Università degli Studi Roma Tre
Dipartimento di Scienze

SCUOLA DOTTORALE IN

GEOLOGIA DELL'AMBIENTE E DELLE RISORSE (SDIGAR)

SEZIONE GEOLOGIA DELL'AMBIENTE E GEODINAMICA

XXV CICLO

PhD Thesis

The origin of mesetas in the Iberian Chain (Spain)

Candidata

Valentina Nicole Scotti

Tutor

Prof. Claudio Faccenna
Dott.ssa Paola Molin

ABSTRACT

Topography results from the interaction of tectonics that moves rock masses and surface processes that shape and lower them. In this study we investigated the recent evolution of the Iberian Chain landscape, an intraplate orogen located in the central-eastern Spain. It originated during the alpine orogeny in Upper Cretaceous-Middle Miocene. In the whole Iberia, the Iberian Chain represents a unique case of dome-shaped topography. Its central sector is dominated by an extensive planation surface which lies at an altitude of 1300 m. This surface records a period of tectonic quiescence (Upper Neogene?) during which most of previous compressive structures were almost completely eroded creating a wide peneplain. In Late Pliocene (?)-Quaternary, this denudation episode was interrupted by the onset of an uplift that controlled the organization of the present fluvial network. The origin and evolution of the high-standing plateau in a relatively tectonically stable region is still a controversial issue.

To quantitatively characterize the influence of surface and tectonic processes, we studied the morphometry of the Iberian Chain. In detail, we analyzed the topography (map of local relief, swath profiles) and the hydrography (basin hypsometric curve and integral, basin asymmetry factor, river longitudinal profiles and relative geomorphic indices) of the Iberian Chain using the SRTM DEM as a main data source. Our results have been coupled with the incision rates of the High Tagus R. and Martin R. areas, calculated using fill terraces dated by the Uranium-series (^{230}Th/U) method carried out on calcareous tufa deposits.

Our morphometric results indicate that rock-type erodibility is the main factors ruling landscape (topography and drainage pattern) evolution of the study area as well as

tectonic uplift. Its dominance is confirmed by the values of incision rate that are very similar throughout the central sector of the range. Nevertheless, the accentuated low values of local relief and intrinsic concavity of the stream longitudinal profiles as well as hypsometric convex curves and relatively high integrals indicate the Iberian Chain landscape is in a transient state in response to a recent uplift. Indeed, the fluvial processes that so weakly incised this landscape are still far from counterbalancing the tectonics input. These results depict the Iberian Chain as a well distinct topographic unit with respect to the rest of Iberia.

To simulate the evolution of a landscape characterized by the same tectonic and erosion inputs of the Iberian Chain area, we performed 3-D numerical experiments. We tested the models combining process laws (hillslope diffusion, fluvial incision, sedimentation) and physical parameters calibrated on the field, radiometric, and morphometric data. For our purposes, we used SIGNUM (Simple Integrated Geomorphological Numerical Model), a Matlab TIN-based landscape evolution model able to simulate tectonic uplift, hillslope diffusion and river incision.

A validation of the parameters obtained from 3-D numerical simulations was performed by the inversion of synthetic 2-D longitudinal profiles.

The comparison between real and simulated 3-D landscapes provide us a quantitative view on the origin of present topographic features of the Iberian Chain. In detail, 3-D models show that the onset of the tectonic uplift occurs at ~3.2 Myr with non-uniform rates that range between 0.5 mm/yr in the interior sector to 0.25 mm/yr. The inversion of the drainage network, starting at around 2 Ma, occurs after the onset of the uplift, through the topographic barriers that preserve the landscape in the inner Iberian Chain at high elevation

TABLE OF CONTENTS

LIST OF FIGURES

Fig. 1.5. Histogram of modal distribution of slope (A) and local relief (B), and comparison of elevation with slope (C) and local relief (D). (E): Correlation between local relief and slope. The analysis concern only data within the Iberian Chain. SRTM DEM elevation data have been divided into height intervals of 50 m. For each height interval, the corresponding slope and local relief mode value has been calculated.

Fig. 1.4. A) DEM of the study area and location of traces of the four swath profiles; B) swath profiles showing the trend of maximum, minimum, and mean topography of the Iberian Chain. In each profile Local relief has been computed by subtracting minimum and maximum elevation. IC: Iberian Chain; TB: Teruel Basin; MB: Madrid Basin; JB: Jiloca Basin; GB: Guadiana Basin; EB: Ebro Basin; CM: Cameros Massif.

Fig. 1.6. Map of the analyzed drainage basins of Eastern Central System and Iberian Chain with their asymmetry factor. The plotted arrows indicate the direction of the asymmetry and their colors indicate the intensity of the asymmetry. Alberche (Al), Guadarrama(Gr), Jarama (Jr); Madrid Basin side: Henares (He), Tajuña (Ta), Tajo (Tj); Júcar (Ju), Cabriel (C), Magro (Mg), Turia (Tu), Mj=Mijares (Mj); Guadalope (Gp), Martìn (Mt), Aguasvivas (Ag), Huerva (Hu), Jiloca (Ji) and Jalón (Ja).

Fig. 1.7. A-C) Hypsometric curves of the studied drainage basins. *H*: maximum elevation within the basin; *h*: elevation; *A*: total surface area of the basin; *a*: area within the basin above a given elevation *h*; D) values of hypsometric integral for the analyzed drainage basins displayed from the SE to the NE following a counterclockwise direction; E-G) Variation of normalized drainage area values of analyzed basins as function of elevation; H) values of concavity and steepness indices of longitudinal

profiles of the studied rivers, displayed from the SE to the NE following a counterclockwise direction.

Fig. 1.8. Map of channel steepness indices extracted throughout the Iberian Chain and its surroundings from SRTM DEM using the Stream Profiler tool, available at www.geomorphtools.org, with procedures described in Wobus et al.(2006). Steepness indices are normalized (k_{sn}) to a reference concavity (θ_{ref}) of 0.45 (Wobus et al., 2006).

Fig. 1.9. River longitudinal profiles (A-F: Madrid Basin side rivers; G-M: Mediterranean side rivers; N-S: Ebro Basin side rivers): each plot consists of two diagrams: elevation vs. distance (longitudinal profile) and log slope vs. log area. Longitudinal profile plots: grey arrows show the location of main knickpoints related to rock-types changes and tectonic structures, while black arrows show the location of the knickpoints dividing the profiles in two different segments; *D* indicates dams. Log slope vs. log area plots: blue and cyan lines represent regression lines fitting data with the concavity as a free parameter and the reference concavity θ_{ref}=0.45, respectively. Red squares are log-bin averages of the slope-area data.

Fig. 1.10. A) radiometric ages of strath terraces in Alto Tajo and Martin R. valleys compared with the standard marine oxygen-isotope curve by Martinson et al. (1987); B) local relief map of Iberian Chain showing the location of the analyzed fresh tufa samples (white circles) and the estimated incision rates for each site.

Fig. 1.11. 2-dimensional isochron plots, with 1σ error crosses, of four coeval sub-samples from (A) terrace III (sample 7-2) and (B) terrace IV (sample 12-1), Puente de San Pedro site. The slopes in the ($^{234}U/^{232}Th$) vs ($^{238}U/^{232}Th$) and ($^{230}Th/^{232}Th$) vs

($^{234}U/^{232}Th$) diagrams represent, respectively, the ($^{234}U/^{238}U$) and ($^{230}Th/^{234}U$) activity ratios of the pure carbonate fraction. MSWD: mean square weighted deviation.

Fig. 2.1. Geological map of the study area, analyzed rivers (1= Henares; = Tajuña; 3= Tajo; 4= Júcar; 5= Cabriel; 6= Magro; 7= Turia; 8= Mijares; 9= Guadalope; 10= Martìn; 11= Aguasvivas; 12= Huerva; 13= Jiloca; 14= Jalón) and location of collected fresh tufa samples (RG: Ruguilla, PSP: Puente de San Pedro, MON: Montalban, RP: Las Parras de Martìn.).

Fig. 2.2. A) DEM of the study area and location of traces of the four swath profiles; B) swath profiles showing the trend of maximum, minimum, and mean topography and local relief of the Iberian Chain. IC: Iberian Chain; TB: Teruel Basin; MB: Madrid Basin; JB: Jiloca Basin; GB: Guadiana Basin; EB: Ebro Basin; CM: Cameros Massif.

Fig. 2.3. Local relief map of the Iberian Peninsula.

Fig. 2.4. River longitudinal profiles. A-C: Madrid Basin side rivers; D-H: Mediterranean side rivers; I-P: Ebro Basin side rivers.

Fig. 2.5. A) areas characterized by homogeneous uplift pattern, in which the Iberian Chain has been sub-divided; B) uplift rate pattern implemented in the numerical model.

Fig. 2.6. A-C: initial conditions; D-F: topographies shaped by fluvial and hillslope erosion, obtained from setup A-C, under uplifting condition, after running the model for 3.2 Myr; G-I: topographies obtained with the implementation of sedimentation processes.

Fig. 2.7. Example of the results for iterative variations of the value of *k* to minimize the error between a simulated stream profiles (dotted lines) and a natural stream profile (solid blue curve) under homogenous uplift conditions.

Fig. 2.8. *k* and *f(k)* plot relative to the example of fig. 2.7, showing that the best fit conditions between simulated and natural stream profiles are achieved when *f(k)* decreases to a value $\leq \varepsilon$.

Fig. 2.9. Synthetic stream profile obtained starting from a flat surface under homogeneous uplift conditions (uplift rate U = 0.3 mm/y), implementing a bedrock characterized by two lithologies with different erodibility ($k_2<k_1$). The river evolves starting from the mouth by upstream erosion. When incision reaches the depth of the uplifted contact between the two different layers, a "lithological" knickpoint propagates upstream on the profile.

Fig. 2.10 Example of iterations implemented to achieve a synthetic stream profile (dotted lines) that provides the best approximation of a natural irregular curve (solid blue line). The real stream profile is discretizated in 3 reaches. The simulation is performed finding the best fitting value of *k* between natural and synthetic stream profiles firstly for the upstream reach (A), then for the next reach (B) and one-by-one to the mouth of the river (C).

Fig. 2.11. Comparison between the natural stream profiles (solid red lines) of Tajo (A), Tajuña (B) and Mijares (C) R and the synthetic profiles (dotted blue lines) obtained from 2-D inversion and taking into account the erodibility of outcropping litologies.

LIST OF TABLES

INTRODUCTION

The Iberian Chain is an intraplate range located in the central-eastern Iberian Peninsula, that results from the tectonic inversion of a Permian-Mesozoic basin occurred in Late Cretaceous to Middle Miocene times.

In the whole Iberia Peninsula, the Iberian Chain represents a unique case of dome-shaped topography. Its central sector is dominated by wide erosional high-standing low relief surfaces: during the Upper Neogene, the compressive structures experienced planation processes presently recorded by wide flat surfaces liying at an average altitude of 1300 m a.s.l.

In Late Pliocene (?)-Quaternary, the onset of a regional uplift controlled the organization of the present fluvial network and the dissection of the landscape.

While the origin of the belt is rather well-understood, the formation of the present-day relief of Iberian Chain is under debate.

A multidisciplinary approach has been applied in this Thesis, in order to understand the development and the causes of the recent landscape evolution in Iberian Chain

To quantitatively characterize the influence of surface and tectonic processes, I studied the morphometry of the Iberian Chain.

In detail, in chapter 1, I analyzed the topography (map of local relief, swath profiles) and the hydrography (basin hypsometric curve and integral, basin asymmetry factor, river longitudinal profiles and relative geomorphic indices) of the Iberian Chain using the SRTM DEM as a main data source.

I combined the morphometric analysis with radiometric Uranium-series dating of

calcareous tufas lying on fluvial strath terraces. The obtained ages allowed me to estimate the incision rates that affected the Iberian Chain since Late Pleistocene.

In chapter 2, 3D numerical experiments of geomorphological processes and tectonic uplift have been performed in order to simulate the Plio-Quaternary landscape and drainage network evolution of the Iberian Chain I tested the models using physical parameters calibrated on the field, radiometric, and morphometric data discussed in chapter 1.

For this purpose, I used SIGNUM (Simple Integrated Geomorphological Numerical Model), a Matlab TIN-based landscape evolution model able to simulate tectonic uplift, hillslope diffusion and river incision. Moreover, 2D modeling of some rivers profiles has been performed to verify the parameters implemented in 3D experiments. The comparison between natural and synthetic landscapes provide me a quantitative view on the origin of present topographic features of the Iberian Chain.

I discuss the implications of the whole study and present my conclusions in chapter 3.

This manuscript provides new geomorphic and time constrains to the reconstruction of the topographic growth of the Iberian Chain, a topic still highly debated in the scientific community.

Chapter 1

THE INFLUENCE OF SURFACE AND TECTONIC PROCESSES IN LANDSCAPE EVOLUTION OF THE IBERIAN CHAIN: QUANTITATIVE GEOMORPHOLOGICAL ANALYSIS AND GEOCHRONOLOGY

Abstract

First-order topographic features, drainage system pattern and spatial variation in surface processes rates in tectonically active areas represent proxies to quantitatively characterize the landscape's response to tectonic forcing.

We investigated the recent landscape evolution of the Iberian Chain (NE Spain), an intraplate thrust-belt formed in Late Cretaceous to Middle Miocene times. In the whole Iberia, the Iberian Chain represents a unique case of dome-shaped topography. Its central sector is dominated by a wide high-standing low relief surface, developed during Upper Neogene (?), presently lying at an average altitude of 1300 m. In Late Pliocene (?)-Quaternary, the onset of a regional uplift controlled the organization of the present fluvial network and the dissection of the landscape.

Geomorphic responses to tectonic forcing have been analyzed by the calculation of morphometric parameters, focusing on topography (map of local relief, swath profiles) and hydrography (basin hypsometric curve and integral, basin asymmetry factor, river longitudinal profiles and relative indices), using the SRTM DEM as main data source. Morphometric analysis has been also combined with radiometric Uranium-series dating

of calcareous tufas lying on fluvial terraces. The results allow the estimation of incision rate along the High Tajo and Martin rivers.

Our results indicate that uplift and rock-type erodibility are the main factors ruling landscape evolution of the study area. The values of incision rate are very similar throughout the central sector of the range, indicating that, despite local small variation, the rivers respond mainly to a homogeneous regional uplift.

In conclusion, the Iberian Chain landscape is in a transient state in response to a recent dome-like uplift. Indeed, the fluvial processes that weakly incised this landscape at a rate of ~0.6 mm/yr, are getting close to a radial pattern. On the basis of geological and geomorphic constrains, we hypothesize the uplift started around or after 3 Ma.

Keywords

Landscape evolution; Iberian Chain; uplift; topography; hydrography; incision rate

1.1 Introduction

First-order topographic features, drainage system pattern and spatial variation in surface processes rates in tectonically active areas represent proxies to quantitatively characterize the landscape response to crustal and subcrustal processes. The competing forces of most of these processes that build-up topography and of erosion that shapes it, tend to balance over time. So if a low relief landscape is uplifted, the steepening of river channels and adjacent hillslopes induces a progressive increase in erosion rates that eventually could counterbalance rock uplift rate (Whipple, 2001). In this case, the landscape changes from a transient state of disequilibrium to a steady state. The response times of landscape to tectonic or climatic perturbation range from 10^4 to 10^6 yr (Whipple, 2001; Wegmann et al., 2007). Generally speaking, the timescale of tectonic

input is long with respect to landscape response time, whereas the timescale of recent climate changes is shorter (Whipple, 2001). So the tectonic perturbation influence is more persistent in landscape than climatic fluctuations one. Among the geomorphic systems response to external perturbation, fluvial systems are particular important since they propagate headward the variations in base-level and rule the adjacent hillslope dynamics (Whipple and Tucker, 1999). This makes the study of hydrography and topography fundamental to investigate the role of tectonics and climate in recent landscape evolution. A good example of a transient landscape where topography and hydrography could be an important source of data to reconstruct the recent evolution is the Iberian Chain (north-eastern Spain), a dome range characterized by a high-standing low relief landscape. It is an intraplate mountain belt located within the Iberia Plate, between the Pyrenees to the north, the Central System to the west, and the Valencia Through to the east (Fig. 1.1). The formation of this belt has been related to the Middle Eocene-Middle Miocene compressive inversion of a Mesozoic extensional basin (e.g.: Álvaro et al., 1979). Mounting geomorphological evidences have shown that while the compressive episode vanished in the Neogene, uplift and incision occurred in recent time (Martín-Serrano, 1991; Mather, 1993; Gutiérrez et al., 1996). Therefore, while the origin of the belt is rather well-understood, the formation of the present-day relief is under debate. Some models proposed that the uplift is generated by large scale folding (Cloetingh et al., 2002; De Vicente et al., 2007), by late stage compressive episode or by erosional unloading (Casas-Sainz and De Vicente, 2009), or by the possible action of a mantle upwelling (Boschi et al., 2010; Faccenna and Becker, 2010).

Here, we investigate the geomorphology and the recent landscape evolution of the Iberian Chain. Geomorphic responses to tectonic forcing have been analyzed by the calculation of morphometric parameters, focusing on the first order features of the present topography (map of local relief, swath profiles, frequency plots of slope and

local relief values and their relationships with elevation) and hydrography (basin hypsometric curve and integral, basin asymmetry factor, river longitudinal profiles and relative indices), using the SRTM DEM as main data source. Morphometric analysis has been also combined with radiometric Uranium-series dating of calcareous tufas lying on fluvial terraces in order to estimate incision rates.

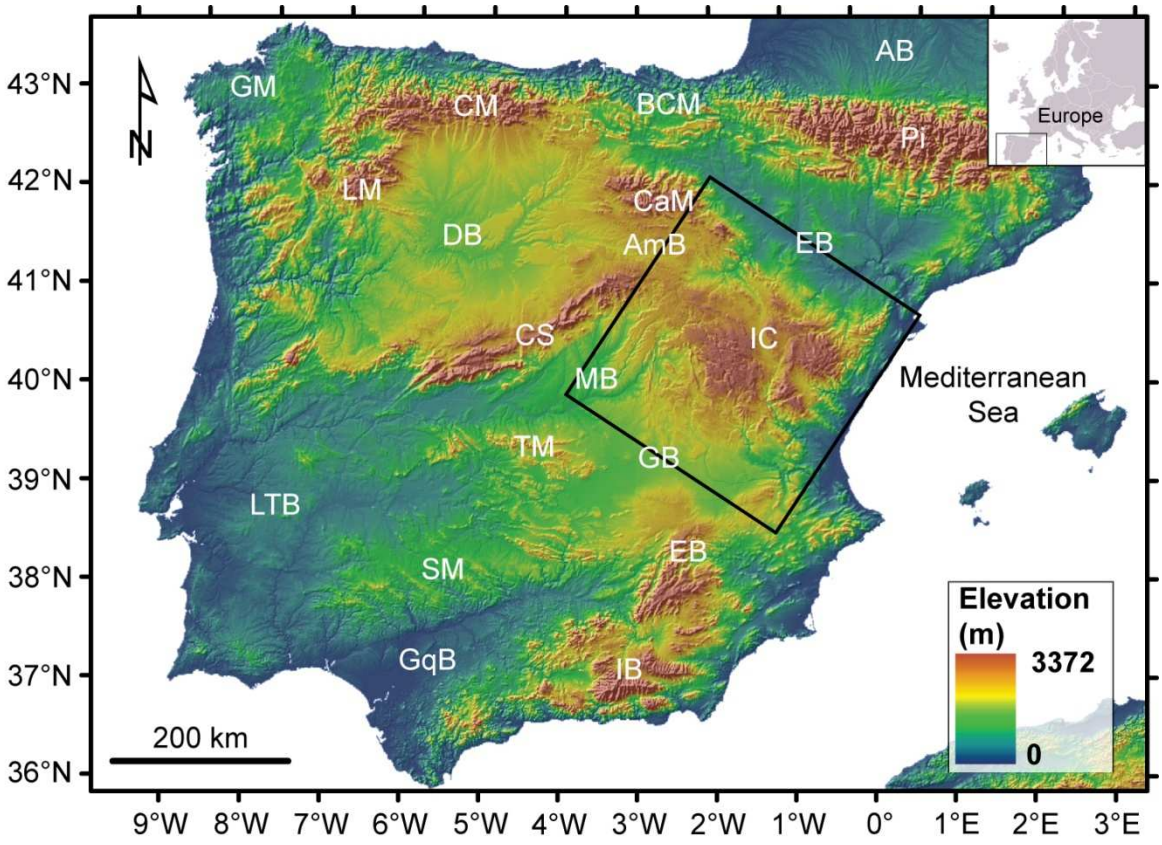

Fig. 1.1. Topography of the Iberian Peninsula (SRTM DEM database). Black box localizes the studied area. Mountain ranges: Galician Massif (GM), Cantabrian Mts (CM), Basque-Cantabrian Mts (BCM), Pyrenees (Pi), Leon Mts (LM), Cameros Massif (CaM), Central System (CS), Iberian Chain (IC), Toledo Mts (TM), Sierra Morena (SM), External Betics (EB), Internal Betics (IB); basins: Aquitaine B. (AB), Duero B. (DB), Almazan B. (AmB), Ebro B: (EB), Madrid (High Tajo) B. (MB), Low Tajo B. (LTB), Guadiana B. (GB), Guadalquivir B. (GqB). Eastings and northings are according to the WGS 1984 grid.

Our goal is to investigate the landscape evolution of an intraplate orogen where crustal or subcrustal processes have driven a regional dome-like uplift. The dominance of this upheaval in geomorphic evolution is just partially disturbed by local rock-type changes

or tectonic features. The results are consistent with a poorly incised landscape where erosion rates are far from counterbalance uplift rate. We used these results to develop a conceptual model for the long-term evolution of the Iberian Chain landscape.

1.2 Geological setting

The *Iberian Chain* is an intraplate double vergent thrust belt, formed as consequence of the convergence between Africa and Iberia (Late Cretaceous-Middle Miocene). The range itself results from the positive inversion of faults originated during the Mesozoic extension of the Iberian Basin (Álvaro et al., 1979; Guimerà et al., 2004), accommodating Cenozoic intraplate shortening (Casas-Sainz and Faccenna, 2001). Estimates of shortening ranges up to 22% (30 km) along the Demanda-Cameros Unit (northwestern sector of the chain) (Casas-Sainz, 1993; Guimerà etal., 1995; Casas-Sainz et al., 2000) decreasing to ~17% in the Montalbán–Utrillas Thrust (Casas-Sainz et al., 2000, Simón and Liesa, 2011), and to ~10% in the Maestrazgo Unit, (De Vicente, 2004; De Vicente and Vegas, 2009) (*Fig.* 1.*2A*). The Castilian (Rodríguez-Pascua and De Vicente, 1998) and Aragonese (Ferreiro et al., 1991; Calvo Hernández, 1993; Cortés-Gracia and Casas-Sainz, 1996; Casas-Sainz et al., 1998) Branches, conversely, show strike-slip component along NW–SE structures with basement-involved positive flower structures (*Fig.* 1.*2B).* Finally, the Altomira Unit, located in the westernmost sector (*Fig.* 1.*2A*), is a north-south trending fold-and-thrust belt, affecting a thin Cretaceous cover, with westward direction of tectonic transport (Muñoz-Martín and De Vicente, 1998; De Vicente, 2004).

The Iberian Chain ends abruptly westward against the Central System *(Fig.* 1.*2A).* The linkage between these ranges is characterized by several NW– SE dextral strike-slip

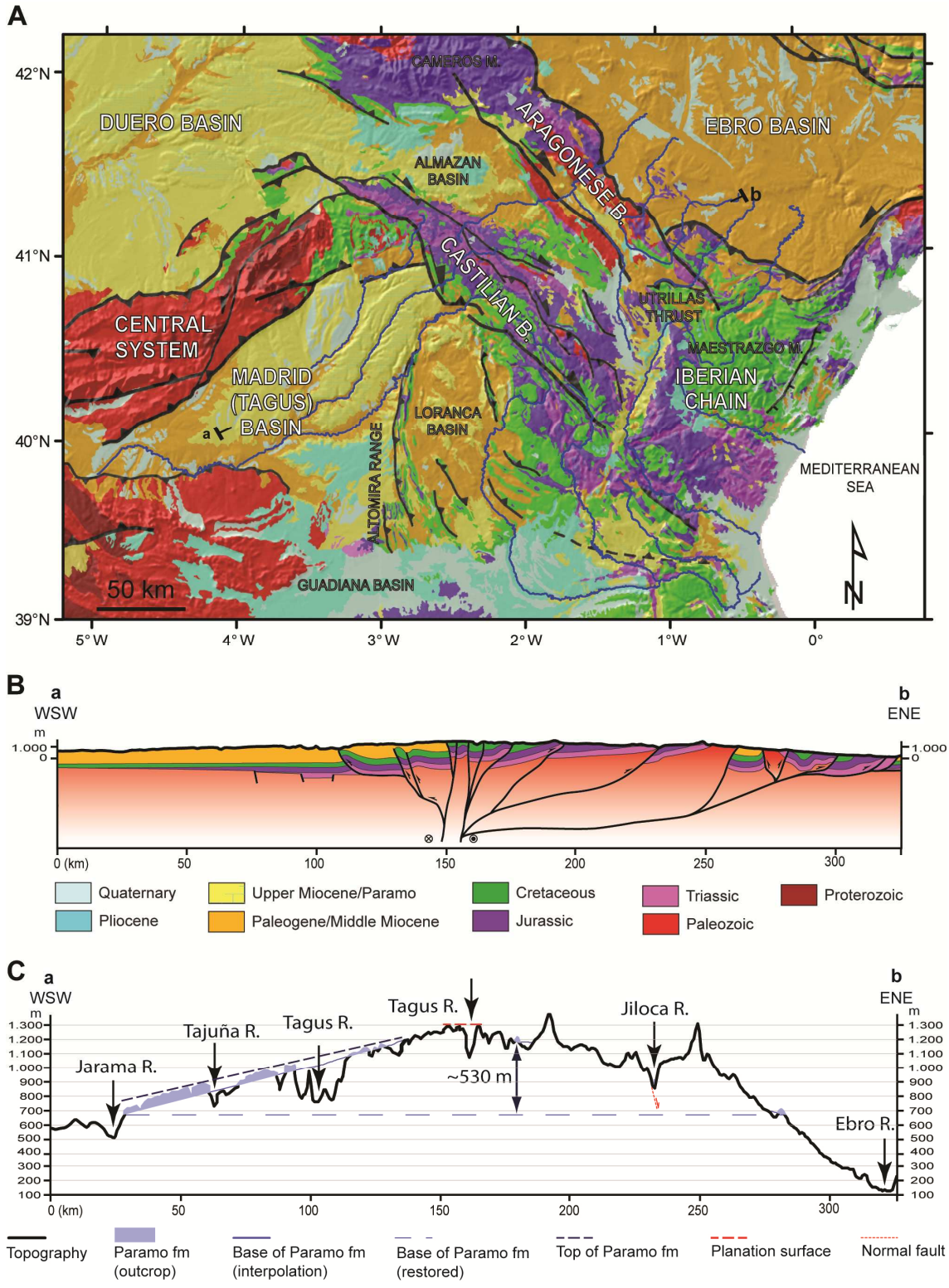
A
42°N
41°N
40°N
39°N
5° W
4° W
3° W
2° W
1°W
0°
DUERO BASIN
CAMEROS M.
ARAGONESE B.
EBRO BASIN
ALMAZAN BASIN
a
b
CASTILIAN B.
UTRILLAS THRUST
CENTRAL SYSTEM
MAESTRAZGO M.
IBERIAN CHAIN
MADRID (TAGUS) BASIN
LORANCA BASIN
ALTOMIRA RANGE
MEDITERRANEAN SEA
50 km
GUADIANA BASIN
N
B
a
WSW
b
ENE
m
1.000
0
0 (km)
50
100
150
200
250
300
Quaternary
Pliocene
Upper Miocene/Paramo
Paleogene/Middle Miocene
Cretaceous
Jurassic
Triassic
Paleozoic
Proterozoic
C
a
WSW
b
ENE
m
1.300
1.200
1.100
1.000
900
800
700
600
500
400
300
200
100
Jarama R.
Tajuña R.
Tagus R.
Tagus R.
~530 m
Jiloca R.
Ebro R.
0 (km)
50
100
150
200
250
300
Topography
Paramo fm (outcrop)
Base of Paramo fm (interpolation)
Base of Paramo fm (restored)
Top of Paramo fm
Planation surface
Normal fault

Fig. 1.2. A) Geological map of the study area compiled from 1:1,000,000 scale map of Iberian Peninsula (IGME, 1995), draped over 1000 m DEM. Major streams of Iberian Chain are displayed for reference. The trace of profile a-b is also shown; B) simplified geological cross-section of Iberian Chain (modified after De Vicente and Vegas, 2009; C) geological cross-section along the trace a-b of the Paramo fm., showing its outcropping and interpolated base, the top surface envelope, and the planation surface developed on the Mesozoic basement. The restored base of Paramo fm before its upwarping is also shown. Note that the maximum uplift of the Paramo fm. is ~500 m.

faults. The Central— System is also a NE-SW, double-vergence intraplate belt in central Iberia, resulting from thick-skinned Tertiary compression involving metamorphic-granitic Hercynian basement (De Vicente et al., 2007).

Tertiary endorheic compressional basins border the thrust belts (e.g.: Calvo et al., 1993; Villena et al., 1996; Alonso-Zarza A. , 2008): the Duero Basin to the NW, the Ebro Basin to the N, the La Mancha Plain Basin to the S, the Alto Tajo Basin to the SW. The latter is divided into two parts separated by the Altomira Unit: the Madrid Basin towards the W and the Loranca piggy-back basin to the E) (*Fig.* 1.*2A*). Conversely, the Teruel and Calatayud-Montalban basins interrupt the general dome-shaped topography of the Iberian Chain and are filled up by Upper Oligocene-Pliocene (4.5-3 Ma) continental sequences deposited in internally drained basins (López-Martínez et al., 1987; Anadón et al., 1990; Anadón and Moissenet, 1996; Alcalá et al., 2000; van Dam and Sanz Rubio, 2003). These basins remained isolated from each other and from the surrounding basins until the Late Miocene, when a widespread deposition of coarse to fine fluvial sediments along the basins margin and lacustrine carbonates located along the depoaxis of each basin (Páramo Fm.) overlapped the entire system (Armenteros et al., 1989; Alonso-Zarza and Calvo, 2000). The origin of these basins is controversial, being related either to compressional episode or to extensional structures that may be correlated with NE-SW extensional structures evident along the Mediterranean coast

and related to the Neogene opening of the Valencia Trough (Guimerà and Alvaro, 1990; Roca and Guimerà, 1992; Vegas, 1992; Cortés-Gracia and Casas-Sainz, 2000).

The topography of the belt is characterized by a regional-scale flat erosion surface, the so-called Main Planation Surface of the Iberian Chain (Birot, 1959; Solé Sabarís, 1979; Simón, 1984; Peña et al., 1984), or by two distinct nested surfaces (Gracia-Prieto et al., 1988; Gutiérrez Elorza and Gracia, 1997). The planation surfaces have been correlated with the top of the Pliocene limestone units, suggesting a coeval development of these planation/sedimentation features (Peña et al., 1984; Gracia-Prieto et al., 1988; Gutiérrez, 1996). Consequently, the Main Planation Surface of the Iberian Chain has been often used as a regional morphological feature marker (Peña et al., 1984; Simón, 1984; Simón, 1989; Gracia-Prieto et al., 1988; Gutiérrez Elorza and Gracia, 1997; Rubio and Simón, 2007). Alternatively, the planation surfaces are considered as originally stepped erosional surfaces (Casas-Sainz and Cortés-Gracia, 2002; Gracia et al., 2003; Benito-Calvo and Pérez-González, 2010) developed either during a compressional uplift of the chain (González et al., 1998; Guimerà and González, 1998; Casas-Sainz and Cortés-Gracia, 2002) or the Neogene stage (Gracia-Prieto et al, 1988, 2003; Benito-Calvo and Pérez-González, 2010).

A regional tectonic uplift occurred producing a general upwarping of the range, smoothly tilting the Páramo carbonates. The present day river network dissects the planation surface. The regressive erosion of Ebro, Tajo and Turia Rivers drove the progressive capture of the intermontane basins and their transformation into exorheic basins from the Pliocene onward (Gutiérrez et al., 2008). At present, Quaternary deposits are confined mostly in still internally drained small intermontane basins.

The timing and extent of uplift of the Iberian chain is poorly constrained. Figure 2C, shows a cross section of the belt illustrating the extent and attitude of the Páramo fm. carbonates and of the Upper planation surface. The Páramo fm. is gently tilted towards

SW, linking the top Madrid Basin infill with the flat Main Planation Surface on top of the belt. Currently, the elevation difference between them is more than 500 m (Fig 2C.). These structural relationships simply indicate that uplift occurred after the deposition of the Páramo, and therefore post-date main compressional phases. Casas-Sainz and De Vicente (2009) interpreted the uplift of the Iberian Chain as the recent stage of a more general uplift that involved the Central Iberia forming by highly elevated flat surfaces (the Iberian Meseta), presently located at 600-800 m a.s.l. These high plains are rimmed by mountain chains reaching heights of up to 1500 m: Cantabrian Mountains, Central System, Iberian Chain, Sierra Morena (Fig. 1.1).

Several hypotheses attempt to explain ages and tectonic origin for the uplift of Central Iberia. Because of the location of granite outcrops, no absolute thermochronological data have been obtained in the Iberian Chain. Fission tracks analyses performed in the Central System (De Bruijne and Andriessen, 2002; Ter Voorde et al., 2004) suggest a pronounced cooling acceleration starting in the Early Pliocene (5 My), as well as in the Catalan Coastal Range (Juez-Larré and Andriessen, 2006).

The mechanisms for uplift of Central Iberia (Cloetingh et al., 2002); De Vicente et al., 2007) invocate the Alpine compression and a lithospheric folding that accommodated shortening. Conversely, an isostatic rebound related to both crustal thickening and erosion due to the endorheic-exorheic drainage transition, is thought to be the source for the late uplift affecting the Iberian Chain (Casas-Sainz and De Vicente, 2009). Other authors (Simón, 1984; 1989; Muñoz-Martín and De Vicente, 1998) invocate extensional doming and uplifting in the eastern Iberian Chain, linked to the evolution of the Valencia Trough and the Mediterranean margin.

1.3. Geomorphology: quantitative morphometric analysis of the Iberian Chain

1.3.1. Topography

At regional scale, we investigated the general features of topography focusing on the spatial variation in minimum, mean, maximum elevations and in local relief values. The maximum topography is represented by a surface (envelope) connecting peaks elevation and displaying topography without river incision. The minimum topography is described by a surface (sub-envelope) corresponding to the general pattern of valley bottoms elevation. The mean topography trend represents the general pattern of landscape at regional scale. Local relief is the residual between maximum and minimum topography and quantifies fluvial incision in a given area (Molin et al., 2004). Since river erosion is driven by the constant competition between tectonics and climate (Burbank, 1992), the local relief variation in an area where climate is almost constant indicates the rivers response to different tectonic inputs.

1.3.1.1. Local relief distribution in the Iberian Peninsula

We extracted a local relief map of the Iberian Peninsula to produce a general overview of the regional spatial variation in fluvial dissection and to compare the Iberian Chain with the other mountain chains of the peninsula. We computed this map as the residual relief between the envelope and the sub-envelope (Fig. 1.3A). These surfaces have been extracted from the raw topography by smoothing the maximum and minimum elevations by a circular moving window 30 km wide. We chose the value of 30 km since it is the average main valley spacing. This allowed us to remove small valleys that would generate a noisy map that misses the regional scale meaning of our analysis.

The values of local relief in the Iberian Chain are anomalously low compared with the other mountain areas (Cantabrian Mts, Pyrenees, Central System, Betics) in Iberia (Fig.

A

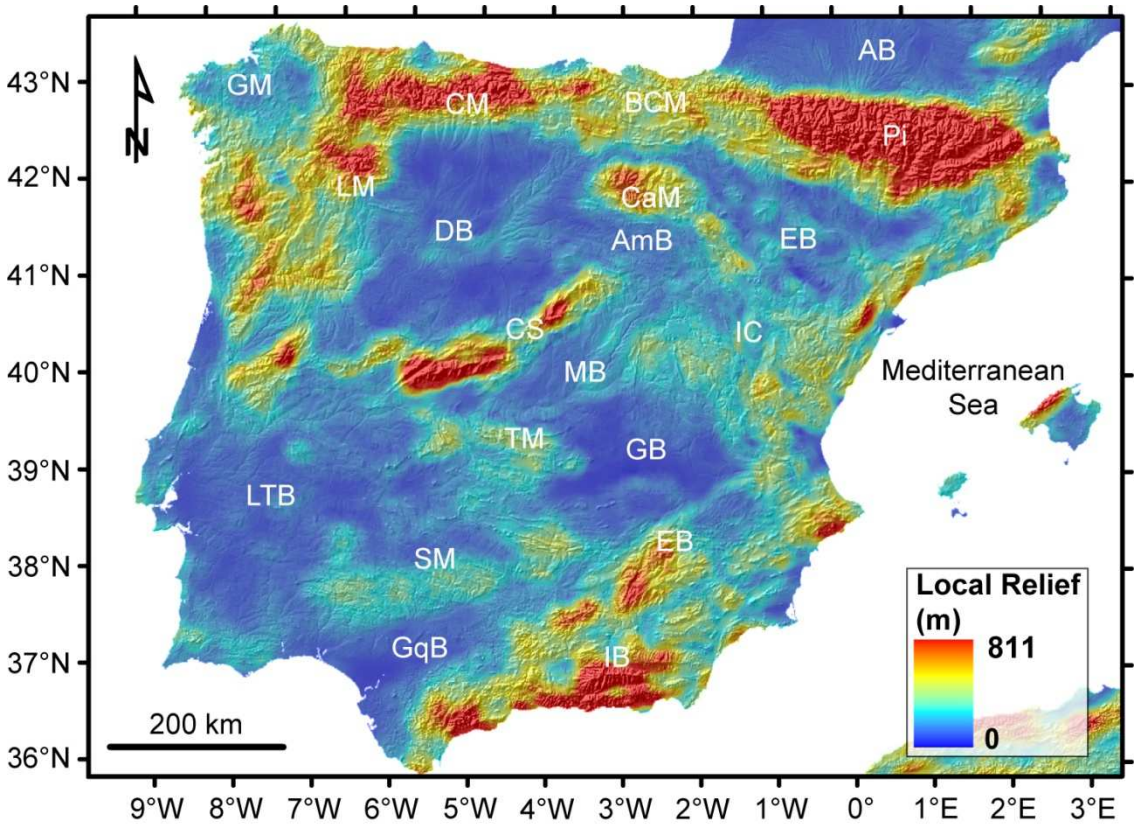
GM
CM
BCM
AB
Pi
LM
CaM
DB
AmB
EB
CS
IC
MB
Mediterranean Sea
TM
GB
LTB
EB
SM
GqB
IB
Local Relief (m)
811
0
200 km
43°N
42°N
41°N
40°N
39°N
38°N
37°N
36°N
9°W
8°W
7°W
6°W
5°W
4°W
3°W
2°W
1°W
0°
1°E
2°E
3°E

B

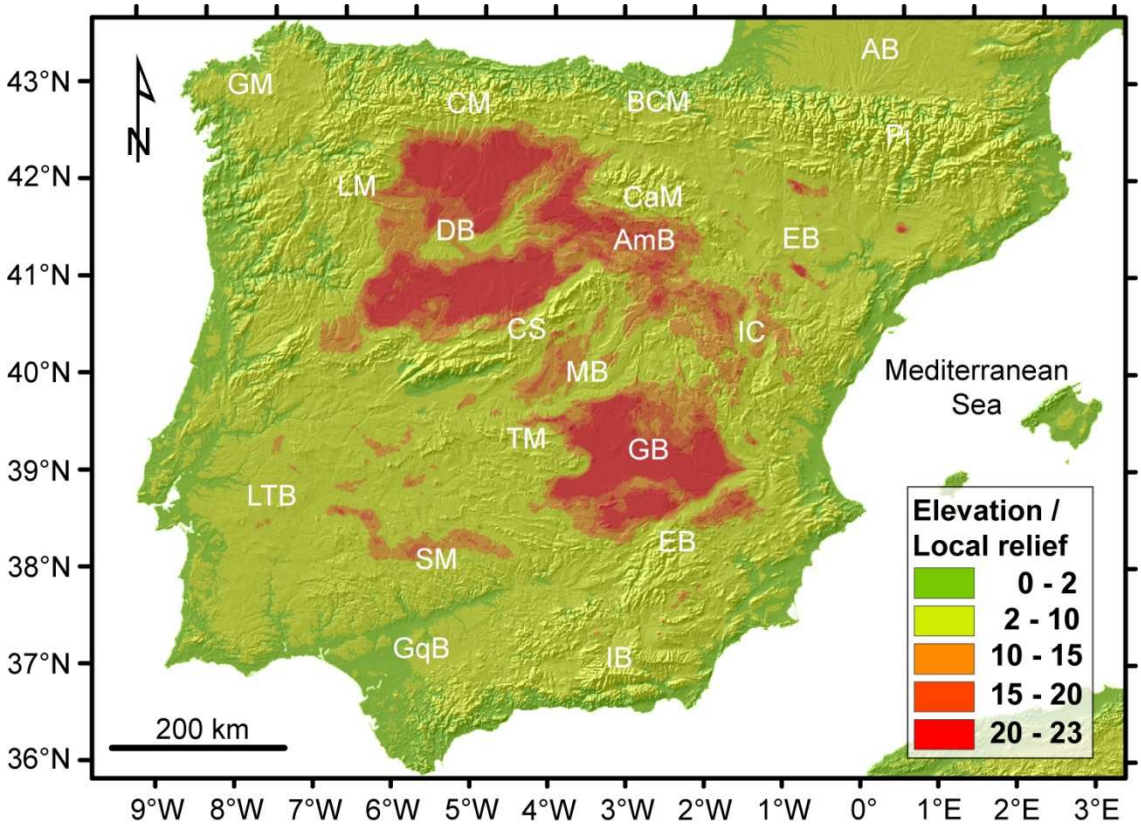
GM
CM
BCM
AB
Pi
LM
CaM
DB
AmB
EB
CS
IC
MB
Mediterranean Sea
TM
GB
LTB
EB
SM
GqB
IB
Elevation / Local relief
0 - 2
2 - 10
10 - 15
15 - 20
20 - 23
200 km
43°N
42°N
41°N
40°N
39°N
38°N
37°N
36°N
9°W
8°W
7°W
6°W
5°W
4°W
3°W
2°W
1°W
0°
1°E
2°E
3°E

Fig. 1.3. A) Local relief map of the Iberian Peninsula, computed by subtracting a minimum from a maximum topography enveloping surfaces (see text for explanation); B) relief anomaly (Local relief/Elevation) map of the Iberian Peninsula.

1.3A). More in detail, the highest values are located in the eastern sector of the Iberian Chain, all along the Mediterranean coast, where active or recent extensional faults are located (Perea et al., 2012; Simón et al., 2012). The rest of chain is characterized by low and very low values.

Observing the whole Iberian Peninsula, all the mountain ranges are characterized by very high values of local relief with the only exception of the Iberian Chain (Fig. 1.3A). To evidence the anomaly of the Iberian Chain topography, we calculated a new parameter (A_R, relief anomaly) normalizing the raw elevation data E of the entire peninsula with respect to the local relief R (Fig. 1.3B).

$$A_R = \frac{E}{R} \qquad (1)$$

The spatial distribution of this parameter shows that the highest values of relief anomaly are located in the Duero, Madrid, and Guadiana basins. On the contrary very low values correspond with all the mountain chains but the Iberian Chain whose A_R values are very similar to the Spanish Central Meseta.

1.3.1.2. Swath profiles

To study and quantify the general pattern of the Iberian chain we extracted four swath profiles from the SRTM DEM. Its ~90-m pixel-size is an acceptable resolution for a regional scale analysis. The topographic sections cut across the Iberian Chain (Fig. 1.4): profile a-a', oriented NW-SE, is perpendicular to the coastal normal fault system and

the Teruel Depression; profile b-b' is oriented E-W, transversally to the tectonic structures and crossing the range to pick the main peaks; profile c-c' is oriented SW-NE, perpendicularly to the major thrusts and strike-slip structures; profile d-d' with a N-S orientation is transversal to the major tectonic alignments.

The observation window of the swath profiles is 40 km wide and about 300 km long to include the entire mountain chain and part of the adjacent basins. In this observation window, we sampled topography at an interval of 1 km along five lines spaced 10 km. These elevation data have been used to generate the trend of maximum, minimum and mean elevation topography and calculate the local relief subtracting arithmetically maximum and minimum elevation (Masek et al., 1994).

The four swath profiles show that the Iberian Chain has a dome-shaped topography (Fig. 1.4). It consists mainly of high-standing plains located at ~1200-1400 m a.s.l. (the Main Planation Surface of Peña et al., 1984), gently dipping towards Madrid and Guadiana basins To the east (profiles a-a' and b-b', Fig. 1.4) and to the north (profiles c-c' and d-d', Fig. 1.4), the relatively steeper flanks of the range make a general asymmetric dome-shape. The general dome-shape is also interrupted by the Teruel and Jiloca intermontane basins (profiles a-a' and b-b', Fig. 1.4), as well as by relics of ancient ridges, consisting of Paleozoic sandstones and shales, usually elevated between 100 and 200 m above the high-standing plain.

Remnants of higher flat surfaces can be also recognized in the interior, standing at ~1650 m and ~1800 m a.s.l. west and east of the Teruel Basin respectively (Fig. 1.4). Presently, these surfaces are not topographically connected with the lower ones.

Generally speaking, throughout the chain, the local relief values are mostly constant, around 200 m, even where the intermontane basins are located (profile a-a', b-b', c-c', Fig. 1.4). This flat pattern indicates a very low spatial variation in fluvial incision in the whole study area. The highest local relief values are along the eastern "Mediterranean"

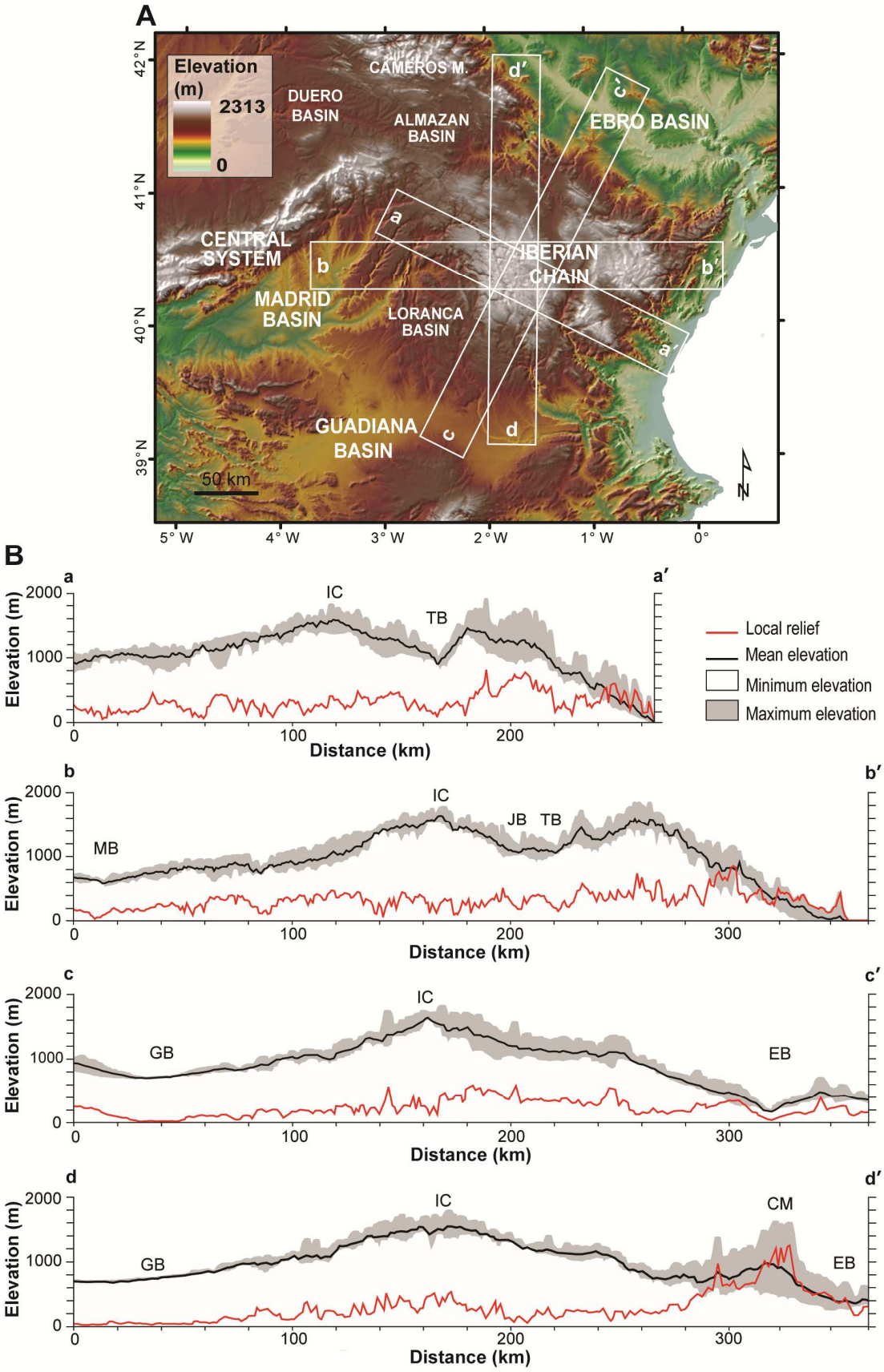
A
Elevation (m)
2313
0
CAMEROS M.
DUERO BASIN
ALMAZAN BASIN
EBRO BASIN
CENTRAL SYSTEM
IBERIAN CHAIN
MADRID BASIN
LORANCA BASIN
GUADIANA BASIN
50 km
42° N
41° N
40° N
39° N
5° W
4° W
3° W
2° W
1° W
0°
B
Elevation (m)
Distance (km)
IC
TB
JB
MB
GB
EB
CM
Local relief
Mean elevation
Minimum elevation
Maximum elevation

Fig. 1.4. A) DEM of the study area and location of traces of the four swath profiles; B) swath profiles showing the trend of maximum, minimum, and mean topography of the Iberian Chain. In each profile Local relief has been computed by subtracting minimum and maximum elevation. IC: Iberian Chain; TB: Teruel Basin; MB: Madrid Basin; JB: Jiloca Basin; GB: Guadiana Basin; EB: Ebro Basin; CM: Cameros Massif.

flank, east of Teruel Basin (swath profile a-a', Fig. 1.4), where active or recent extensional faults are located (e.g.: Perea et al., 2012). To the north, a small increase in local relief is where the Ebro R. tributaries are located. On the contrary, the lowest values (~0 m) are along the southern flank where the Iberian Chain topography decreases gently down to the Guadiana Basin (swath profile c-c' and d-d', Fig. 1.4).

1.3.1.3. Slope and local relief distribution in the Iberian Chain

We calculated the frequency of slope and local relief (fig. 1.5) and we investigated the relationships between elevation, slope and local relief to quantify the first order features of the Iberian Chain. A slope map and a local relief map were used as data sources. We divided the raw elevation data into altitude intervals of 50 m and we extracted the slope and local relief modal value for each of them. These values have been plotted in frequency diagrams (Fig. 1.5A, B).

The slope distribution in Fig. 1.5A is strongly shifted to the left, and characterized by the modal value of 1.27°. The frequency plot of local relief (Fig. 1.5B) exhibits a slightly asymmetric unimodal distribution with a highest peak at ~84 m and two local maxima at ~25 m and ~60 m.

The variation in slope mode with respect to elevation (Fig. 1.5C) increases gently from 0.8° to 3° in the altitude range 0-1500 m a.s.l.. This general trend is interrupted by the lowest value at ~650 m a.s.l., but increases abruptly to the maximum of 9° at ~2500 m above 1500 m of elevation.

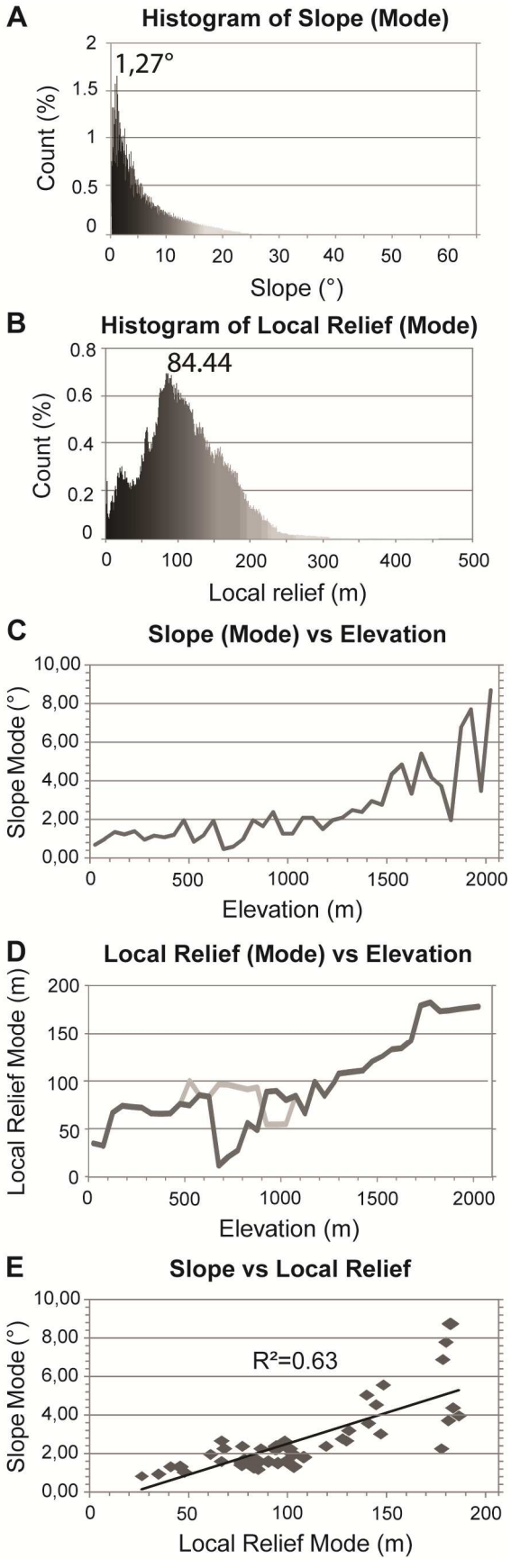
A
Histogram of Slope (Mode)
1,27°
Count (%)
Slope (°)
B
Histogram of Local Relief (Mode)
84.44
Count (%)
Local relief (m)
C
Slope (Mode) vs Elevation
Slope Mode (°)
Elevation (m)
D
Local Relief (Mode) vs Elevation
Local Relief Mode (m)
Elevation (m)
E
Slope vs Local Relief
R²=0.63
Slope Mode (°)
Local Relief Mode (m)

Fig. 1.5. Histogram of modal distribution of slope (A) and local relief (B), and comparison of elevation with slope (C) and local relief (D). (E): Correlation between local relief and slope. The analysis concern only data within the Iberian Chain. SRTM DEM elevation data have been divided into height intervals of 50 m. For each height interval, the corresponding slope and local relief mode value has been calculated.

The variation in local relief mode with respect to elevation (Fig. 1.5D) increases rapidly up to ~75 m at around 100 m of elevation, and remains almost constant (70-110 m) between 150 and 1450 m a.s.l. This flat or slightly increasing pattern is abruptly interrupted by a minimum (10 m) around 600-700 m of elevation. Above 1500 m, where topography includes mostly relic ranges, the local relief increases at a higher rate up to 185 m (around 1700 m of elevation), but then it remains constant in correspondence with the remnants of higher flat surfaces. In Fig. 1.5D, a less sensitive curve– has been extracted for the elevation interval of 500-1000 m. It shows an opposite pattern with respect to the more sensitive curve. Between 500 and 900 m a.s.l. the less sensitive curve shows higher values with a constant pattern of ~90-100 m, related to the relief in the Mediterranean side area. Between 900 and 1100 m a.s.l., the less sensitive curve has a constant value of 50 m and reflects the significant amount of low relief upland in the internal sector of the chain.

Generally speaking, a very similar pattern characterizes the local relief and the slope as functions of elevation (Fig. 1.5C, D). In particular, a linear relationship links these morphometric indices up to ~1500 m a.s.l (Fig. 1.5E). This correlation underlines the different morphometric features that characterize the landscape below the mean elevation of the planation surface, where relief contrasts and slopes are not pronounced, and above it, where the topographic roughness increases, although including upland low relief surfaces.

1.3.2. Drainage network analysis

1.3.2.1. Drainage pattern

The Iberian Chain constitutes the dividing ridge between the three main drainage basins of Iberia (Duero, Tajo and Ebro rivers), as well as between the basins flowing to the Atlantic Ocean and to the Mediterranean Sea in the central-western sector of the peninsula (Fig. 1.6).

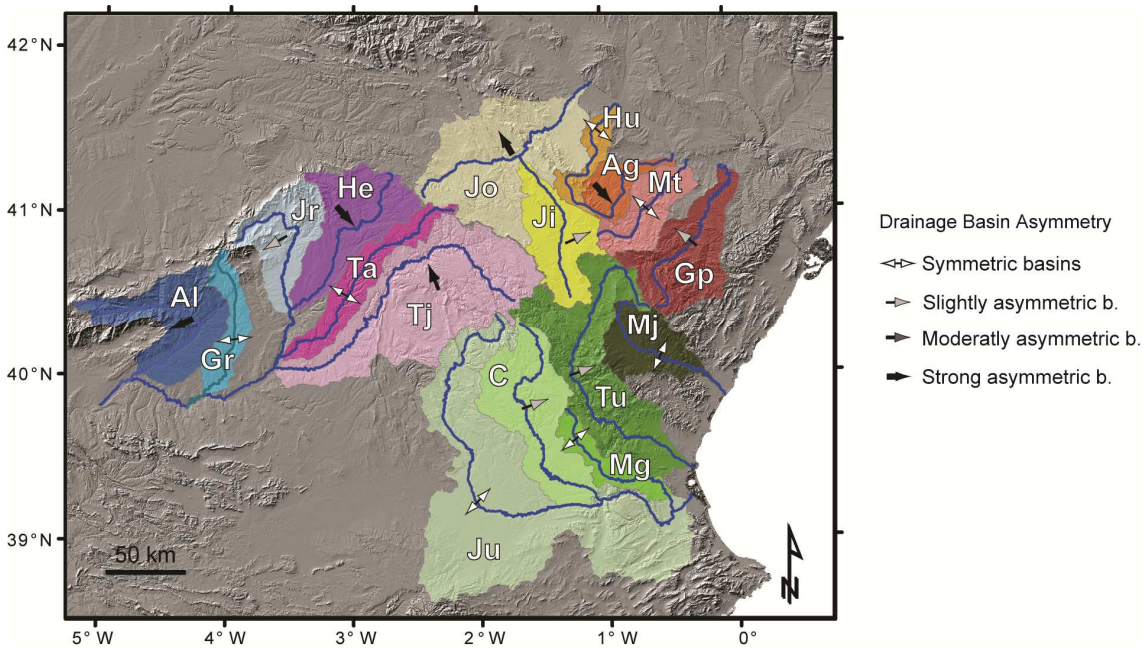

Fig. 1.6. Map of the analyzed drainage basins of Eastern Central System and Iberian Chain with their asymmetry factor. The plotted arrows indicate the direction of the asymmetry and their colors indicate the intensity of the asymmetry. Alberche (Al), Guadarrama(Gr), Jarama (Jr); Madrid Basin side: Henares (He), Tajuña (Ta), Tajo (Tj); Júcar (Ju), Cabriel (C), Magro (Mg), Turia (Tu), Mj=Mijares (Mj); Guadalope (Gp), Martìn (Mt), Aguasvivas (Ag), Huerva (Hu), Jiloca (Ji) and Jalón (Ja).

The rivers draining the Iberian Chain could be separated into three groups: the Alto Tajo R. and its tributaries in the south-western sector, the rivers flowing directly into the Mediterranean Sea in the eastern sector, and the Ebro R. tributaries in the north-eastern sector.

The drainage network exhibits a general radial pattern (Fig. 1.6) where the main trunks are roughly spaced about 30 km. Most of the streams drain just the flanks of the Iberian Chain, whereas only three rivers reached its interior: Tajo, Turia and Jiloca. Erodibility variations related to tectonic structures and/or rock-types play an important role on the orientation of trunk channels. This influence is apparent by the pattern of the Ebro tributaries: upstream these rivers flow SE–NW following the highly erodible syn-orogenic units in intermontane basins and downstream they change direction, cutting across tectonic structures and less erodible rock-types. Similarly, Tajo R. follows tectonic structures in its upstream portion and the Turia and Jiloca rivers captured intermontane basins.

To quantitatively characterize the hydrography of the study area, we performed a morphometric analysis on 14 rivers that drain the Iberian Chain. We also included 3 rivers draining the eastern Central System for comparing results regarding streams developed in adjacent mountain chains. The analysis was focused on the shape of drainage basins (drainage basin asymmetry, hypsometry) and on stream longitudinal profiles.

1.3.2.2. Basin asymmetry

Regional and local tectonic tilting could be recorded in the shape of drainage basin in plan view if the basin is favorably oriented with respect to the tilting axis. The asymmetry factor (AF) is defined as (Hare and Gardner, 1985; Gardner, et al., 1987; Keller and Pinter, 2002):

$$AF = 100 \cdot \frac{A_r}{A_t} \qquad (2)$$

where A_r is the area of the basin on the downstream right of the main trunk, and A_t is the total area of the drainage basin. AF values close to 50 are typical of symmetric drainage basins, AF values greater than 50 indicate that the channel has shifted towards the downstream left and values less than 50 are indicative of channel shifting towards the downstream right.

According to Perez-Peña et al. (2010), we classified the AF using the index:

$$AF^* = \left| 50 - 100 \cdot \frac{A_r}{A_t} \right| \qquad (3)$$

where AF<5 defines symmetric basins, AF=5–10 gently asymmetric basins, AF=10–15 moderately asymmetric basins, and AF>15 strongly asymmetric basins.

As shown in table 1.1 and in Fig. 1.7, in the Iberian Chain 6 basins are symmetric and 4 are gently asymmetric, equally distributed in the eastern and southern sector of the range. In the north-western sector a moderately to strongly asymmetric pattern can be recognized. The Tajo R., Jalón R. and its tributary Jiloca R. point their shift toward the peripheral areas of the chain, while the Henares R. shows a shifting to the south-east. In the eastern Central System, the results shows an increase of the asymmetry toward SW.

1.3.2.3. Basin hypsometry

The hypsometric curve of a drainage basin represents the relative amount of the basin area below (or above) a given height (Strahler, 1952). As it is related to the degree of dissection of the basin, the hypsometric curve is a suitable indicator for the relative dominance of fluvial incision or hillslope processes in landscape evolution.

The shape of the hypsometric curve is influenced by climate, tectonics and lithology (Hurtrez et al., 1999). The scale dependence of hypsometry on basin area has been

shown in a natural setting and by numerical and experimental modeling of basin evolution (Willgoose and Hancock; 1998; Hurtrez et al., 1999).

The area below the hypsometric curve is called hypsometric integral (HI) and it is used to quantitatively characterize the curve. Its value varies from 0 to 1: convex-up hypsometric curves with high HI values are associated with poorly dissected landscapes where hillslope processes dominate. This shape could be also associated to low relief uplands uplifted by tectonic and not yet reached by regressive fluvial erosion; S-shaped curves (concave upwards at high elevations and concave downwards at low elevations) characterize landscapes where fluvial incision and hillslope processes are in equilibrium; concave-up shape with low values of the HI are typical of deeply dissected landscapes (Weissel et al., 1994; Moglen and Bras, 1995; Willgoose and Hancock, 1998; Hurtrez et al., 1999; Keller and Pinter, 2002; Huang and Niemann, 2006). Uplift rate (Lifton and Chase, 1992) and climate (Masek et al., 1994) have a positive correlation with hypsometry, while lithology appears to influence mostly at local scales (up to 100 km^2, Lifton and Chase, 1992; Walcott and Summerfield, 2008).

We extracted the hypsometric curve and calculated the relative integrals to get possible evidence of spatial variation in the competition between fluvial incision and hillslope processes within the Iberian Chain. In this analysis we included also the three rivers draining the Eastern Central System to compare the study area with an adjacent mountain belt.

For each studied river we extracted the hypsometric integrals and curves from SRTM by the GIS extension CalHypso (Pérez-Peña et al., 2009), available at http://www.iamg.org/CGEditor/index.htm. Since the hypsometric curve does not show the distribution of basin area relative to specific elevation values, we determine the amount of drainage area for elevation class intervals of 50 m and we plot the area of

each height interval. To compare all the analyzed catchments, we normalized the obtained area by the total drainage basin area.

Low values of the HI (0.18-0.28) and concave-up shape of the hypsometric curves characterize the three streams draining the eastern Central System (Fig. 1.7A and D, Table 1.1). Conversely, the hypsometric curves of Iberian Chain rivers show a wider variety of shapes and relative higher integral values (0.38-0.55) (Fig. 1.7A, B, C, D and Table 1.1). The Henares R., flowing at the boundary between the two chains, is characterized by a hypsometric integral (0.28) similar to those of the Central System rivers, and a curve shape intermediate with respect to those of the rivers that drain the two ranges (Fig. 1.7A and D). Regarding the south-western flank of the Iberian Chain, where Tajuña and Alto Tajo rivers flow down to the Madrid Basin, the values of the hypsometric integral (0.48, 0.38 respectively) as well as the curve shapes indicate drainage systems dominated by fluvial incision although almost counterbalanced by hillslope processes (Fig. 1.7A e D).

The HI of the rivers that flow straight to the Mediterranean Sea, are relatively high (0.44-0.55) and the shapes of the hypsometric curves are peculiar (Fig. 1.7B and D). Jucar, Turia and Mijares rivers have asymmetrical S-curves indicating that most part of the basin topography is at high elevation and poorly incised, whereas their steep toe is a possible indicator of a relative lowering of the base level. Cabriel and Magro rivers, tributaries of the Jucar R., have very irregular hypsometric curves characterized by relatively high values of the HI (Fig. 1.7B and D). This irregularity appears mostly to be related to fluvial piracy. Furthermore, the Turia and Magro rivers hypsometric curves show a concave-up trend in their lowest part. Similar hypsometric curves and values of the HI (0.42-0.51) characterize the tributaries of the Ebro R. that drain the northern flank of the Iberian Chain (Fig. 1.7C and D). The curves of the Aguasvivas, Jiloca and Jalon rivers, located to the west, show asymmetric S-shape with steep toes that indicate

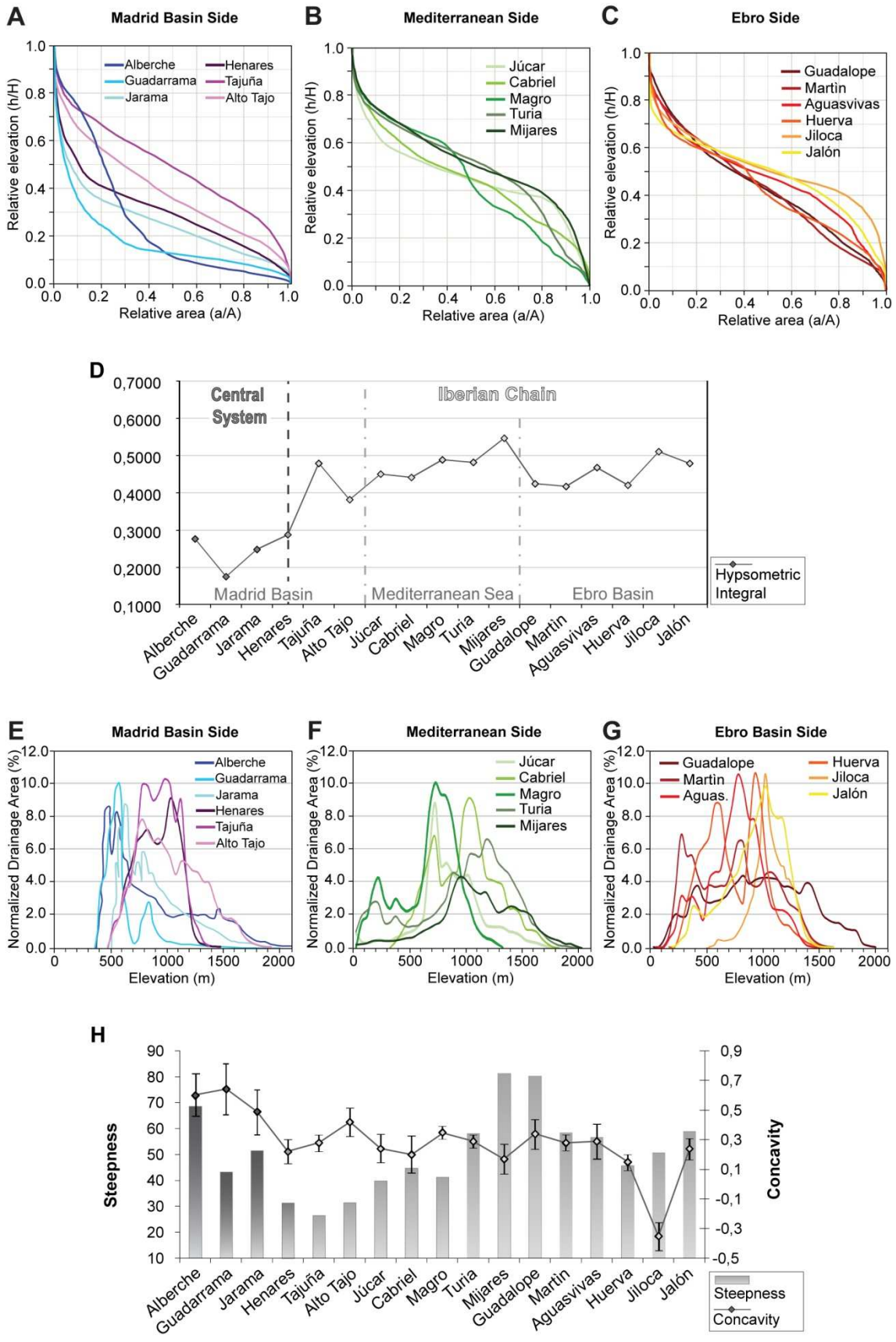
A
Madrid Basin Side
Alberche
Guadarrama
Jarama
Henares
Tajuña
Alto Tajo
Relative elevation (h/H)
Relative area (a/A)
B
Mediterranean Side
Júcar
Cabriel
Magro
Turia
Mijares
C
Ebro Side
Guadalope
Martìn
Aguasvivas
Huerva
Jiloca
Jalón
D
Central System
Iberian Chain
Madrid Basin
Mediterranean Sea
Ebro Basin
Hypsometric Integral
E
Madrid Basin Side
Normalized Drainage Area (%)
Elevation (m)
F
Mediterranean Side
G
Ebro Basin Side
Aguas.
H
Steepness
Concavity

Fig. 1.7. A-C) Hypsometric curves of the studied drainage basins. *H*: maximum elevation within the basin; *h*: elevation; *A*: total surface area of the basin; *a*: area within the basin above a given elevation *h*; D) values of hypsometric integral for the analyzed drainage basins displayed from the SE to the NE following a counterclockwise direction; E-G) Variation of normalized drainage area values of analyzed basins as function of elevation; H) values of concavity and steepness indices of longitudinal profiles of the studied rivers, displayed from the SE to the NE following a counterclockwise direction.

a base level lowering. Guadalope, Martin and Huerva rivers have an almost straight curve with more or less pronounced irregularities, indicating a landscape poorly dissected. Similarly to Turia and Magro rivers, also the Ebro tributaries hypsometric curves show a concave-up trend in the lowest part, progressively less pronounced from SE to NW.

In Fig. 1.7E, that shows the variation of normalized drainage area vs. elevation, the drainage basins belonging to the Central System attain the maximum area distribution at low altitudes (400-600 m a.s.l.). Conversely, in the catchments that drain the Iberian Chain, the elevation where the drainage areas reach their maximum values is generally included between ~800 and ~1200 m a.s.l. and the curves show a roughly bell-shape distribution, with a particular bimodal distribution for the Jiloca and Cabriel R. (Fig. 1.7E, F, and G). This peak area progressively narrows from the southern flank to the eastern and northern ones. Generally, for higher altitudes, the distribution curves abruptly decrease, even thought a more gently decreasing can be recognized in the Alto Tajo, Turia and Mijares rivers. The Guadalope R. represents an exception, because its area distribution does not show distinct high peaks, but a more smoothed curve. However, its highest values range between ~800 and ~1200 m (Fig. 1.7G). Moreover, often the curve of the basins located along the northern and eastern side of the range, shows a distinct peak at low altitude, particularly high along the Ebro side. It mainly corresponds to the drainage area located downstream of the litho-structural boundary

between the Permo-Mesozoic bedrock of the mountain chain and the softer sediments of the bordering basins.

1.3.2.4. Stream longitudinal profiles

Empirical observations carried out in mountain belt under a wide range of geological settings, reveal that river channels in steady state have a smooth, concave shape described by the following power law relationship (Hack, 1957; Flint, 1974):

$$S = k_s A^{-\theta} \quad (4)$$

where S is the local channel gradient, A is the contributing drainage area, k_s is the steepness index, a measure of channel gradient, and θ is the concavity index, a morphometric marker describing the rate of change of channel gradient with drainage area (Hack, 1957; Flint, 1974). Several recent studies (e.g., Snyder et al., 2000; Kirby and Whipple, 2001; Wobus et al., 2006; Kirby et al., 2007) demonstrate the dependence of the steepness index on uplift rate, arguing for a linear scaling relationship between them. Moreover, theoretical considerations (Whipple and Tucker, 1999) consistent with empirical data (Tarboton et al., 1989; Snyder et al., 2000; Kirby and Whipple, 2001; Whipple, 2004; Wobus et al., 2006; Whipple et al., 2007) suggest that under steady-state conditions the θ value is expected to fall in a range between 0.4 and 0.6, normally ~0.45. Deviations from the concave-up shape, called knickpoint or knickzone according to their length, indicate that the river is in a transient state of disequilibrium as a consequence of lithologic, tectonic, climatic, or eustatic perturbations.

We extracted 17 river profiles and calculated the relative indices using “Streamprofiler”, a tool for GIS and MATLAB (available at: http://geomorphtools.org) developed by

Wobus et al. (2006) and Whipple et al. (2007). The indices are calculated directly using a linear regression analysis of channel slope and drainage basin area in a log-log plot: longitudinal profile concavity and steepness represent the slope and y-intercept of the regression line respectively. Since θ and k_s are autocorrelated, we normalized the steepness index by a reference concavity θ_{ref} =0.45 (e.g.: Wobus et al., 2006). This allows an effective comparison of river longitudinal profiles despite the widely varying drainage area.

In addition, to reveal the general variation in steepness index values, we extracted the k_{sn} throughout the Iberian Chain and the surrounding areas (Fig. 1.8).

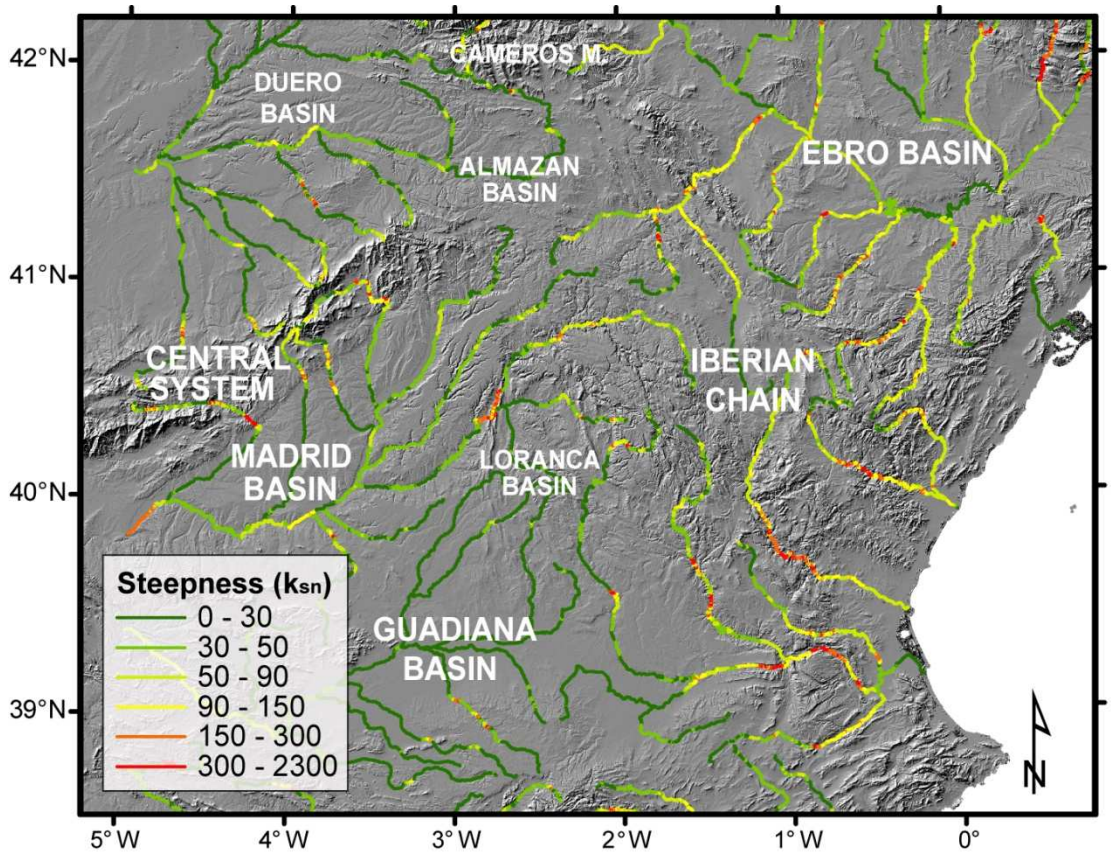

Fig. 1.8. Map of channel steepness indices extracted throughout the Iberian Chain and its surroundings from SRTM DEM using the Stream Profiler tool, available at www.geomorphtools.org, with procedures described in Wobus et al.(2006). Steepness indices are normalized (k_{sn}) to a reference concavity (θ_{ref}) of 0.45 (Wobus et al., 2006).

Table 1.1. Morphometric indexes of the analysed rivers.

River	AF* *(asymmetry factor)*	HI *(hyps. integral)*	θ *(concavity)*	ksn *(steepness)*
Madrid Basin Side				
Alberche*	-	0.27	0.60±0.15	68.6
Guadarrama*	-	0.17	0.67±0.085	43.3
Jarama*	-	0.24	0.49±0.17	51.6
Henares	12.77	0.28	0.22±0.085	31.3
Tajuña	0.22	0.47	0.28±0.063	26.5
Alto Tajo	-11.05	0.38	0.42±0.100	31.4
Mediterranean Side				
Júcar	-1.90	0.4502	0.24±0.098	39.9
Cabriel	5.85	0.44	0.20±0.130	44.8
Magro	-0.08	0.48	0.35±0.047	41.3
Turia	6.31	0.48	0.29±0.057	58.1
Mijares	-2.59	0.54	0.17±0.098	81.4
Ebro Basin Side				
Guadalope	5.86	0.42	0.34±0.096	80.4
Martìn	2.08	0.41	0.28±0.048	58.5
Aguasvivas	-21.06	0.46	0.29±0.13	56.6
Huerva	-1.02	0.42	0.15±0.055	45.7
Jiloca	-5.84	0.51	-0.35±0.28	50.7
Jalón	17.97	0.47	0.24±0.071	58.9

*: Rivers draining the Central System.

In the Iberian Chain, the river profile concavity ranges from 0.15 to 0.42 with the exception of the Jiloca R. that has a negative concavity (-0.35) (Table 1.1, Fig. 1.9). In general the rivers that drain the Iberian Chain are characterized by low or very low values of concavity (average value θ = 0.27), suggesting they are in a transient state of disequilibrium. The concavity of the rivers that drain the Central System is higher (0.49-0.67), indicating that here the hydrography is much closer to the equilibrium state (Figs. 1.7H, 1.9, Table 1.1).

The analysis does not show any clear relationship between θ and k_{sn} (Fig. 1.7H). The values of the normalized steepness index vary from 26.5 to 81.4 (Table 1.1): the lowest values are relative to the rivers flowing through the southern flank of the Iberian Chain.

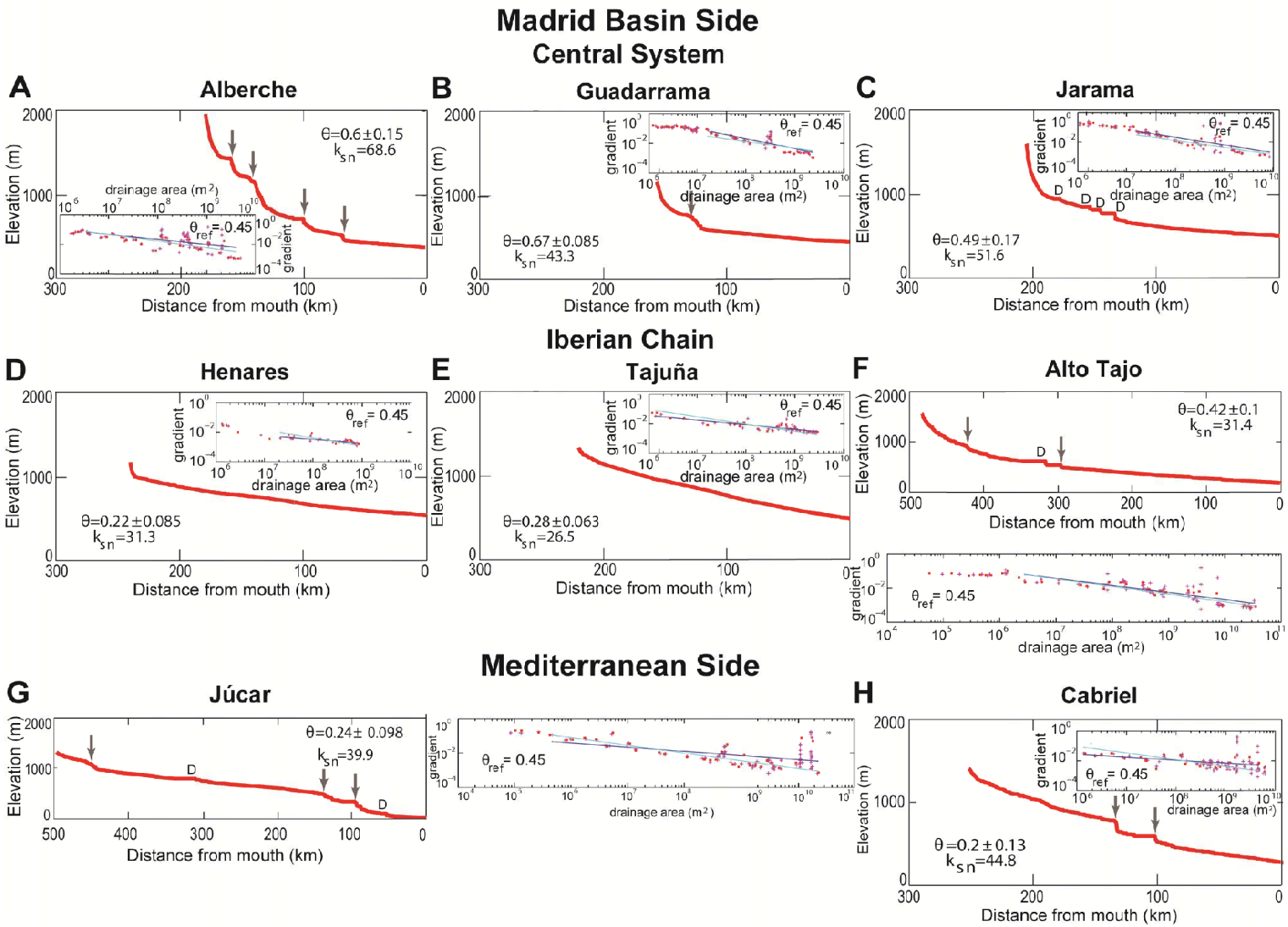
Madrid Basin Side
Central System
A
Alberche
θ=0.6±0.15
k sn=68.6
drainage area (m²)
θ ref = 0.45
gradient
Elevation (m)
Distance from mouth (km)
B
Guadarrama
θ=0.67±0.085
k sn=43.3
C
Jarama
θ=0.49±0.17
k sn=51.6
D
Iberian Chain
Henares
θ=0.22±0.085
k sn=31.3
E
Tajuña
θ=0.28±0.063
k sn=26.5
F
Alto Tajo
θ=0.42±0.1
k sn=31.4
Mediterranean Side
G
Júcar
θ=0.24± 0.098
k sn=39.9
H
Cabriel
θ=0.2 ± 0.13
k sn=44.8

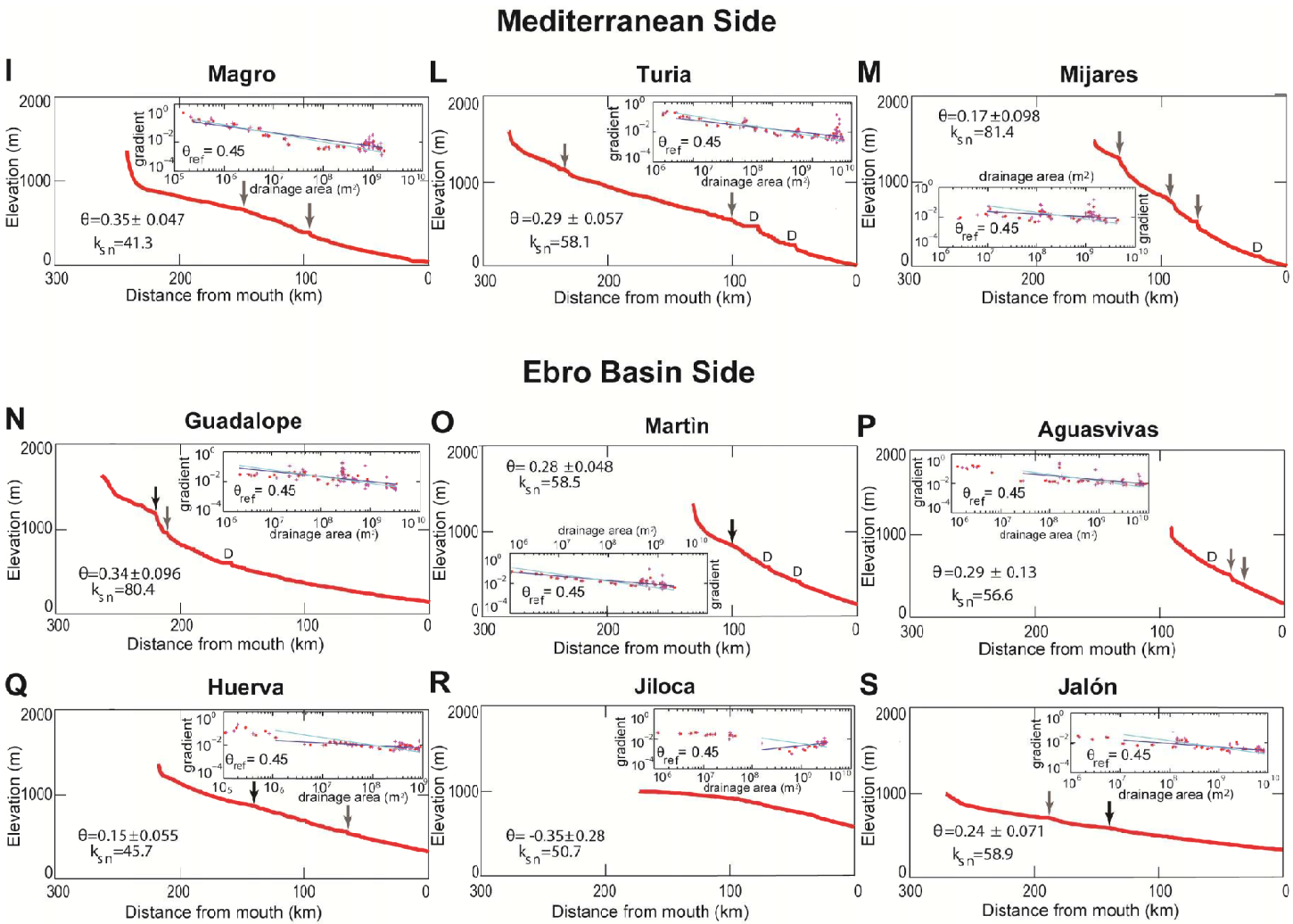
Mediterranean Side
I
Magro
θ=0.35± 0.047
k sn=41.3
L
Turia
θ=0.29 ± 0.057
k sn=58.1
M
Mijares
θ=0.17±0.098
k sn=81.4
Ebro Basin Side
N
Guadalope
θ=0.34±0.096
k sn=80.4
O
Martìn
θ= 0.28 ±0.048
k sn=58.5
P
Aguasvivas
θ=0.29 ± 0.13
k sn=56.6
Q
Huerva
θ=0.15±0.055
k sn=45.7
R
Jiloca
θ= -0.35±0.28
k sn=50.7
S
Jalón
θ=0.24 ± 0.071
k sn=58.9
θ ref = 0.45
gradient
drainage area (m²)
Elevation (m)
Distance from mouth (km)
D

Fig. 1.9. River longitudinal profiles (A-F: Madrid Basin side rivers; G-M: Mediterranean side rivers; N-S: Ebro Basin side rivers): each plot consists of two diagrams: elevation vs. distance (longitudinal profile) and log slope vs. log area. Longitudinal profile plots: grey arrows show the location of main knickpoints related to rock-types changes and tectonic structures, while black arrows show the location of the knickpoints dividing the profiles in two different segments; *D* indicates dams. Log slope vs. log area plots: blue and cyan lines represent regression lines fitting data with the concavity as a free parameter and the reference concavity θ_{ref}=0.45, respectively. Red squares are log-bin averages of the slope-area data.

The highest values are relative to Mijares and Guadalope rivers whose source is located where the chain topography is more elevated (Figs. 1.2, 1.7H, 1.9B). A general increase in normalized steepness index occurs from the SW flank of the Iberian Chain to its NE corner; from here the values decrease to the NW (Fig. 1.7H). The rivers of the Central System have values of k_{sn} higher than the ones of the adjacent Henares, Tajuña and Alto Tajo rivers (Fig. 1.8H).

Fig. 1.8 shows that anomalously high values of steepness index are widely present in the lower segment of channels located in the northern and eastern flank of the Iberian Chain (k_{sn}=50-150, excepting knickpoints and knickzones), whereas low gradient reaches (k_{sn}=0-50) characterize the plateau-like interior. In contrast, the southern flank is characterized by lower normalized gradients for most of the channels length (k_{sn}=30-50), except for discrete knickpoints and part of the upper portion of the Tajo R. (k_{sn}=50-150). The rivers draining the eastern sector of the Central System have low-gradient reaches (k_{sn}=0-50) downstream, but high steepness indices (k_{sn}=50-150) upstream. Guadiana, Loranca, Duero, Almazan basins and Pyrenean side of Ebro Basin show a similar general pattern characterized by low-gradient profiles.

The longitudinal profiles of the rivers draining the eastern sector of the Central System are characterized by concave–up shape, with knickzones related to the presence of less erodible granites (Fig. 1.9A).

Among the streams that drain the south-eastern flank of the Iberian Chain and flow down to the Madrid basin (fig. 1. 9 D-F), Henares and Tajuña rivers profiles exhibit a rectilinear shape, while the Alto Tajo R. reveals a concave–up shape interrupted by some knickpoints mainly related to rock-type changes. All the rivers that flow to the Mediterranean Sea show almost rectilinear profiles. Júcar and Magro R. present an uneven shape, with a change in slope at ~630 m a.s.l. that defines an upstream low gradient segment (θ~0.48, k_{sn}~28 for θ_{ref} = 0.45), related to the low-relief surfaces of the eastern part of the Iberian Chain (Fig. 1.9A).

The two upstream knickpoints, above 1000 a.s.l., of Turia and Mijares rivers define the segments where they flow along the Teruel basin and the Mijares Graben, respectively. The downstream segments exhibit several knickpoints, some of which located in correspondence with lithologic changes.

Among the tributaries of Ebro R. (Fig. 1.9B), variations in channel slope can be recognized in most of river profiles and in general a knickpoint divides the profiles into two segments: a short concave reach upstream and a straight one downstream. Upper segments have low k_{sn} values (20.9-53.2) and θ~0.40. Downstream segments show higher k_{sn} values (0.7-0.95), whereas the θ index measurements are affected by a too high error to be taken into account. These knickpoints correspond with the abrupt change of valley orientation at the contact between rocks with a different susceptibility to erosion. In map view, all these knickpoints are located along a NW-SE oriented line. They are more pronounced and at an elevation progressively higher from NW to SE. Here the Guadalope R. profile presents this major knickpoints at a much higher elevation. An exception is the Jiloca R. that is the only case of clearly convex profile without knickpoints: the wide knickzone corresponds to the intermontane basin of Catalayud and Jiloca.

Moreover, litho-structural knickpoints are located at the boundary between the Permo-Mesozoic bedrock and the more erodible sediments of the basins bordering the range. These knickpoints are just upstream the elevation where the values of drainage areas analyzed in Fig. 1.8G show a distinct peak. Presently, most of these knickpoints are now used for dams (Fig. 1.9).

1.4. Geochronology: U/Th dating of calcareous tufa terraces and incision rates

To provide a geochronological framework for Iberian Chain river systems and to calculated incision rates we dated calcareous tufas resting on top of fluvial strath terraces by U/Th Serie method. We always chose to consider just strath terraces because the shaping of the strath surface and the deposition of the overlying thin fluvial deposits could be considered simultaneous (maximum time span 10^2-10^3 years) (Pazzaglia et al., 1998). The overlying calcareous tufas that are usually just few meters thick, should have deposited in few thousands of years, considering that deposition rates are around 1 or few mm/yr (Ordoñez et al., 2005; Vázquez-Urbez et al., 2010). So, we calculated fluvial incision rates taking into consideration the strath surface that is a common, evident feature for most of the sampled terraces and that is just few thousand years younger than the dated tufas. This time lag is partially included into the error of the dating method and allows us to provide conservative estimation of incision rate.

According to the most recent classifications (Ford and Pedley, 1996; Glover and Robertson, 2003; Pedley et al., 2003; Pedley, 2009), we used the term “calcareous tufa” referring to carbonates deposited under cool or ambient temperature water conditions, in climate controlled fluvial/palustrine systems. Several studies highlight how local and global climate conditions regulate tufa deposition. In particular, the maximum tufa

development in Europe occurred during Quaternary interglacial and interstadial periods in non-arid and temperate climates (e.g.: Henning et al., 1983; Baker et al., 1993; Dramis et al., 1999; Horvatinčić et al., 2000).

1.4.1. Sampling and method

Calcareous tufas have been dated by the uranium-series disequilibrium method (Ivanovich and Harmon, 1992), using alpha spectrometry. This method is based on the measurement of authigenic ^{230}Th, developed from radioactive decay of ^{234}U. Calcareous tufas are mixture of calcium carbonate and detrital minerals, in which the radionuclides are present both in the authigenic and detrital fractions. Only the authigenic fraction enables to estimate the age of the carbonates. Four sub-samples from each outcrop were collected at the same stratigraphic level within a distance of 1 m in order to obtain coeval samples with different proportions of homogeneous detrital and authigenic carbonate. Samples were obtained from compact, micritic layers.

About 30 g of sample were dissolved in 1N HNO_3 and filtered to separate the leachates from the insoluble residue. The leachate was heated at 100°C after adding few millilitres of hydrogen peroxide in order to destroy the organic matter. The residue was dissolved in HF+HClO4, dried and redissolved in 1N HNO_3. Both fractions were then combined and spiked with a ^{228}Th/^{232}U tracer. Chemical separation and extraction of the isotopic complexes of uranium and thorium were performed using chromatography columns containing organic resin, eluated with HNO_3 and HCl. The ages of tufas were calculated following the technique outlined for impure carbonates in (Bischoff and Fitzpatrick, 1991), the so-called total-sample dissolution (TSD) procedure. This method was chosen over using leachates alone (Schwarcz and Latham, 1989) because the leaching method gives reliable results only in the case of selective dissolution of the

carbonate fraction, without any removal of U and Th isotopes from the detrital component, or when U and Th are leached without any fractionation. Generally, this condition is not verified because U and Th are often fractionated and Th can be reabsorbed into the residual component. When analysing samples consisting of simple mixtures of carbonate and a detrital component, the use of the TSD method is preferred to determine the age because the sample is totally dissolved and consequently no preferential leaching or re-adsorption can occur. The presence of detrital fraction was marked by ^{232}Th deriving from the surrounding environment. Corrections required in presence of non-radiogenic ^{230}Th were performed for samples with $^{230}Th/^{232}Th$ activity ratio less than or equal to 50. We measured the $^{230}Th/^{232}Th$, $^{234}U/^{232}Th$, and $^{238}U/^{232}Th$ activity ratios of four coeval sub-samples in order to obtain the value of the $^{230}Th/^{234}U$ and $^{234}U/^{238}U$ activity ratios in the pure carbonate fraction. These values were respectively calculated from the slopes of the regression lines in the $^{230}Th/^{232}Th$ vs $^{234}U/^{232}Th$ and $^{234}U/^{232}Th$ vs $^{238}U/^{232}Th$ isochron plots. The ages were calculated using ISOPLOT, a plotting and regression program for radiogenic-isotope data (Ludwig, 2003). The goodness of data points fitting was quantified through the statistical index Mean Square Weighted Deviation (MSWD). Errors were expressed as $\pm 1\sigma$. The age of calcareous tufas free from non-radiogenic ^{230}Th (samples PSP 3-1, RUG 4, MON 3, RP 1, table 1.2) were obtained using the $^{230}Th/^{234}U$ and $^{234}U/^{238}U$ activity ratios of a single sample.

The regression line of sample RUG3 (table 1.2) was not statistically significant, probably because the detrital fraction of the tufa was inhomogeneous. The age were consequently corrected assuming that all the detrital thorium had an average upper crustal $^{230}Th/^{232}Th$ activity ratio of 0.85 ± 0.36 (Wedepohl, 1995).

1.4.2. Results

The radiometric dating was performed on seven samples collected from tufa units located in four different sites (fig 1.10B). In the southern flank of the Iberian Chain three samples were collected from three different terraces of Alto Tajo R. (PSP 3-1, 7-2, 12-1), and two samples were gathered from tufa deposits along the Ruguilla R. (RUG 3, 4). Two samples were collected along the upper channel segment of Martín R. (MON 3, RP 1), a tributary of the Ebro R. The radiometric dating results from all investigated samples are displayed in Table 1.2

1.4.2.1. Ruguilla (Ruguilla River)

The Ruguilla R. is a small drainage characterized by several remnants of a tufa terrace close to the confluence with the Tajo R. The calcareous tufa buildup consists of a platform located near the Ruguilla village. The platform is gently dipping (2°-3°) toward SW and overlies a 1 m-thick fining upward alluvial deposit. This deposit unconformably rests on the substrate, mainly consisting of sands and polygenic conglomerates related to a syn-orogenic basin (Depresión Intermedia). The strath surface is ~60 m above current thalweg, whereas the platform is approximately 10 m thick. The calcareous tufas consist of massive and grossly stratified phyto (leaf moulds and vegetal frustules) - microhermal texture and reddish sands grading upward to thinly laminated silts and sub-horizontally layered micritic tufas, concordant with the top surface. These features suggest a paludal sedimentary environment. The calculated age of these tufa deposits is 89±6 kyr (MIS 5b, fig. 1.10A).

It was obtained from the uncontamined sample RUG 4, and later verified with the sample RUG 3, collected at the base of the buildup. Consequently, the estimated incision rate is 0.69±0.04 mm/yr (fig. 1.10B). Our results differ from previous datings

Table 1.2. Isotope data and ages for calcareous tufa sub-samples of Iberian Chain

Sample	Sub-sample	U (ppm)	$^{230}Th/^{232}Th$	$^{234}U/^{238}U$	$^{230}Th/^{234}U$	$^{234}U/^{232}Th$	$^{238}U/^{232}Th$	$^{230}Th/^{234}U_c$	$^{234}U/^{238}U$	Age (kyr)
RUG 3	RUG 3b	0.129 ± 0.004	1.569 ± 0.052	1.169 ± 0.040	0.711 ± 0.030	2.210 ± 0.101	1.891 ± 0.087	0.595 ± 0.043*	-	96 ± 11
RUG 4	RUG 4a	0.141 ± 0.005	138.773 ± 22.313	1.167 ± 0.041	0.567 ± 0.026	-	-	-	-	89 ± 6
PSP 3-1	PSP 3-1d	0.095 ± 0.003	143.322 ± 42.751	1.079 ± 0.038	0.624 ± 0.027	-	-	-	-	105 ± 8
PSP 7-2	PSP 7-2a	0.090 ± 0.003	1.340 ± 0.208	1.323 ± 0.055	0.132 ± 0.010	17.631 ± 1.397	13.318 ± 1.063	0.0449 ± 0.00	1.435 ± 0.023	5 ± 0.8
	PSP 7-2b	0.103 ± 0.004	2.639 ± 0.335	1.395 ± 0.055	0.047 ± 0.004	55.016 ± 6.174	39.411 ± 4.430			
	PSP 7-2d	0.086 ± 0.003	4.174 ± 0.619	1.426 ± 0.056	0.059 ± 0.006	70.543 ± 9.612	49.472 ± 5.545			
	PSP 7-2e	0.087 ± 0.003	24.646 ± 6.802	1.366 ± 0.052	0.050 ± 0.004	492.195 ± 133.784	360.260 ± 97.456			
PSP 12-1	PSP 12-1a	0.071 ± 0.003	4.233 ± 0.608	1.325 ± 0.075	0.089 ± 0.009	47.283 ± 6.525	35.697 ± 4.955	0.023 ± 0.003	1.413 ± 0.129	2.54 ± 0.33
	PSP 12-1b	0.074 ± 0.002	3.618 ± 0.501	1.495 ± 0.058	0.144 ± 0.014	25.067 ± 3.166	17.099 ± 2.169			
	PSP 12-1c	0.076 ± 0.004	3.654 ± 0.260	1.450 ± 0.081	0.067 ± 0.007	31.003 ± 3.365	21.378 ± 2.348			
	PSP 12-1e	0.070 ± 0.002	4.828 ± 0.688	1.431 ± 0.054	0.054 ± 0.005	82.277 ± 11.744	54.481 ± 8.231			
MON 3	MON 3b	0.296 ± 0.012	80.632 ± 13.780	1.331 ± 0.034	0.315 ± 0.017	-	-	-	-	41 ± 2
RP 1	RP 1b	0.200 ± 0.010	92.480 ± 21.498	1.264 ± 0.040	0.581 ± 0.031	-	-	-	-	91 ± 7

Errors are quoted as 1σ. (230Th/234U)c and (234U/238U)c are referenced to the pure carbonate fraction used in the calculation of the age.
*Age has been corrected for initial (230Th/232Th) activity ratio of 0.85 ± 0.36 (upper crust value, Wedepohl, 1995).

obtained by aminoacid racemization method on ostracod caparaces (sample RR1.1, Ortiz et al., 2009) and by U/Th method (sample M-3, Ordóñez et al., 1990), that provide ages of 301±61 kyr and >350 kyr, respectively. In our opinion, the latter result could be considered uncertain because of the significant detrital contamination of the sample ($^{230}Th/^{232}Th$ is lower than 50 and $^{230}Th/^{234}U$ is much higher than 1.

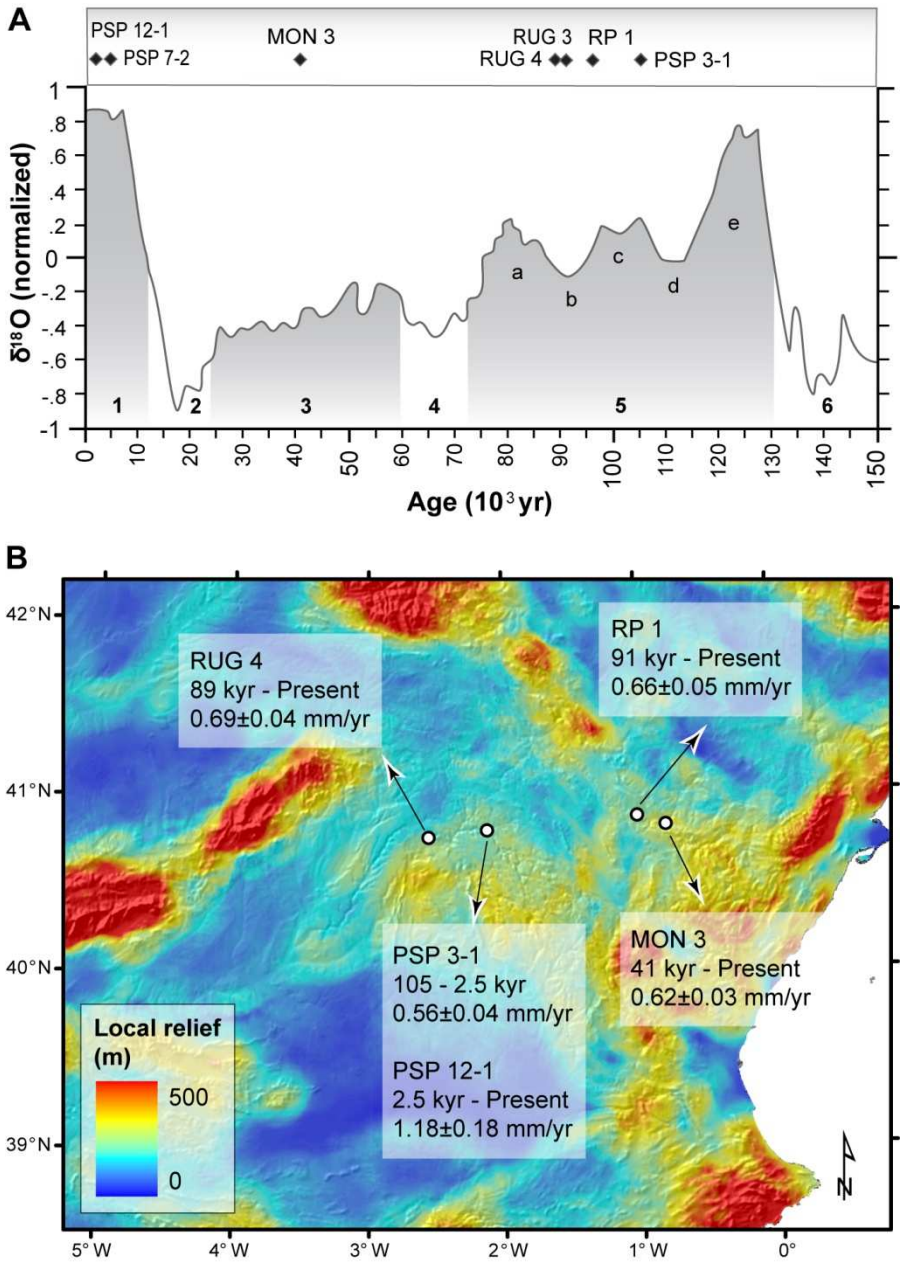

Fig. 1.10. A) radiometric ages of strath terraces in Alto Tajo and Martin R. valleys compared with the standard marine oxygen-isotope curve by Martinson et al. (1987); B) local relief map of Iberian Chain showing the location of the analyzed fresh tufa samples (white circles) and the estimated incision rates for each site.

1.4.2.2. Puente de San Pedro (Alto Tajo River)

The calcareous tufa outcrops of Puente de San Pedro are located along the upper course of the Tajo R. Here the river incised a ~350 m deep valley into the upland surface and the underlying Jurassic and Cretaceous limestones and dolostones. The tufa deposits are located close to the confluence with the Gallo R., where the Tajo R. valley locally widens. At Puente de San Pedro the tufas overlie the fluvial deposits of four orders of terraces.

The base of the ~35 m-thick tufas of the I order terrace is located at ~60 m above the present river thalweg. It buries 2 m thick fluvial terrace deposits that unconformably overlay the bedrock. The strath surface is 58 m above the Tajo channel. Tufas mainly consists of clinostratified microhermal deposits associated with grain supported phytoclats (gentle to steep slope facies) and sub-vertical structures with microhermal and phytohermal textures (rapid and cascade facies). U/Th dating, obtained from the sample PSP 3-1, provides an age of 105±8 kyr (MIS 5c, fig. 1.10A). This value shows a good correspondence with the radiometric (U/Th) age previously obtained by López Vera and Martínez Goytre (1989).

The II order terrace shows a wide flat top surface located at 50-60 m above the current thalweg position, while the bottom surface is not exposed.

The terrace is mainly composed of reddish fluvial deposits: horizontal- and cross-bedded. The terrace is mainly composed of reddish fluvial deposits: horizontal- and cross-bedded siliciclastic and carbonate silty sands with lenticular interbeds of gravels. Sub-horizontal and massive fine sand deposits associated with organic-rich silt layers and malacofauna (shallow lacustrine/paludal facies) dominate the upper part of the terrace deposit. Locally, the detrital sediments are replaced by lenticular bodies and

drapes of concretionary calcareous tufa characterized by weathered highly porous, detrital facies that are not suitable for U/Th dating method.

The top surface of III order terrace is at 25-30 m above current riverbed. Gentle slope phytoclast facies characterize the terrace. The outer part of the calcareous body is often covered by vertical hanging festoons and drapes of crystalline cascade lithofacies. Radiometric dating on these laminated layers (sample PSP 7-2, fig. 1.11A) provides an age of 5±0.8 kyr (MIS 1, fig. 1.10A). Since the strath surface does not outcrop, this result was not suitable for incision rate calculation.

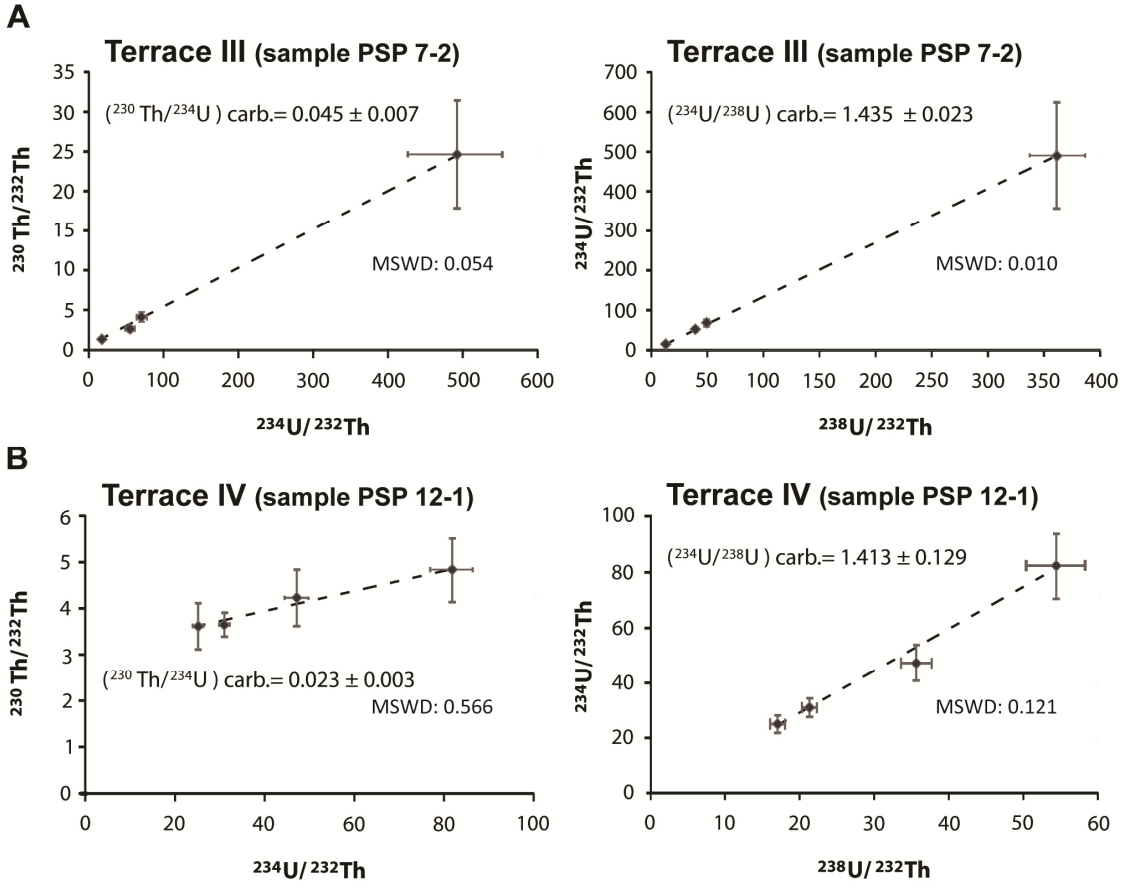

Fig. 1.11. 2-dimensional isochron plots, with 1σ error crosses, of four coeval sub-samples from (A) terrace III (sample 7-2) and (B) terrace IV (sample 12-1), Puente de San Pedro site. The slopes in the ($^{234}U/^{232}Th$) vs ($^{238}U/^{232}Th$) and ($^{230}Th/^{232}Th$) vs ($^{234}U/^{232}Th$) diagrams represent, respectively, the ($^{234}U/^{238}U$) and ($^{230}Th/^{234}U$) activity ratios of the pure carbonate fraction. MSWD: mean square weighted deviation.

The IV order terrace has the strath surface at 10 m above the present channel, and unconformably overlies the bedrock with colluvial and fluvial deposits. Highly porous and friable sub-horizontal tufa facies rich in phytoclast and associated with sandy and gravel bodies (fluvial environment) dominate the terrace lithology. The age calculated from the sample PSP 12-1 (fig. 1.11B), is 2.54±0.33 kyr (MIS 1, fig. 1.10A).

The radiometric analysis provides the following incision rates: 0.56±0.04 mm/yr for the time interval 105 - 2.54 kyr, and 1.18±0.18 for the last 2.54 kyr (fig. 1.10B).

1.4.2.3. Montalbán (Martín River)

Tufa deposits outcrop near the city of Montalbán along the Martín R. valley, ~2 km upstream of the major knickpoint that divides the longitudinal profile in two main segments (fig 9O). The river flows on the soft continental deposits of the intermontane syn-orogenic Montalbán Basin. The valley shows a 300-500 m wide flat floor and few orders of terraces. The analyzed outcrop is a remnant of a horizontal tabular-shaped deposit. Its base is located at 25 m above the present thalweg and overlies a 3 dm-thick alluvial conglomerate unconformably lying on the substrate. The stratigraphic sequence is ~5 m thick and can be referred to paludal environment located in marginal zones of a floodplain. The tufa is characterized by phytoclastic sands, massive and stratified lime mud and marls associated with organic-rich silt layers and gastropods. The outcrop shows on top a polygenic breccia. Sample MON 3 revealed an age 41±2 kyr (MIS 3, fig. 1.10A), that allows the calculation of an incision rate of 0.62±0.03 mm/yr (fig. 1.10B) with respect to the elevation of the strath surface.

1.4.2.4. Las Parras de Martín (Martín River)

The tufa outcrop is situated close to the village Las Parras de Martín, along the valley of one of the uppermost tributary of the Martín River, ~4 km upstream of their confluence. The narrow V-shaped valley cuts across the Utrillas thrust and the Mesozoic rock units. The strath surface of the terrace is located at 60 m above the present riverbed. The tufas are built up over thin colluvial and alluvial deposits. The 10 m thick tufa sequence mainly consists of clinostratified structures composed primarily of highly porous bryophyte facies. Horizontally stratified sands intercalated with pebbles lens record limited deposition events. The age of this terrace (sample RP1) is 91±7 kyr (MIS 5b, fig. 1.10A), the relative incision rate is 0.66±0.05 mm/yr (fig. 1.10B).

1.5. Discussion

We studied the landscape evolution of the Iberian Chain by a morphometric analysis of the massif and the surrounding area, focusing on topographic and hydrographic features. We coupled morphometry with field survey and calcareous tufa datings to obtain geological and time constraints in the reconstruction of landscape evolution. Our results describe a poorly incised topography characterized by upland low relief surfaces, indicating this landscape is in a transient state in response to a dominant regional tectonic input: a long wavelength uplift. Indeed, the more representative values of slope and local relief for the entire chain are 1.27° and 84.44 m respectively (Fig. 1.5). In particular, the swath profiles (Fig. 1.6) show that the local relief has a mostly uniform pattern throughout the chain that suggests the river network is incising equally the Iberian Chain in response to the dominant regional uplift. Moreover, in general there is no significant local relief variations across the intermontane basins (Fig. 1.4), indicating

that these depressions could constitute pre-existing topographic features with respect to the regional uplift. Moreover, despite the high altitude, the central sector of the range records the lowest local relief values, showing more similarity with the surrounding Madrid and Duero basins than with all the other mountain belts of the Iberian Peninsula (Figs. 3, 4). The longitudinal profiles of rivers draining the Iberian Chain are characterized by low values of concavity (average value: 0.27), indicating that the basins are in a transient state of disequilibrium. All these results evidence how the Iberian Chain constitutes a well defined physiographic unity in the whole Iberian Peninsula where river incision is poor and the relative parameters are almost constant.

The relationship between elevation and modal values of both slope and local relief (Fig. 1.5) allows us to recognize two domains characterized by different topographic features. From ~100 to 1400 m a.s.l. slope and local relief slightly increase, defining a landscape with almost constant metrics. Within this elevation interval, the analysis of swath profiles (Fig. 1.4) allows to distinguish between two sub-domains: the flanks of the chain and a flat surface above ~700 a.s.l., that correspond with a poorly dissected surface drained by low gradient channels (Fig. 1.9), interpreted as a relict landscape, (Figs. 1.3 and 1.4).

From ~1500 to ~2000 m a.s.l., slope and local relief abruptly increase with elevation (Fig. 1.5), defining essentially the topographic roughness of remnants of ranges rising from the upland flat surface. Above ~1700 m, the local relief records again a homogeneously dissected landscape, that corresponds with an older flat surface now preserved just locally in the interior of the range (Fig. 1.4C and D).

Most of the stream longitudinal profiles of the Ebro R. tributaries show a knickpoint related to the capture of intermontane basins, part of the relic landscape located in the inner sector of the chain. Upstream of this knickpoint, channels are characterized by concave profiles (θ~0.40) and low steepness indices (k_{sn}<50 for θ ref = 0.45, Fig. 1.8).

These features suggest that the reaches are in an equilibrium state with respect to base-level conditions different from the present ones. The upland low relief surfaces together with the remnants of ranges (1500-2000 m) are part of an old landscape that developed in stable base-level conditions with which the upstream reaches were in equilibrium. Similar features are present in all of the flanks of the chain (Fig. 1.7 E, F, G): the basin drainage areas reach their maximum values in the elevation interval comprised between 700 and 1200 m a.s.l. This evidence, together with the S-shaped hypsometric curves of many of the analyzed catchments, suggests that the basins are more developed where they reflect the river network of the old landscape. All these considerations confirm that the headward erosion of the currently exorheic drainage does not reach the interior of the chain, preserving the old landscape and its relative river network. This erosional wave induced by the regional uplift and the change from endorheic to exorheic drainage is still confined along the flanks of the range. Indeed, here channels are characterized by rectilinear profiles and high steepness, suggesting the rivers are far from equilibrium. The landscape of the Iberian Chain flanks is poorly dissected as marked by low values of slope and local relief (Figs. 3, 4, and 5) and by peculiar hypsometric curves (Fig. 1.7). However, Fig. 1.8 shows that the steepness indices along the northern and eastern sides of the chain are in general higher with respect not only to the southern side, but also to the areas surrounding the Iberian Chain. This suggests that a stronger and/or more recent tectonic activity possibly affects the north-eastern sector of Iberian Chain, generating a differential uplift.

At more local scale, the present-day drainage pattern partly reflects the distribution of erodibilities in consequence of rock-type changes and local tectonics. In some cases rivers follow faults bounded by highly deformed rock (e.g.: Tajo R. in the Castilian Branch fault zone) or flow across highly erodible rocks (e.g.: soft facies of the

intermontane basins drained by the Ebro R. tributaries and Turia R. or Paleozoic shaly units interbedded within more competent rocks).

The values of AF* (asymmetry factor) calculated for the drainage basins of the Iberian Chain and the almost radial pattern of the main trunks suggest a differential uplift, roughly maximum at the center of the chain, but gradually decreasing towards the low-standing basins bordering the range (Fig. 1.1). This generated a tilting of the Iberian Chain flanks, so that the channels oriented transverse to the tilting shift toward the peripheral areas (for example, Tajo, Jalón, and Jiloca rivers), and those slightly transversal (Cabriel, Turia, and Guadalope rivers) tend to rotate towards an orientation parallel to the maximum slope of the chain flanks, similarly to the symmetric basins pattern (Tajuña, Júcar, Magro, Mijares, Martìn, Huerva R.). The Central System, topographically higher than the Iberian Chain, seems to control the direction of migration of the Henares R. trunk, located in between the two ranges (Fig. 1.1). These considerations suggest that, apart the local variation in erodibility and possible differential uplift, the main factor driving the evolution of the drainage network is the regional uplift.

Along the Mediterranean flank of the Iberian Chain, homogeneous substrate properties and no spatial climatic variations allow to use k_{sn} as indicator of differential uplift (Fig. 1.7H). From SW to NE, the steepness progressively increases reaching the highest value (also with respect to all the analyzed rivers) of the Mijares R. A similar value is also relative to the Guadalope R., an Ebro R. tributary draining the same sector of the chain (Fig. 1.6). The HI values have a trend similar to the steepness index (Fig. 1.7D). The Mijares R. basin records the highest value, much higher than 0.5, indicating an active tectonic area (Keller and Pinter, 2002). This is confirmed by the relative low value of concavity of the Mijares R. profile and by the not particularly resistant bedrock. So, these anomalies delineate a localized area in the NE sector of the Iberian Chain

characterized by the highest elevation of the range and by parameters that speak to a landscape in stronger disequilibrium. Those can be signals of a differential higher rock uplift. In particular, this area presents remnants of planation surfaces even at high altitude (~2020 m a.s.l.) and is affected by extensional faults related to the opening of the Valencia Through.

In the Iberian Chain (e.g.: (Martínez-Tudela et al., 1986; Peña et al., 1984; Ordoñez et al., 2005; Domínguez-Villar et al., 2011) as well as in the rest of Europe (e.g.: Henning et al., 1983), the Quaternary climate variation (interglacial and interstadial stages) favoured intense calcareous tufa deposition. In agreement to these previous studies, our radiometric datings of fresh calcareous tufa indicate ages corresponding to MIS 1, 3, 5 (Table 1.2, Fig. 1.10A). Moreover, the datings of calcareous tufas located on top of strath fluvial terraces provide a good approach for estimating incision rates because these deposits accumulate rapidly (Andrews, 2006), and consequently the shaping of the strath surface and the deposition of the overlying deposits could be considered simultaneous. The obtained ages yield average incision rates of 0.6 mm/yr for Late Pleistocene, but the values increase to 1.2 mm/yr for Holocene time. Although we sampled calcareous tufas in basins draining both southern and northern flanks of the range, the value of 0.6 mm/yr is homogeneous throughout the central sector of the chain. This evidence confirms that, at least in the chain interior, rivers incise mainly in response to a dominant regional input rather than to local ones such as: i) the drastic base level fall due to the diachronous capture of the *endorheic* basins, that occurred during Late Pliocene-Late Pleistocene (Gutiérrez et al., 2008); ii) the lithology of river-bed basement, both poorly consolidated sediments (Martín and Ruguilla rivers) and stronger limestone (Tajo R.). Therefore, we interpreted the homogeneous erosion rates of central Iberian Chain as related to regional rock uplift.

In the Alto Tajo R., at Puente de San Pedro, the incision rate calculated from the age (2.54±0.33 kyr, MIS 1) of the Holocene terrace, is much higher (1.18±0.18 mm/yr) than the Late Pleistocene rates. This increase has been recognized in the nearby areas by dating similar tufa deposits by ostracode shell amino acid racemization (Torres et al., 2005; Ortiz et al., 2009). This phenomenon, reported also in many river systems all over the world, is interpreted as the fluvial response to the declining sediment input since the Last Glacial Maximum (Hancock and Anderson, 2002; Pederson et al., 2006),

We compared the geomorphic indices of rivers (all Tajo R. tributaries) that drain the southern Iberian Chain and the eastern flank of the Central System, an area climatically homogeneous. The shape of both longitudinal stream profiles and hypsometry curves indicate a progressive change from W to E from a landscape in almost steady state to a transient landscape. Indeed, the catchments draining the Central System have concave–up longitudinal profiles with θ ranging between 0.49 and 0.67, suggesting steady-state conditions (e.g.: Whipple and Tucker, 1999, Snyder et al., 2000). Moreover they have concave hypsometric curves characterized by low values of HI (0.18 and 0.28). The concave-up shape of the hypsometric curves points to a deeply dissected landscapes where a long-term equilibrium between uplift and erosion rates has been achieved (e.g.: Strahler, 1952). The Henares R. show intermediate characters with respect to both ranges. The comparison of morphometry data shows that the landscape of the Central System in close to steady state, whereas the one of the Iberian Chain is transient. So, the Central System could have a much longer uplift history during which erosion succeeded in counterbalancing uplift. Apatite fission tracks analysis evidence a rapid cooling phase of the Central System from the Early Pliocene (5 Ma) to Recent (De Bruijne and Andriessen, 2002; Ter Voorde et al., 2004). On the basis of these considerations, we hypothesize the Iberian Chain has a recent uplift history, younger than 5 Ma. An important geologic constraint to understand the uplift of the Iberian chain is the Paramo

fm. and its geometry. This carbonatic unit, Late Miocene-Early Pliocene in age, is the last lacustrine record before exorheism stage. The Paramo fm. reaches the maximum elevation of ~1200-1300 m in the Iberian Chain, with shallow dips of few degrees towards the low-standing basins where it becomes horizontal, as preserved in the area of Madrid Basin (Fig. 1.2). The envelope given by the attitude of Paramo fm. forms a ~300 km wide gentle asymmetric dome whose northern flank is steeper than the southern one (Fig. 1.2). The maximum uplift of the dome is ~600 m.

1.5.1. Tectonic implication

The morphometry data coupled with field investigation and calcareous tufa datings describes the landscape of the Iberian Chain as a poorly incised high-standing plain, probably Miocene-Early Pliocene in age. This morphology is a relic of an old landscape characterized by low values of local relief, surrounded by huge endorheic lakes. During or just after the Early Pliocene, the uplift of the Iberian Chain started reaching a maximum uplift of ~600 m. This provides a minimum uplift rate of ~0.2 mm/yr, that possibly increases up to ~0.6 mm/yr in the Late Pleistocene. Roughly at the same time the change from endorheism to exorheism occurred, so that rivers should respond to a tectonic input, the uplift, and variation in base level related to a change from lake to sea. Anyway this last contribution should not be that strong since so big endorheic lakes could not continue to exist for several million of years at an elevation far from sea level.

As for the origin of the uplift, few hypotheses can be proposed (Casas-Sainz and De Vicente, 2009). The uplift of the Iberian chain post-date the compressional episodes, which vanished in the Middle Miocene. Hence, the uplift of the belt cannot be related to crustal thickening. In addition, the small amount of erosion and the immature river network do not support the hypothesis of an isostatic uplift related to unloading due to

erosion. Therefore, we can reasonably rule out that the uplift is related to crustal isostasic adjustment.

Two alternative hypotheses can be suggested. One possibility is that the Iberian Chain underwent uplift under compression producing large scale folding (Cloetingh et al., 2002; De Vicente et al., 2007). This is indeed quite possible also considering the possible prosecution of the Iberian chain to the west in the Central System. In this case, we should then consider that the lithospheric large scale folding post-dated the compressional episode. The other possibility is that the large and smooth morphology of the uplifted dome and the relatively low uplift rate is instead due to deeper causes related to mantle dynamics. In this case, the uplift could result from the progressive erosion of the lithosphere mantle due, for example, to conduction of a mantle thermal anomaly. The other solution is that the support is more related to an upwelling process of the uppermost mantle. Tomography images and dynamic topography model indeed indicate a slow velocity anomaly beneath central western Iberia (Wortel and Spakman, 2000; Piromallo and Morelli, 2003; Li et al., 2008; Schmid et al., 2008; Boschi et al., 2009; 2010; Faccenna et al., 2010). This anomaly could have produced a positive dynamic topography of few hundreds of meters, as predicted by dynamic topography model (Boschi et al., 2010). In this case, we could imagine that the intraplate recent volcanism of the area, as the Late Miocene–Late Pliocene Calatrava leucitites in central Spain (e.g., Cebriá and Lopez-Ruiz, 1995) and the Quaternary basanites from Olot–Garrotxa in northeast Spain (Cebriá et al., 2000), would be related to that deep process. Similarly the uplift of the Valencia Gulf and of the Costal Chain could have been related to this large scale process. More refined seismological model is needed to support this hypothesis and the result of the more local project could give definitive answer to those questions.

1.6. Conclusions

Topography results from the interaction of crustal tectonics and/or subcrustal processes that move rock masses and surface processes that erode, transport and deposit materials. So, landscape approximates tectonic processes and the study of its features at local and regional scale provides important information to reconstruct the role of tectonics in landscape evolution.

Our morphometry analyses coupled with U-Th datings and field investigation in the Iberian Chain evidence the topographic and hydrographic features that result more sensitive to a main tectonic input, a regional uplift, in an intraplate context. This dominance is only slightly influenced by local geologic and tectonic features. A summary of our results includes the followings:

1) The landscape of the Iberian Chain is characterized by a poorly incised interior constituted by a low relief topography including planation surfaces and remnants of ranges. Just three rivers could integrate into the chain interior, whereas the rest of the hydrography drains its flanks. The lack of Late Pliocene-Quaternary deposits, except for small intermontane basins, suggest that erosion is a dominant process mainly in response to regional uplift. This consideration indicates the beginning of uplift as at least Late Pliocene in age.
2) The morphometric analysis on drainage basins and stream longitudinal profiles describe a landscape in which rivers are still adjusting a dominant tectonic input. The shape of longitudinal profiles, quantitatively measured by concavity and steepness indices, indicate that the rivers are far from equilibrium. The hypsometric curves and the relative HI confirm that the Iberian Chain landscape is poorly incised by hydrography and that preserve an old landscape in its interior. This setting is validated by comparing the

morphometry of the Iberian Chian with the adjacent Central System. This range, that experienced a rapid uplift since 5 Ma, is in steady state.

3) The U-Th dating of calcareous tufas located on top of strath fluvial terraces allows us to calculate a homogeneous incision rate of 0.6 mm/yr for Late Pleistocene. In the Holocene a strong increase in incision (1.2 mm/yr) has been related to the declining sediment input in fluvial systems since the Last Glacial Maximum.

In summary, we conclude that the Iberian Chain is an intraplate orogen that is experiencing a recent dome-like uplift. The rivers are responding to this input incising topography at a rate of 0.6 mm/yr, getting close to a radial pattern. The comparison with the adjacent Central System, that experienced an increase in uplift since the beginning of Pliocene, the age and geometry of the carbonates of the Paramo fm., and the almost complete lack of Late Pliocene-Quaternary sediments in the chain interior allows us to hypothesize the uplift started at or after ~3 Ma.

Acknowledgements

The Authors want to thank Gerardo De Vicente for helpful discussion, Valerio Olivetti and Giovanny Jimenez Diaz for logistic support on the field.

References

Alcalá, L., Alonso-Zarza, A. M., Álvarez Sierra, M. A., Azanza, B., Calvo, J. P., Cañaveras, J. C., van Dam, J.A., Garcés, M., Krijgsman, W., van der Meulen, A.J., Morale, J., Peláez-Campomanes, P., Pérez Gonzalez, A., Sánchez Moral, S., Sancho, R., Sanz Rubio, E., 2000. El registro sediment ario y faunístico de las cuencas de Calatayud-Daroca y Teruel. Evolución paleoambiental y pal eoclimática durante el Neógeno. Revista de la Sociedad Geológica de España, 13, 323–343.

Alonso-Zarza, A., 2008. El Neógeno: de las crisis tectónicas a la tranquilidad de los lagos someros. In: Calonge, A., Rodríguez, M.,Segura M. (Eds.), Geología de Guadalajara, Guadalajara (Spain), 151–165.

Alonso-Zarza, A., Calvo, J., 2000. Palustrine sedimentation in an episodically subsiding basin: the Miocene of the northern Teruel Graben (Spain). Palaeogeography, Palaeoclimatology, Palaeoecology, 160, 1–21.

Álvaro, M., Capote, R., Vegas, R., 1979. Un modelo de evolución geotectónica para la Cadena Celtibérica. Acta Geológica Hispanica, 14, 172-177.

Anadón, P., Moissenet, E., 1996. Neogene basins in the Eastern Iberian Range. In: Friend, P., Dabrio C., Tertiary basins of Spain, the stratigraphic record of crustal kinematics. Cambridge University Press, Cambridge (UK),. 68-76.

Anadón, P., Moissenet, P., Simón, J., 1990. The Neogene Grabens of the Eastern Iberian Chain (Eastern Spain). In: Agustí, J., J. Martinell, Iberian Neogene Basins: Field Guideboook.. Paleont. Evol. Especial Publ., 2, 97 – 130.

Andrews, J. E., 2006. Palaeoclimatic records from stable isotopes in riverine tufas: Synthesis and review. Earth-Science Reviews, 75, 85–104.

Armenteros, I., Dabrio, C., Guisado, R., Sanchez de Vega, A., 1989. Megasecuencias sedimentarias del terciario del borde oriental de la Cuenca de Almazan (Soria – Zaragoza). Studia Geologica Salmanticensia, Special Volume 5, 107–127.

Baker, A., Smart, P. L., Ford, D. C., 1993. Northwest European palaeoclimate as indicated by growth frequency variations of secondary calcite deposits. Palaeogeography, Palaeoclimatology, Palaeoecology, 100, 291–301.

Benito-Calvo, A., Pérez-González, a., 2010. Erosion surfaces and Neogene landscape evolution in the NEDuero Basin (north-central Spain). Geomorphology, 88, 226-241.

Birot, P., 1959. Esquisse morphologique des Monts Celtibériques orientaux. Bull. Comm. Trav. Hist. Sci., Sect. Geogr., 72, 101–130.

Bischoff, J., Fitzpatrick, J. A., 1991. U-series dating of impure carbonates: an isochron technique using total sample dissolution. Geochimica et Cosmochimica Acta, 55, 543–554.

Boschi, L., Fry, B., Ekström, G., Giardini, D., 2009. The European upper mantle as seen by surface waves. Surveys in Geophysics, 30, 463–501, doi:10.1007/s10712-009-9066-2.

Boschi, L., Faccenna, C., Becker, T. W., 2010. Mantle structure and dynamic topography in the Mediterranean Basin. Geophysical Research Letters, 37, doi: 10.1029/2010GL045001.

Burbank, D. W., 1992. Characteristic size of relief. Nature, 359, 483–484.

Calvo Hernandez, J. M., 1993. Cinematica da las fallas discontinuas en el sector central de la Cordillera Iberica. PhD Thesis, Universuty of Zaragoza, Spain.

Calvo J.P., Daams, R., Morales, J., López-Martínez, N., Agusti, J., Anadon, P., Armenteros, I., Cabrera, L., Civis, J., Corrochano, A., Diaz-Molina, M., Elizaga, E., Hoyos, M., Martin-suarez, E., Martinez, J., Moissenet, E., Muñoz, A., Perez-Garcia, A., Perez-Gonzalez, A., Portero, J.M., Robles, F., Santisteban, C., Torres, T., van der Muelen, A.J., Vera, J.A., Mein, P., 1993. Up-to-date Spanish continental Neogene synthesis and paleoclimatic interpretation. Revista de la Sociedad Geológica de España, 6, 1–16.

Casas-Sainz, A.M., Cortés, A., Gapais, D., Nalpas, T., Román, T., 1998. Modelización analógica de estructuras asociadas a compresión oblicua y transpresión. Ejemplos del NE peninsular. Rev. Soc. Geol. España, 11 (3-4), 137-150.

Casas-Sainz, A.M., Faccenna, C., 2001. Tertiary compressional deformation of the Iberian Plate. Terra Nova, 13, 281-288.

Casas-Sainz, A. M., Cortés-Gracia, A. L., 2002. Cenozoic landscape development within the Central Iberian Chain, Spain. Geomorphology, 44, 19–46.

Casas-Sainz, A., 1993. Oblique tectonic inversion and basement thrusting in the Cameros Massif (Northern Spain). Geodinamica Acta, 6 (3), 202–216.

Casas-Sainz, A., De Vicente, G., 2009. On the tectonic origin of Iberian topography. Tectonophysics, 474, 214–235.

Casas-Sainz, A.M., Cortés, A.L., MaestroA.2000. Intra-plate deformation and basin formation during the Tertiary at the Northern Iberian Plate: origin and evlution of the Almazán Basin. Tectonics, 19, 258-289.

Cebriá, J.M., Lopez-Ruiz, J., 1995. Alkali basalts and leucitites in an extensional intracontinental plate setting: the late Cenozoic Calatrava volcanic province (Central Spain). Lithos, 35, 27–46.

Cebriá, J.M., Lopez-Ruiz, J., Doblas, M., Oyarzun, R., Hertogen, J., Benito, R., 2000. Geochemistry of the Quaternary alkali basalts of Garrotxa (northeast volcanic province, Spain): a case of double enrichment of the mantle lithosphere. Journal of Volcanology and Geothermal Research, 102, 217–235.

Cloetingh, S., Burov, E., Beekman, F., Andeweg, B., Andriessen, P. A., García-Castellanos, D., De Vicente, G., Vegas R., 2002. Lithospheric folding in Iberia. Tectonics, 21 (5), 1041.26 p.doi:10.1029/2001TC901031.

Cortés Gracia, A.L., Casas-Sainz, A.M., 1996. Deformación alpina de zócalo y cobertera en el borde norte de la Cordillera Ibérica. Rev. Soc. Geol. España, 9 (1-2), 51-66.

Cortés-Gracia, A.L., Casas-Sainz, A.M., 2000. ¿Tiene el sistema de fosas de Teruel origen extensional? Revista de la Sociedad Geológica de España, 13 (3-4), 445-470.

De Bruijne, C., Andriessen, P., 2002. Far field effects of alpine plate tectonism in the Iberian microplate recorded by fault-related denudation in the Spanish Central System. Tectonophysics, 349, 161–184.

De Vicente, G., (ed.) 2004. Estructura alpine del Antepaís Ibérico. In:Geología de España (J.A. Vera, Ed.), SGE-IGME, Madrid, 587–634.

De Vicente, G., Vegas, R., Muñoz Martín, A., Silva, P., Andriessen, P., Cloetingh, S., González Casadod, J.M., Van Weesc, J.D., Álvareza, J., Carbóa A., Olaiza A. (2007). Cenozoic thick-skinned deformation and topography evolution of the Spanish Central System. Global and Planetary Change, 58, 335–381.

De Vicente, G., Vegas,R., 2009. Large-scale distributed deformation controlled topography along the western Africa–Eurasia limit: Tectonic constraints. Tectonophysics, 474, 124–143.

Domínguez-Villar, D., Vázquez-Navarro, J. A., Cheng, H., Lawrence Edwards, R., 2011. Freshwater tufa record from Spain supports evidence for the past interglacial being wetter than the Holocene in the Mediterranean region. Global and Planetary Change, 77, 129– 141.

Dramis, F., Materazzi, M., Cilla, G., 1999. Influence of climatic changes on freshwater travertine deposition: a new Hypothesis. Phys. Chem. Earth (A), 24 (10), 893-897.

Faccenna, C., Becker, T.W., Lallemand S., Lagabrielle Y., Funiciello F., Piromallo, C., 2010. Subduction-triggered magmatic pulses: A new class of plumes? Earth Planetary Science Letters, 299, 54–68, doi:10.1016/j.epsl.2010.08.012.

Faccenna, C., Becker, T.W., 2010. Shaping mobile belt from small scale convection. Nature, 465, doi:10.1038/nature09064.

Ferreiro, E., Ruiz, V., Lendínez, A., Lago, M., Meléndez, A., Pardo, G., Ardevol, L., Villena, J., Hernández, A., Alvaro, M., Gómez, J.J., Carls, P., 1991. Mapa y memoria explicativa de la Hoja 40 (Daroca) del Mapa Geológico Nacional a escala 1:200.000, ITGE, 239 p..

Flint, J. J., 1974. Stream gradient as a function of order, magnitude, and discharge. Water Resources Research, 10, 969–973.

Ford, T. D., Pedley, H. M., 1996. A review of tufaand travertine deposits of the world. Earth Science Review, 41, 117–175.

Gardner, T. W., Back, W., Bullard, T. F., Hare, P. W., Kesel, R. H., Lowe, D. R., Menges, C.M., Mora, S., Pazzaglia, F.J., Sasowsky, I.D., Troester, J.W., Wells, S.G., 1987. Central America and the Caribbean. In: Graf, W. L. (Ed.), Geomorphic systems of North America: Boulder, Colorado. Geological Society of America, Centennial Special 2, 343–401.

Glover, C., Robertson, A., 2003. Origin of tufa (cool-water carbonate) and related terraces in theAntalya area, SW Turkey. Geological Journal, 38, 329–358.

González, A., Guimerà, J., Luzón, A., 1998. Edad Oligoceno superior-Mioceno inferiore para las superfícies de erosión conservadas en el flanco SW de la cubeta de Bordón (Provincia de Teruel, España). Geogaceta, 24, 155-158.

Gracia, F.J., Gutiérrez, F., Gutiérrez, M., 2003. The Jiloca karst polje-tectonic graben (Iberian Range, NE Spain). Geomorphology 52, 215-231. doi:10.1016/S0169-555X(02)00257-X

Gracia-Prieto, F. J., Gutiérrez-Elorza, M., Leránoz Istúriz, B., 1988. Las superficies de erosión neógenas en el sector central de la Cordillera Ibérica. Revista de la Sociedad Geológica de España, 1 (1-2), 135-142.

Guimerà, J., Alonso, A., Mas, J. R., 1995. Inversion of an extensional ramp basin by a newly formed thrust: the Cameros basin (N. Spain). In: Buchanan, J. G., Buchanan, P. G., Basin Inversion. Geol. Society London, Spec. Publ., 88, 433–453.

Guimerà, J., Alvaro, M., 1990. Structure et évolution de la compression alpine dans la Chaîne Ibérique et al Chaîne Côtière Catalane. Bulletin de la Société géologique de France, 8 (6), 339–348.

Guimerà, J., González, A., 1998. El relieve de la Cadena Ibérica como producto de la compresión alpina. Geogaceta, 24, 163-166.

Guimerà, J., Más, R., Alonso, A., 2004. Intraplate deformation in the NW Iberian Chain: Mesozoic extension and contractional inversion. Journal of Geological Society of London, 16, 291–303.

Gutiérrez Elorza, M., Gracia, F. J., 1997. Environmental interpretation and evolution of the Tertiary erosion surfaces in the Iberian Range (Spain). In: Widdowson, M., Palaeosurfaces: Recognition, Reconstruction and Palaeoenvironmental Interpretation. Geol. Soc., Spec. Publ. 120, 147-158, doi:10.1144/GSL.SP.1997.120.01.10

Gutiérrez, F., 1996. Gypsum karstification induced subsidence: effects on alluvial systems and derived geohazards (Calatayud Graben, Iberian Range, Spain). Geomorphology, 16, 277–293.

Gutiérrez, F., Gracia, F.J., Gutiérrez, M., 1996. Consideraciones sobre el final del relleno endorreico de las fosas de Calatayud y Teruel y su paso al exorreismo. Implicaciones morfo estratigráfi cas y estructurales. In: Grandal D'Anglade, A., Pagés Valcarlos, J. (Eds.), IV Reunión Nacional de Geomorfología. Cadernos do Laboratorio Xeolóxico de Laxe, 21, 23–43.

Gutiérrez, F., Gutiérrez, M., Gracia, F. J., Mc Calpin, J. P., Lucha, P., and Guerrero, J., 2008. Plio-Quaternary extensional seismotectonics and drainage network development in the central sector of the Iberian Chain (NE Spain). Geomorphology, 102, 21–42.

Hack, J. T., 1957. Studies of longitudinal profiles in Virginia and Maryland. U. S. Geological Survey Professional Paper, 294 (B), 45–97.

Hancock G.S., Anderson, R.S., 2002. Numerical modeling of fluvial strath-terrace formation in response to oscillating climate. GSA Bulletin; 114 (9), 1131–1142.

Hare, P. W., Gardner, T. W., 1985. Geomorphic indicators of vertical neotectonism along converging plate margins, Nicoya Peninsula, Costa Rica. In: Morisawa, M., Hack, J.T., Tectonic Geomorphology. Proceedings of the 15th Annual Bighamton Geomorphology Symposium, Allen and Unwin, Boston, 75–104.

Hennig, G. J., Grünn, R., Brunacker, K., 1983. Speleothems, travertines and paleoclimates. Quaternary Research, 20, 1–29.

Horvatinčić, N., Čalič, R., Geyh, M., 2000. Interglacial growth of tufa in Croatia. Quaternary Research, 53, 185–195.

Huang, X., Niemann, J. D., 2006. Modelling the potential impacts of groundwater hydrology on long-term drainage basin evolution. Earth Surface Processes and Landforms, 31, 1802–1823.

Hurtrez, J. E., Sol, C., Lucazeau, F., 1999. Effect of drainage area on hypsometry from an analysis of small-scale drainage basins in the Siwalik Hills (Central Nepal). Earth Surface Processes and Landforms, 24 (9), 799-808.

Ivanovich, M., Harmon, R. S., 1992. Uranium-series disequilibrium: applications to Earth, Marine, and Environmental Sciences. Clarendon Press, Oxford.

Juez-Larré, J., Andriessen, P., 2006. Tectonothermal evolution of the northeastern margin of Iberia since the break-up of Pangea to present, revealed by low-temperature fission-track and (U-Th)/He thermochronology. A case history of the Catalan Coastal Ranges. Earth and Planetary Science Letter, 243, 159-180.

Keller, E., Pinter, N., 2002. Active Tectonics. Earthquakes, Uplift, and Landscape.Prentice Hall, New Jersey.

Kirby, E., Johnson, C., Furlong, K., Heimsath, A., 2007. Transient channel incision along Bolinas Ridge, California: Evidence for differential rock uplift adjacent to the San Andreas fault. Journal of Geophysical Research 112(F3): doi: 10.1029/2006JF000559. issn: 0148-0227.

Kirby, E., Whipple, K. X., 2001. Quantifying differential rock-uplift rates via stream profile analysis. Geology, 29, 415–418.

Li, C., van der Hilst, R. D., Engdahl, E. R., Burdick, S., 2008. A new global model for P-wave speed variations in Earth's mantle. Geochemistry, Geophysics, Geosystems, 9, Q05018, doi:10.1029/2007GC001806.

Lifton, N., Chase, C. G., 1992. Tectonic, climatic and lithologic influences on landscape fractal dimension and hypsometry: implications for landscape evolution in the San Gabriel Mountains, California. Geomorphology, 5, 77–114.

López Vera, F., Martínez Goytre, J., 1989. Edad radiogénica y estratigrafía isotópica de los edificios travertínicos del Puente de San Pedro (Guadalajara). Boletín Geológico y Minero, 100 (2), 248-258.

López-Martínez, N., Agusti, J., Cabrera, L., Calvo, J., Civis, J., Corrochano, A., Daams, R., Diaz, M., Elizaga, E., Hoyos, M., Martinez, J., Morales, J., Portero, J. M., Robles, F., Santisteban, C., Torres, T., 1987. Approach to the Spanish continental Neogene

synthesis and paleoclimatic interpretation. Annales. Instituti Geologici Publici Hungarici, 70, 383 – 391.Ludwig, K. (2003). Using Isoplot/Ex, Version 3. A Geochronological Toolkit for Microsoft Excel. Berkeley Geochronology Center Special Publication, 4 .

Ludwig, K., 2003. Using Isoplot/Ex, Version 3. A Geochronological Toolkit for Microsoft Excel. Berkeley Geochronology Center Special Publication, 4.

Martınez Tudela, A., Cuenca, F., Santisteban, C., Grun, R., Hentzsch, B., 1986. Los travertinos del rio Matarraña, Beceite (Teruel) como indicadores paleoclimaticos del Cuaternario. In: Lopez-Vera, F. (Ed.), Quaternary Climate in Western Mediterranean. Universidad Autonoma de Madrid, Madrid, 307-324.

Martín-Serrano, A., 1991. La definición y el encajamiento de la red fl uvial actual sobre el Macizo Hespér ico en el marco de su geodinámica alpina. Revista de la Sociedad Geologica de España 4, 337–351.

Martinson, D.G., Pisias, N.G., Hays, J.D., Imbrie, J., Moore, T.C., Shackleton, N.J., 1987. Age dating and the orbital theory of the ice ages: Development of a high-resolution 0 to 300,000-year chronostratigraphy. Quaternary Research, 27 (1), 1–29.

Masek, J., Isacks, B., Gubbels, T., Fielding, E., 1994. Erosion and tectonics at the margins of continental plateau. Journal of Geophysical Research, 99 (B7) , 13941-13956.

Mather, A. E., 1993. Basin inversion: some consequences for drainage evolution and alluvial architecture. Sedimentology, 40, 1069–1089.

Moglen, G., Bras, R. L., 1995. The effect of spatial heterogeneities on geomorphic expression in a model of basin evolution. Water Resources Research, 31, 2613–2623.

Molin, P., Pazzaglia, F., Dramis, F., 2004. Geomorphic expression of active tectonics in a rapidly-deforming forearc, Sila massif, Calabria, southern Italy. American Journal of Science, 304 (7), 559-589.

Muñoz-Martín, A., De Vicente, G., 1998. Origen y relacion entre las deformaciones y esfuerzos alpinos de la zona centro-oriental de la Peninsula Ibérica. Revista de la Sociedad Geológica de España, 11, 57-70.

Ordóñez, S., González Martín, J. A., García del Cura, M. A., 1990. Datacion radiogénica (U-234/U-238 y Th-230/U-234) de sistemas travertinicos del Alto Tajo (Guadalajara). Geogaceta, 8, 53–56.

Ordoñez, S., González Martín, J. A., García del Cura, M. A., Pedley, M., 2005. Temperate and semi-arid tufas in the Pleistocene to recent fluvial barrage system in

the Mediterranean area: the Ruidera Lakes Natural Park (central Spain). Geomorphology, 69, 332–350.

Ortiz, J. E., Torres, T., Delgado, A., Reyes, E., Dìaz-Bautista, A., 2009. A review of the Tagus river tufa deposits (central Spain): age and palaeoenvironmental record. Quaternary Science Reviews, 28, 947–963.

Pazzaglia, F. J., Gardner, T. W., Merritts, D., 1998. Bedrock fluvial incision and longitudinal profile development over geologic time scales determined by fluvial terrace. In: Wohl, E., Tinkler, K., Rivers over rock, Fluvial Processes in Bedrock Channels. American Geophysical Union, Geophysical Monograph Series, 107, 207–236..

Pederson, J.L., Anders, M.D., Rittenhour, T.M., Sharp, W.D., Gosse, J.C., Karlstrom, K.E., 2006. Using fill terraces to understand incision rates and evolution of the Colorado River in eastern Grand Canyon, Arizona. Journal of Geophysical Research: Earth Surface, 111 (F2), DOI: 10.1029/2004JF000201

Pedley, M., 2009. Tufas and travertines of the Mediterranean region: a testing ground for freshwater carbonate concepts and developments. Sedimentology, 56, 221–246.

Pedley, M., González Martín, J., Ordóñez, S., García del Cura, M., 2003. Sedimentology of Quaternary perched springline and paludal tufas: criteria for recogni-tion, with examples from Guadalajara Province, Spain. Sedimentology, 50, 23–44.

Peña, J. L., Gutiérrez, M., Ibáñez, M. J., Lozano, M. V., Rodríguez, J., Sánchez, M., Simón, J.L., Soriano, A., Yetano, M. ,1984. Geomorfología de la Provincia de Teruel. Teruel. Instituto de Estudios Turolenses. Excma. Dip. Provincial de Teruel (Spain).

Perea, H., Masana, E., Santanach, P., 2012. An active zone characterized by slow normal faults, the northwestern margin of the València trough (NE Iberia): a review. Journal of Iberian Geology, 38(1), 31-52.

Perez-Peña, J. V., Azor, A., Azañon, J. M., Keller, E. A., 2010. Active tectonics in the Sierra Nevada (Betic Cordillera, SE Spain): insights from geomorphic indices and drainage pattern analysis. Geomorphology, 119, 74–87.

Pérez-Peña, J., Azanon, J. M., Azor, A., 2009. CalHypso: An ArcGIS extension to calculate hypsometric curves and their statistical moments. Applications to drainage basin analysis in SE Spain. Computers and Geosciences, 35, 1214–1223.

Piromallo, C., Morelli, A., 2003. P-wave tomography of the mantle under the Alpine‐Mediterranean area. Journal of Geophysical Reseach, 108 (B2), doi:10.1029/2002JB001757.

Roca, E., Guimerà, J., 1992. The Neogene structure of the eastern Iberian margin: structural constraints on the crustal evolution of the Valencia trough (western Mediterranenan). Tectonophysics, 203, 203–218.

Rodríguez-Pascua, M., De Vicente, G., 1998. Análisis de paleoesfuerzos en cantos de depósitos conglomeráticos terciarios de la cuenca de Zaorejas (rama castellana de la Cordillera Ibérica). Revista Sociedad Geoligica España 11, 169–180.

Rubio, J.C., Simón, J.L. (2007) Tectonic subsidence vs. erosional lowering in a controversial intramontane depression: the Jiloca basin (Iberian Chain, Spain). Geological Magazine 144 (1), 127-141

Schmid, C., S. van der Lee, J. C. VanDecar, E. R. Engdahl, and D. Giardini (2008). Three‐dimensional S velocity of the mantle in the Africa‐Eurasia plate boundary region from phase arrival times and regional waveforms. Journal of Geophysical Research, 113, B03306, doi:10.1029/2005JB004193.

Schwarcz, H., Latham, A. G., 1989. Dirty calcites 1. Uranium-series dating of contaminated calcite using leachate alone. Chemical Geology, 80, 35-43.

Simón, J.L., Liesa, C.L., 2011. Incremental slip history of a thrust: diverse transport directions and internal folding of the Utrillas thrust sheet (NE Iberian Chain, Spain). In: Poblet, J., Lisle, R. J. (eds), Kinematic Evolution and Structural Styles of Fold-and-Thrust Belts. Geological Society, London, Special Publications, 349, 77-97.

Simón, J. L., 1984. Compresión y distensión alpinas en la Cadena Ibérica oriental. Instituto de Estudios Turolenses, Teruel (Spain).

Simón, J. L., 1989. Late Cenozoic stress field and fracturing in the Iberian Chain and Ebro Basin (Spain). Journal of Structural Geology, 11, 285-294.

Simón, J., Arlegui, L., Lafuente, P., Liesa, C., 2012. Active extensional faults in the central-eastern Iberian Chain, Spain. Journal of Iberian Geology, 38(1), 127-144.

Snyder, N., Whipple, K. X., Tucker, G. E., Merritts, D. J., 2000. Landscape response to tectonic forcing: Digital elevation model analysis of stream profiles in the Mendocino triple junction region, northern California. Geological Society of America Bulletin, 112 (8), 1250-1263.

Solé Sabarís, L., 1979. La Meseta. In: Teràn, D., Geográfia de España. Ariel, Madrid (Spain), 42 – 62.

Strahler, A., 1952. Hypsometric (area–altitude) analysis of erosional topography. Geological Society of America Bulletin, 63, 1117–1142.

Tarboton, D. G., Bras, R. L., Rodriguez-Iturbe, I., 1989. Scaling and elevation in river networks. Water Resources Research, 25, 2037–2051.

Ter Voorde, M., De Bruijne, C., Cloetingh, S., Andriessen, P., 2004. Thermal consequences of thrust faulting: simultaneous versus successive fault activation and exhumation. Earth and Planetary Science Letter, 223, 397-415.

Torres, T., Ortiz, J., Garcia de la Morena, M. A., Llamas, F. J., Goodfriend, G., 2005. Ostracode-based aminostratigraphy and aminochronology of a tufa system in central Spain. Quaternary International, 135, 21–33.

van Dam, J., Sanz Rubio, E., 2003. Late Miocene and Pliocene small mammals from the Calatayud Basin (Central Spain). Coloquios de Paleontología, 1, 115-126.

Vázquez-Urbez, M., Arenas, C., Sancho, C., Osácar, C., Auqué, L., Pardo, G., 2010. Factors controlling present-day tufa dynamics in the Monaterio de Piedra Natural Park (Iberian Range, Spain): depositional environmental settings, sedimentation rates and hydrochemistry. International Journal of Earth Sciences, 99, 1027–1049.

Vegas, R., 1992. The Valencia trough and the origin of the western Mediterranean basins. Tectonophysics, 203, 249–261.

Villena, J., Pardo, G., Pérez, A., Muñoz-Jiménez, A., González, A.. 1996. Tertiary of the Iberian margin of the Ebro Basin: 1) Stratigraphic synthesis. In: Friend, P., Dabrio, C. (eds) Tertiary basins of Spain, Serie World and Regional Geology. Cambridge University Press, 77-82.

Walcott, R., Summerfield, M. A., 2008. Scale dependence of hypsometric integrals: an analysis of southeast African basins. Geomorphology, 96, 174–186.

Wedepohl, K., 1995. The composition of the continental crust. Geochimica et Cosmochimica Acta, 59, 1217-1239.

Wegmann, K.W., Zurek, B.D., Regalla, C.A., Bilardello, D., Wollenberg, J.L., Kopczynski, S.E., Ziemann, J.M., Haight, S.L., Apgar, J.D., Zhao, C., Pazzaglia F.J., 2007. Position of the Snake River watershed divide as an indicator of geodynamic processes in the greater Yellowstone region, western North America. Geosphere, 3, 272‑281, doi:10.1130/GES00083.1.

Weissel, J., Pratson, L. F., Malinverno, A., 1994. The length-scaling properties of topography. Journal of Geophysical Research, 99 (B7), 13997–14012.

Whipple, K. X., 2004. Bedrock rivers and the geomorphology of active orogens. Annu. Rev. Earth Planetary Sci., 32 , 151-185.

Whipple, K. X., 2001. Fluvial landscape response time: how plausible is steady state denudation? Am. J. Sci., 301, 313‑325, doi:10.2475/ajs.301.4-5.313.

Whipple, K. X., Tucker, G. E., 1999. Dynamics of the stream-power river incision model: implications for height limits of mountain ranges, landscape response timescales, and research needs. Journal of Geophysical Research, 104, 17,661-17,674.

Whipple, K.X., Wobus, C., Crosby, B., Kirby, E., Sheehan, D., 2007. New Tools for Quantitative Geomorphology: Extraction and Interpretation of Stream Profiles from Digital Topographic Data. Geological Society of America Annual Meeting, Short Course Guide: http://www.geomorphtools.org, Denver.

Willgoose, G., Hancock, G., 1998. Revisiting the hypsometric curve as an indicator of form and process in transport-limited catchment. Earth Surface Processes and Landforms, 23, 611– 623.

Wobus, C., Whipple, K. X., Kirby, E., Snyder, N., Johnson, J., Spyropolou, K., Crosby, B., Sheehan, D., 2006. Tectonics from topography: Procedures, promise, and pitfalls. In: Willett, S., Hovius, N., Brandon, M.T, Fisher, D.M. (Eds), Tectonics, Climate, and Landscape Evolution. Geol. Soc. Am. Spec. Pap., 398, 55 –74.

Wortel, M. J. R., Spakman, W., 2000. Subudction and slab detachment in the Mediterranean‑Carpathian region. Science, 290, 1910–1917, doi:10.1126/science.290.5498.1910.

Chapter 2

NUMERICAL SIMULATIONS OF PLIO-QUATERNARY LANDSCAPE EVOLUTION OF THE IBERIAN CHAIN (SPAIN)

Abstract

The Iberian Chain is an intraplate range located in the central-eastern Iberian Peninsula, showing a dome-shaped topography characterized by a low relief landscape located at a mean elevation of 1300 m a.s.l.

The mountain range results from the late Cretaceous-middle Miocene compression. During the Upper Neogene, compressive structures experienced planation processes presently recorded by wide erosion surfaces. Since about 2.5 Myr (?), a regional tectonic uplift occurred guiding the organization of the present fluvial network.

We performed numerical experiments to simulate landscape evolution characterized by the same tectonic and erosion inputs of the Iberian Chain area, using a range of physical parameters calibrated on field, radiometric and morphometric data. To test the evolution of different initial topographies, we used SIGNUM (Simple Integrated Geomorphological Numerical Model), a Matlab, TIN-based landscape numerical model. The results show that the initial topography that better matches the geomorphological features encountered in the present-day landscape consists of a wide plain with a slightly higher relief to the NE. This plain was surrounded by endorehic areas.

After running the SIGUM, this initial synthetic landscape evolves into a topography that reaches a mean elevation quite similar to the Iberian Chain high-standing plain,

preserves small internally drained areas in its interior and is poorly incised by hydrography.

Our results, coupled with geological and gemorphological data, allowed us to conclude that:

1) in Miocene-Middle Pliocene a relief of few hundred meters was located in the NE sector of the Iberian Chain; lakes occupied the rest of the present range;

2) in Late Pliocene-Quaternary a regional uplift occurred, causing the progressive capture of endorheic lakes. Topographic barriers played an important role preserving the landscape in the inner Iberian Chain at high elevation through time.

3) the time span necessary to obtain a synthetic topography morphologically similar to the present-day Iberian Chain is ~3.2 Myr.

4) the estimate uplift rates are non-uniform and range between 0.5 mm/yr in the interior sector to 0.25 mm/yr;

5) the inversion of the drainage network and the opening of the internally drained basins occurs after the onset of the uplift, and starts at around 2 Ma.

Keywords

Iberian Chain, landscape evolution, numerical modeling.

2.1. Introduction

Modern process geomorphologists use the term landscape evolution to describe the interactions between form and process that are played out as measurable changes in landscapes over geologic as well as human time scales (Pazzaglia, 2003).

Numerical models that describe landscape evolution by representing one or more geomorphic process and landscape characteristics through mathematical expressions are

called *Landscape Evolution Models (LEM).*

Here, we simulate the Plio-Quaternary landscape and drainage network evolution of the Iberian Chain (Central-Eastern Spain) through numerical models that integrate tectonic uplift and geomorphological processes calibrated on previous geomorphic analysis by using raster and radiometric data.

In detail, our approach to numerically simulate the landscape evolution of Iberian Chain mainly consisted in solving an inverse problem: "if, given some information on the values of some measured quantities, we try to use a theoretical relationship in order to obtain information on the values of the set of parameters, then we are solving an 'inverse problem'. (…) For an inverse problem, the data are the results of some measurements, and the unknowns are the values of the parameters" (Tarantola & Valette, 1982).

Our geomorphological inverse problem has been formulated combining the following input data:

1) initial data: 90m pixel-size DEM, present-day topographic features geological records, a time interval for the uplift onset; paleo-environmental reconstruction of the area);
2) values of some unknowns (incision rates, morphometric inedexes of river profiles, the amount of the total regional uplift inferred from topographic analysis).

Then, we used theoretical relationships in order to combine data and unknowns, such as stream power laws for river incision and geomorphic transport, as well as the erodibility of outcropping lithologies. We obtained the values of the unknowns: initial conditions, uplift onset, uplift rates, uplift spatial distribution, erodibility in the stream power model.

In detail, we performed 62 3-D TIN-based numerical experiments of landscape

evolution to calibrate geomophological processes, tectonic uplift rates and pattern to the present-day topography.

Furthermore, we validated the results obtained from 3D numerical simulations by a 2D inversion of synthetic longitudinal river profiles and comparing them with natural channels.

2.2. Geological setting

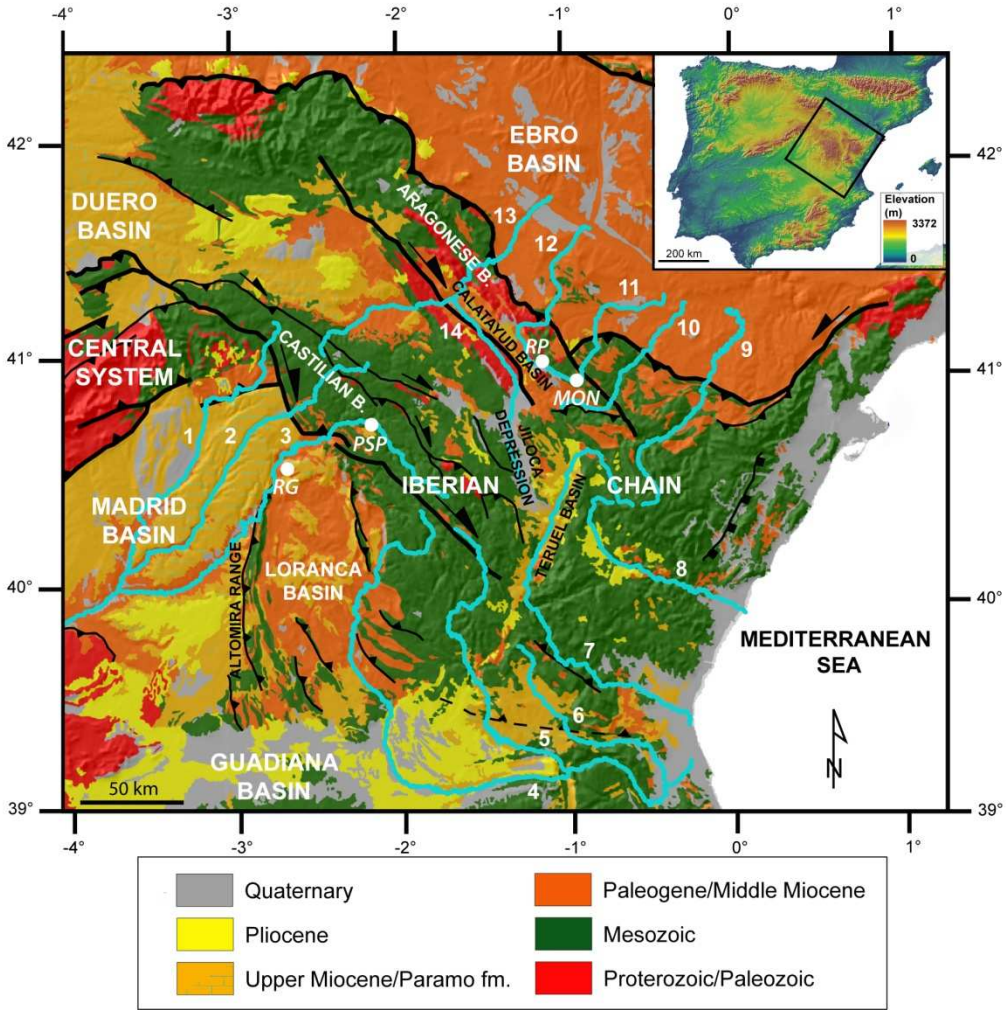

Fig. 2.1. Geological map of the study area, analyzed rivers (1= Henares; = Tajuña; 3= Tajo; 4= Júcar; 5= Cabriel; 6= Magro; 7= Turia; 8= Mijares; 9= Guadalope; 10= Martìn; 11= Aguasvivas; 12= Huerva; 13= Jiloca; 14= Jalón) and location of collected fresh tufa samples (RG: Ruguilla, PSP: Puente de San Pedro, MON: Montalban, RP: Las Parras de Martìn.).

The Iberian Chain (North-Eastern Iberian Peninsula) is an example of intraplate range, formed during Late Cretaceous-Middle Miocene times as consequence of the convergence between Africa and Iberia (fig. 2.1). The resulting deep imprint of the intraplate deformation (Casas-Sainz and Faccenna, 2001) inverted the pre-existing Mesozoic Iberian Basin (Álvaro et al., 1979; Guimerà et al., 2004).

Along the borders of the Iberian Chain as well as of the adjacent ranges, compressive tectonic structures favored the development of tertiary internally drained basins (e.g.: Calvo et al., 1993; Villena et al., 1996; Alonso-Zarza A., 2008): the Ebro B., the Madrid B., the Loranca B. and the Duero B. (fig. 2.1). In the interior of the Iberia Chain several small endorheic intermontane basins also developed, such as Calatayud-Montalban and Teruel basins (fig. 2.1). They are filled up by Upper Oligocene-Pliocene (4.5-3 Myr) continental sequences (López-Martínez et al., 1987; Anadón et al., 1990; Anadón and Moissenet, 1996; Alcalá et al., 2000; van Dam and Sanz Rubio, 2003). During Early Pliocene times, the final sedimentary stages of all these basins are characterized by the widespread deposition of lacustrine limestones, the so-called Páramo Fm. (Armenteros et al., 1989; Alonso-Zarza and Calvo, 2000). This unit is considered coeval with an extensive planation surface (the so-called Main Planation Surface: Birot, 1959; Solé Sabarís, 1979; Simón, 1984; Peña, 1984, Gracia-Prieto et al., 1988; Gutiérrez, 1996) that currently dominates the central sector of the range. This wide surface records a period of tectonic quiescence (Upper Neogene?), during which most of previous compressive structures were almost completely levelled. In Late Pliocene (?)-Quaternary, this denudation episode was interrupted by the onset of a regional uplift that produced a general upwarping of the range, well defined by the smoothly tilting of the Páramo Fm. carbonates from the inner sector of the range toward the Madrid Basin. Moreover, the uplift controlled the organization of the present fluvial network and drove

the regressive erosion of Ebro, Tajo and Turia Rivers, as well as the progressive capture of the intermontane basins and their transformation into exorheic basins from the Pliocene onward (Gutiérrez et al., 2008).

The timing and extent of uplift of the Iberian chain is poorly constrained, although recently Scotti et al. (2013) suggest the upheaval started at or after ~3 Myr, on the basis of an extensive morphometry analysis coupled with geological, geomorphological data and radiometric datings.

2.3. Theoretical background and methods

In order to perform numerical experiments on the Plio-Quaternary geomorphological evolution of the Iberian Chain, we use a TIN-based, numerical landscape evolution model (LEM) called SIGNUM (Simple Integrated Geomorphological NUmerical Model) (Refice et al., 2012).

SIGNUM is a multi-process, 3D, geomorphological numerical model and its code is written in Matlab. SIGNUM provides a simple and integrated numerical framework for the simulation of some important processes that shape real landscapes at different space and time scales.

The majority of LEMs use a raster-based approach, i.e. they represent surfaces approximated as a regular grid of points in the (x, y) plane. An alternative is to use a triangulated irregular network (TIN)-based structure, which represents a surface by a list of points arbitrarily disposed on the plane. The use of TIN-sparse points presents some advantages compared to fixed grids: TINs allow more uniform sampling of some surface parameters such as point distances and drainage directions; sampling density in

TINs can be dynamically and spatially varied, allowing to selectively increase detail on particular areas compared to others, and thus optimizing computational costs.

SIGNUM operates by defining a triangulated mesh of points on a surface, defined as pairs of (x; y) coordinates in arbitrary units (for this study coordinates units are in meters). To each point is associated a unique height value z. The initial list of point coordinates and heights must be passed to SIGNUM as Matlab arrays, which can be created by any means, either by loading external data (e.g. sampling a real elevation field) or creating one from scratch, i.e. by simulating synthetic landscapes. In SIGNUM, the Voronoi polygon area, calculated for each TIN point, is used as approximation of the elementary drainage area associated to each point. The flow routing network is determined through a "steepest descent" algorithm: each point is linked through a "following" pointer to its neighbor with the steepest slope. Once the flow routing network is built, contributing areas are determined by cumulating elementary drainage areas over the network. The main program then operates in successive time cycles, modifying the surface states (i.e. point coordinates, hydrologic and geomorphic variables etc.), at each cycle according to predefined rules. These rules are coded into individual process functions, which are called from the main program through evaluation of Matlab commands from text strings, which are passed to the program from a parameter file.

The parameter file is a list of overriding definitions for any variable with respect to their default value. Of these, the most important ones are the initial coordinate lists x, y, z and the boundary condition list b of the same size. Additional variables which can be overridden in the main program through the parameter file are: the total duration of the simulation in years, Nt; the save time frequency Ns (data are saved to disk in a .mat file

every Ns years); the seed name of the sequence of output mat files containing all the surface parameters, which are saved periodically to disk; the plot time frequency Np, to have a 3D plot of the surface on screen in a Matlab figure window every Np years; text strings containing alternate calls to Matlab functions encoding the chosen diffusion, erosion, and channeling processes; parameter definitions for each of the above functions (for instance, kd for the diffusion; Kc, m, n, for the channeling; U for the uplift modules; respectively).

The main program updates the model heights at each iteration, according to the chosen processes. Time is simulated as a sequence of discrete steps. At each iteration, height changes due to the simulated geomorphological processes are calculated in sequence, and then applied to all points of the TIN. This corresponds to a simple forward-in-time explicit resolution scheme, equal for all the equations pertaining to the various processes. The size of each time step is determined by taking into account the Courant-Friedrichs-Lewy (CFL) condition (Courant et al., 1967), in order to avoid numerical instabilities in the solutions.

Every Ns simulated years, a .mat file named with a user-defined seed character string and an additional string equal to the current time numerical value (for instance, for a seed name such as “SIGNUM_exp”, if Ns = 1000, a sequence of files named SIGNUM_exp_1000.mat, SIGNUM_exp_2000.mat, etc.) is saved to disk. Each of these .mat files contains the whole Matlab memory content at the saving time. This simple data storage scheme helps successive processing of the simulated data to extract useful information.

2.3.1. Geomorphic processes

All the approaches to landscape modeling picture the evolution of the Earth surface through the interaction of three broad classes of processes, one driven by tectonic, large-scale surface deformation, another describing the smoothing effects associated to diffusive processes, and a third one encoding the erosive power of water flow, represented by advective processes. These three basic process classes which I label here with the terms of surface uplift, diffusion, and channeling, respectively, are implemented in a large variety of ways, and the study of their interactions, rates, and forms, constitutes most of the current research effort in the field.

They can be represented in a symbolic mathematical form by writing:

$$\frac{\partial x}{\partial t}(x, y, z, t) = U(x, y, z, t) + D(x, y, z, t, \nabla^2 z) + C(x, y, z, t, \nabla z)$$

(1)

where the dependence of each process class on points' positions, time, as well as derived states such as surface curvature (∇2z) or slope (∇z), are explicated for clarity. The exact mathematical form of the three processes is of course dependent on several assumptions, and additional parameters must be assigned to each of them in practical experiments.

2.3.1.1. Hillslope diffusion

Diffusion modifies the height *z* of each point by implementing the formula:

$$\frac{\partial \mathrm{z}}{\partial \mathrm{t}} = \nabla \cdot q_s \qquad (2)$$

i.e. height variation is proportional to the divergence of sediment flux over the surface. The simplest expression for the flux q_s is a linear function of the surface slope, so that the final height variation equation for linear diffusion can be written:

$$\frac{\partial z}{\partial t} = k_d \nabla^2 z \quad (3)$$

where k_d is the diffusion coefficient which must be set in the *parameterfile*. The linear diffusion process is implemented through the approximation (see Tucker et al., 2001):

$$\frac{\partial z_i}{\partial t} = \frac{k_d}{A_i} \sum_{j=1}^{n} \lambda_{ij} \frac{z_j - z_i}{L_{ij}} \quad (4)$$

where A_i is the area of its Voronoi polygon, the sum is over all the n points adjacent to i, the ratio $(z_j - z_i)/L_{ij}$ represents the slope of the segment (height differences divided by the length of the mesh edge L_{ij}) and λ_{ij} is the length of the corresponding Voronoi edge. In the adopted first-order, forward-in-time scheme, $\Delta z = \Delta t \cdot f(z, t)$, the size of the time step Δt is chosen by calculating the minimum CFL factor over all the TIN arc lengths L_{ij}:

$$\Delta t_{max} < min_{i,j} \left(\frac{L^2{}_{ij}}{2k_d} \right) \quad (5).$$

The actual relevance of an equation as (3) in modeling hillslope processes is currently subject to scientific debate (see e.g. Tucker and Bradley, 2010; Foufoula-Georgiou et al., 2010). Often, an alternative mathematical equation has been invoked to account for nonlinear dependency of sediment fluxes on terrain slope instead of the linear relation implied by (3), such as (e.g. Roering et al., 1999):

$$q_s = \frac{k_d \nabla z}{1-\left(\frac{|\nabla z|}{S_c}\right)^2} \quad (6)$$

which is used for values of ∇z smaller than the critical slope S_c.

Since $lim_{\nabla z \to Sc}\, q_s = \infty$, as the local slope increases, it tends asymptotically to the value S_c without overcoming it. This kind of nonlinear diffusion is implemented in SIGNUM by using the nonlinear expression (6) in (2), and approximating as finite volumes, analogously to (4), as:

$$\frac{\partial z_i}{\partial t} = \frac{k_d}{A_i} \sum_{j=1}^{n} \lambda_{ij} \frac{\frac{z_j - z_i}{L_{ij}}}{1-\left(\left|\frac{z_j - z_i}{L_{ij}}\right| / S_c\right)^2} \quad (7)$$

The determination of the CFL limit for a nonlinear diffusion equation is quite tricky (see e.g. Pelletier, 2008; Press et al., 1992). I calculate an approximate limit as:

$$\Delta t_{max} \ll min_{i,j}\left(\frac{{L^2}_{ij} - \frac{|z_j - z_i|}{{S_c}^2}}{2k_d}\right) \quad (8)$$

where the inequality is forced by multiplying the right-hand side by a factor such as 0.1 or less. The last expression must be evaluated at each iteration, since it depends on the surface slopes.

2.3.1.2. Channeling

Channel-forming advective processes are usually simulated through mathematical relations linking vertical erosion rates with channel slope and contributing areas, with a

huge variety of additional parameters influencing the particular erosion process (see a review in Gasparini et al., 2007). One of these models, widely used, is the stream-power erosion equation, representing the fluvial incision rate as a power law function of water discharge and local channel gradient:

$$\frac{\partial z}{\partial t} = -K_c A^m \nabla z^{\mathrm{n}} \quad (9).$$

The contributing area *A* is used as a proxy for the water and thus the sediment flux (detachment-limited erosion regime), K_c is a constant including surface erodibility, as well as other terms such as the link between runoff and contributing area (see Willgoose et al., 1991), and *m* and *n* are positive constants which depend generally on the erosion process being simulated. This is a common model for detachment-limited erosion, in which deposition of sediment is not considered, as all eroded material is assumed to exit the surface from one or more fluvial outlets. Much has been written about the significance, applicability, and verifiability of the above equation (see e.g. Whipple and Tucker, 1999, and references therein). Commonly used values for *m* and *n* are around 0.5 and 1, respectively, although a range of values can be found in the literature, based on various assumptions about processes at work and surface characteristics (Gasparini and Brandon, 2011). Nevertheless, many such derivations maintain a value of the *m/n* ratio in a small interval around 0.5.

In SIGNUM, the process is simulated through the approximation:

$$\frac{\partial z_i}{\partial t} = -K_c {A_i}^m \left(\frac{|z_j - z_i|}{L_{ij}}\right)^n \quad (10)$$

where *j* is the index of the point which point *i* is draining to (as determined in the flow routing algorithm, i.e. in this version of SIGNUM, the steepest descent point linked to point *i* in the TIN), and $L_{i\,j}$ is the length of the TIN arc linking points *i a*nd *j*, while A_i is the contributing area of point *i*, as defined in the preceding section.

The adopted explicit finite-volume scheme requires again a CFL upper limit for the time step, which in this case can be written:

$$\Delta t_{max} < min_{i,j}\left[\frac{L_{ij}}{K_c A_i^m \left(\frac{|z_j - z_i|}{L_{ij}}\right)^{n-1}}\right] \quad (11)$$

with the *min* calculated over all the TIN arcs.

2.3.1.3. Lacustrine areas

Internally drained areas, widespread in most of Iberia during Miocene, and their transition into exorheic areas in Pliocene and Quaternary, represents a first-order feature of the topography that we try to simulate in our landscape evolution model. Therefore an ad-hoc numerical treatment of closed topographic depressions is required by the aim of this study, namely modeling the interplay between tectonic uplift and drainage network organization. Hence, we develop a simple explicit method to simulate sediment transport and deposition in a closed basin: all points on the TIN having a steepest-descent slope $S_{st} \geq 0$ (meaning that all neighbors points have elevation $z \geq$ point *i*) are flagged as lake-points; thus, no erosion is allowed by the model in these points and the sediment flux *Qs* from an upstream cell is deposited in the lake-point cell, or redistributed down-slope of a lake-point. Then the model checks if the elevation of the lake-point *i* is higher than the minimum elevation of all its neighbor and non-lake

upstream points; if it does, excess of sediment is redistributed to neighbors downstream lake-points of lake-point *i*. When a basin is overfilled by sediments and an external river captures an endorheic area by headward erosion on a flank of the lake, a new outlet opens: rivers flowing upstream the endorheic area can flow out, the erosion starts again doing work on the undissected deposition surface of the lake and produces an exorheic, self-organized drainage network. This numerical method represents the simplest way to numerically simulate the filling of closed depressions or sedimentary basins.

2.3.1.4. Tectonic uplift

*S*urface uplift is intended here as a class of processes modifying the mesh nodes according to some global rule. Common choices include uniform uplift at a constant rate, or episodic base level fall in a selected number of surface edges, or even no uplift, to simulate lowering of the relief in a region. More complex phenomena can be simulated by changing the spatial/temporal patterns of the uplift rate. Rigorous simulation of surface uplift due to crustal movements, such as those detected close to faults, requires in principle to track mass displacements within the earth surface by allowing the points representing the surface to move also in the horizontal plane. This approach would require updating the mesh grid during the simulation, as mesh nodes migrate laterally. This solution is adopted in some models such as Braun & Sambridge (1997), and could be coded in an ad hoc future SIGNUM uplift module. In many cases, however, a simplified approach not involving node movements can be used as a good approximation of the superficial manifestation of ground height variations due to tectonic motions. In this scenario, the surface effects of some complex tectonic motion schemes, such as thrusts or normal faults, can be simulated by allowing points to change their elevation at different times during the simulation. This scheme corresponds in

practice to an “eulerian” approach as opposed to the “lagrangian” point of view implied by the mesh migration algorithms. Eulerian simulation of the propagation of “uplift shock waves” through the simulated mesh can indeed reproduce the phenomenology of surface uplift quite faithfully, provided numerical stability of the simulation, which is assured if the time step satisfies the CFL condition:

$$\Delta t_{max} < min_{i,j}\left(\Delta x_{ij}/v_c\right) \quad (12).$$

with v_c some parameter representative of the lateral migration velocity of the ground movement phenomenon, and the maximum calculated over all the mesh arcs (*i*; *j*).

2.4. Quantitative constraints

2.4.1 Geomorphological constraints

In order to simulate the uplift of the Iberian Chain and the relative river incision into bedrock, we implemented some parameters in the numerical model SIGNUM. They are derived from morphometric features of the Iberian Chain topography, such as swath profiles, local relief map and stream longitudinal profiles (Scotti et al., submitted). Our main data source is the SRTM DEM of the Iberian Chain, whose resolution of ~90 m pixel size is good enough for a regional analysis. Incision rates have been also calculated from U-Th dating of calcareous tufas overlying fluvial strath terraces in the inner sector of the range (Scotti et al., submitted).

2.4.1.2. Swath profiles and local relief map

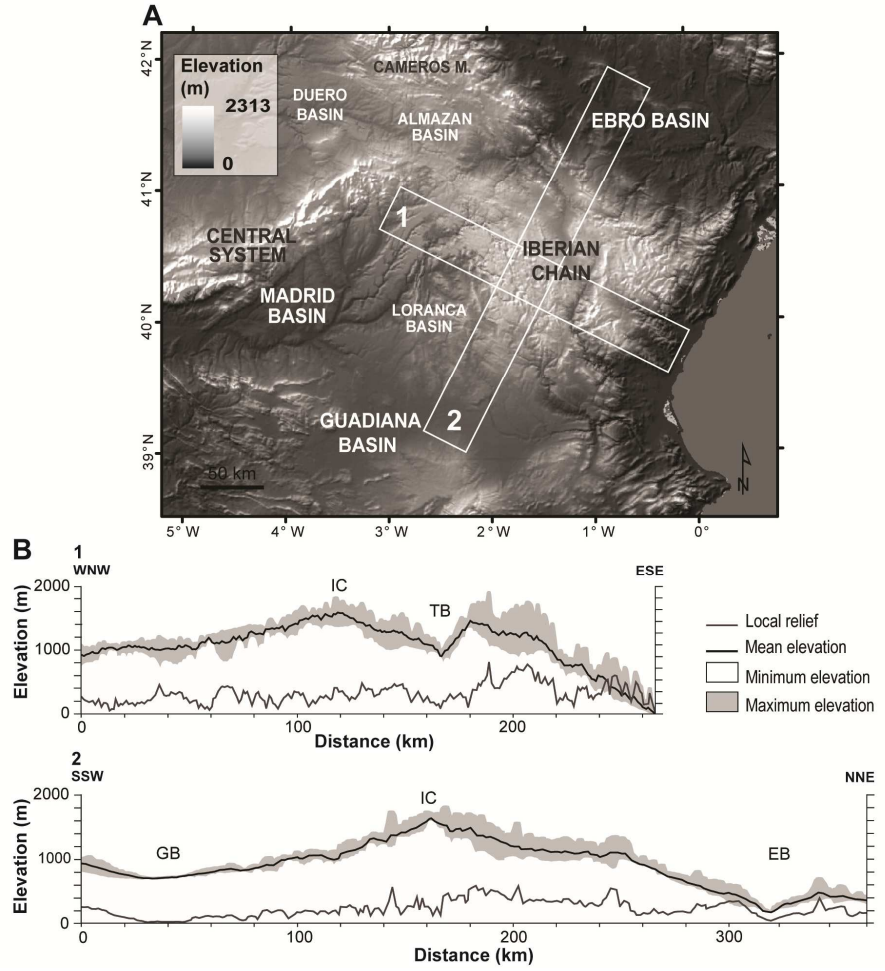

Fig. 2.2. A) DEM of the study area and location of traces of the four swath profiles; B) swath profiles showing the trend of maximum, minimum, and mean topography and local relief of the Iberian Chain. IC: Iberian Chain; TB: Teruel Basin; MB: Madrid Basin; JB: Jiloca Basin; GB: Guadiana Basin; EB: Ebro Basin; CM: Cameros Massif.

To characterize the Iberian Chain topography we focused our morphometric analysis on several swath profiles and a map of local relief (fig 2.2). We extracted four swath profiles to describe the general trend of the maximum, minimum and mean topography included in an observation window 40 km wide and about 300 km long. A curve of the local relief has been generated subtracting arithmetically the minimum from the maximum elevations.

The swath profiles (fig 2.2) reveals the Iberian Chain has a dome-shaped topography, characterized by a widespread low-relief surface, standing at ~1300 m a.s.l. in its

interior. Comparing the swath profiles with the geological map in fig. 2.1, the connection between the high standing surface and the Miocene-Pliocene lacustrine deposits in the Madrid and Guadiana basins is apparent. To the E and NE, the high-standing plateau is interrupted along the Mediterranean and Ebro sides of the massif. Remnants of ranges characterized by an older low relief surface rise from the plateau reaching elevation of more than 1600 m.

The curve of local relief (fig. 2.2) shows an almost homogeneous almost plat pattern, suggesting rivers are incising in response to an unique tectonic main input.

In order to describe the spatial variation in river incision throughout the study area, we also elaborated a map of local relief by arithmetically subtracting two surfaces describing the general configuration of valley bottoms and peak elevations (fig 2.3).

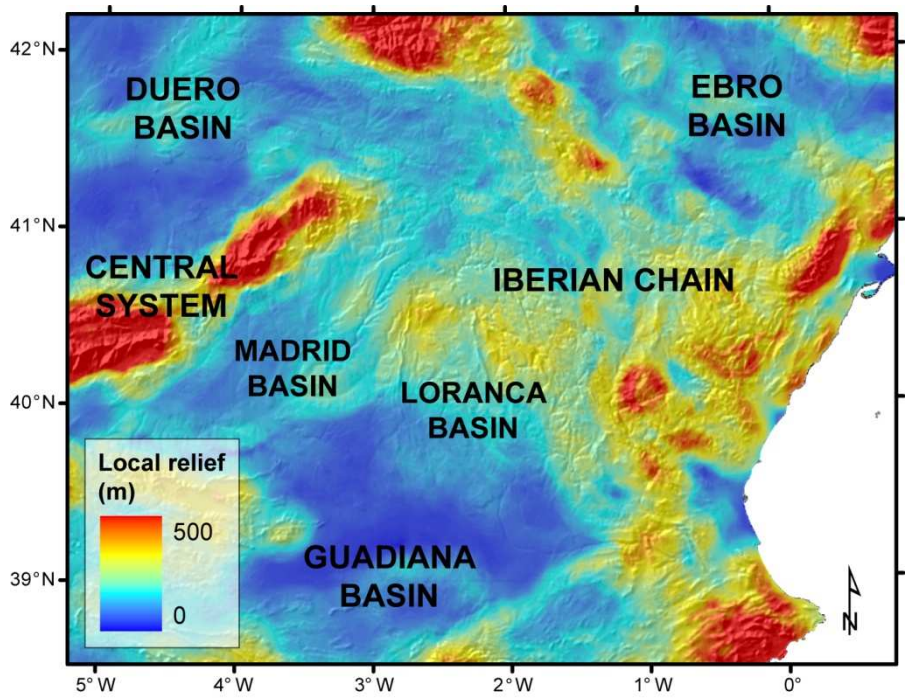

Fig. 2.3. Local relief map of the Iberian Peninsula.

These two surfaces have been extracted by smoothing the raw topography by a circular moving window 30 km wide. The resulting map indicate the values of local relief are low or very low (~200 m), especially considering that it reaches elevations of 2000 m.

High values are in the eastern sector of the Iberian Chain, along the Mediterranean coast, where active or recent extensional faults are located (Perea et al., 2012; Simón et al., 2012). The widespread low values of local relief indicate the Iberian Chain is poorly incised by hydrography.

2.4.1.3. Longitudinal stream profiles

We extracted the longitudinal profiles of 14 main rivers draining the Iberian Chain (fig. geological map) and we quantified their shape calculating the values of the concavity index (θ), that describes the rate of change of channel gradient with respect to drainage area, and the steepness index (k_{sn}), a measure of channel gradient normalized by a reference concavity θ_{ref} =0.45 (Hack, 1957; Flint, 1974, fig long profile). As shown in Table 2.1, results indicate that most of the river profiles are characterized by low values of concavity (average value: 0.27) to respect to the values expected under steady-state conditions (θ = 0.4 - 0.6; Tarboton et al., 1989; Snyder et al., 2000; Kirby and Whipple, 2001; Whipple, 2004; Wobus et al., 2006; Whipple et al., 2007) and are far from the typical concave-up shape traditionally referred to fluvial systems in equilibrium. Conversely, the steepness index progressively increases along both southern and northern flanks of the range, reaching its highest values in the NE sector of the Iberian Chain (Mijares and Guadalope R., fig. 1). This area also shows the highest elevation of the entire chain and remnants of planation surfaces at high altitude (~2020 m a.s.l.), suggesting that the high values of k_{sn} could be indicators of a differential rock uplift.

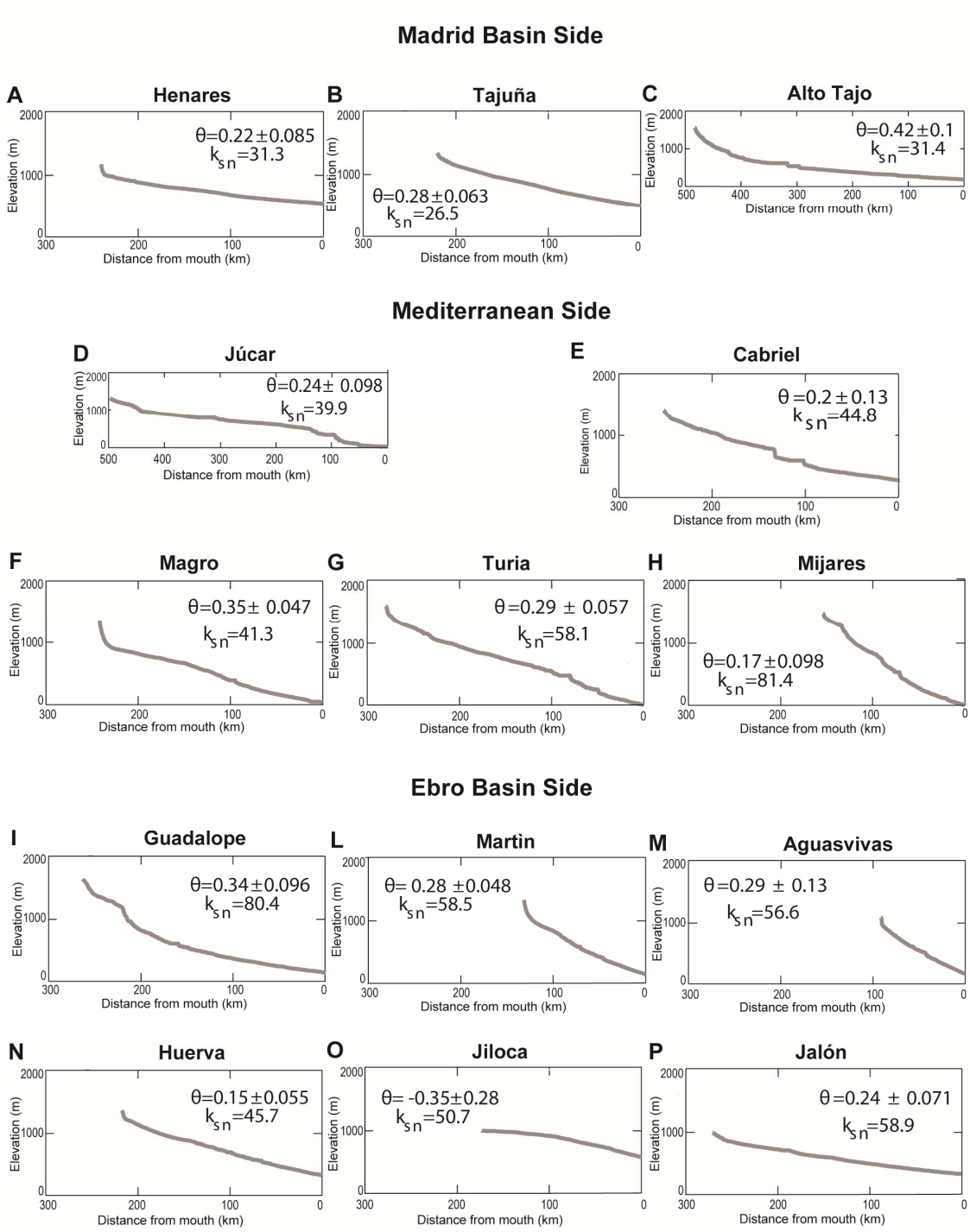

Fig. 2.4. River longitudinal profiles. A-C: Madrid Basin side rivers; D-H: Mediterranean side rivers; I-P: Ebro Basin side rivers.

Table 2.1. Morphometric indexes of the longitudinal stream profiles of the analysed rivers.

River	θ *(concavity)*	k_{sn} *(normalized steepness)*
	Madrid Basin Side	
Henares	0.22±0.085	31.3
Tajuña	0.28±0.063	26.5
Alto Tajo	0.42±0.100	31.4
	Mediterranean Side	
Júcar	0.24±0.098	39.9
Cabriel	0.20±0.130	44.8
Magro	0.35±0.047	41.3
Turia	0.29±0.057	58.1
Mijares	0.17±0.098	81.4
	Ebro Basin Side	
Guadalope	0.34±0.096	80.4
Martìn	0.28±0.048	58.5
Aguasvivas	0.29±0.13	56.6
Huerva	0.15±0.055	45.7
Jiloca	-0.35±0.28	50.7
Jalón	0.24±0.071	58.9

2.4.1.4. Incision rates

We estimated incision rates by ^{230}U-Th datings of calcareous tufas lying on strath terraces along the high courses of Martin, Ruguilla, and Alto Tajo rivers (fig 2.1, Table 2.2). The samples are almost homogeneously distributed throughout the Iberian Chain interior. The results allowed us to calculate an incision rate of 0.6 mm/yr from 105 to 41 kyr (Scotti et al., submitted). The very similar results indicate the rivers are responding to a single regional tectonic input.

Table 2.2. *Age determinations from investigated calcareous tufa deposits on strath terraces and relative incision rate values.*

River	Site	Sample	Elevation strath terrace *(m above current thalweg)*	Age *(kyr)*	Incision rate *(mm/yr)*
Ruguilla	Ruguilla	RUG 4	60	89 ± 6	0.69 ± 0.04
Tajo	Puente de San Pedro	PSP 3-1	60	105 ± 8	0.56 ± 0.04
Martìn	Las Parras de Martìn	RP 1	60	91 ± 7	0.66 ± 0.05
	Montalban	MON 3	25	41 ± 2	0.62 ± 0.03

2.4.2. Model calibration

A 300 km^2 domain is used to represent the natural region of the Iberian Chain. The shape of the real area is well approximated by the square synthetic domain. The landscape is numerically represented by a randomly sampled and triangulated set of points with x, y, z coordinates. The maximum spacing of points is 6 km ± 1.2 km (i.e. ± 20%). This grid size represents a good balance between the size of the landscape features that are analyzed and the size that allows runs to be performed in a relatively short amount of time. We implemented a river incision model considering that the average concavity index $\theta = m/n = 0.3$, as calculated for all main real rivers that drain the mountain belt using an ad hoc GIS based regression tool.

On the basis of topography, and of geomorphic, geological and morphometric constraints, we divided the Iberian Chain and its surroundings in regions defined by homogeneous uplift rates (fig. 2.5A). Area 1 includes the inner and the SW sector of the range. Here we assumed an uplift rate gently decreasing toward WSW. Conversely, along the north-eastern flank (Area 2), we hypothesized a homogeneous uplift rate,

A

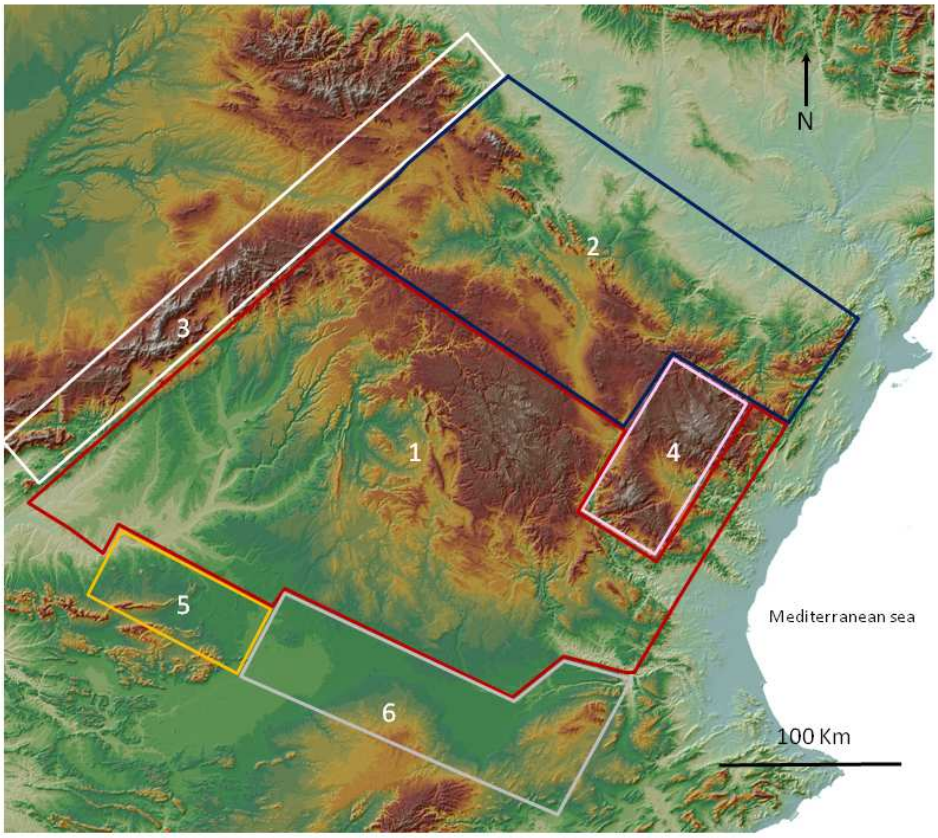

B

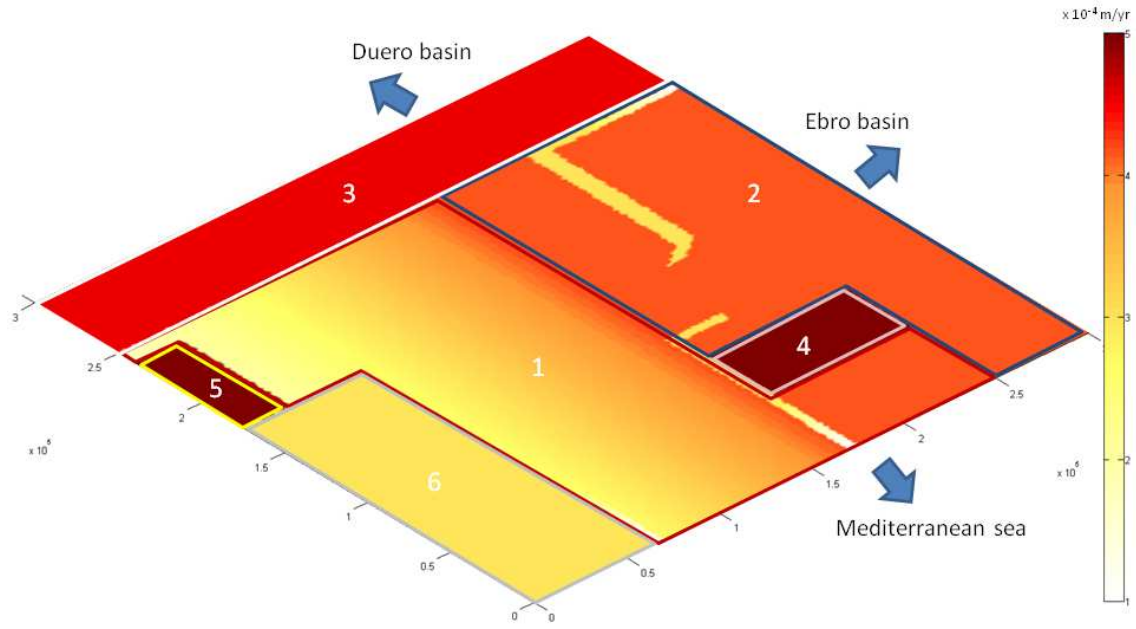

Fig. 2.5. A) areas characterized by homogeneous uplift pattern, in which the Iberian Chain has been sub-divided; B) uplift rate pattern implemented in the numerical model.

since there are no geological and geomorphic evidences that indicate a more complex uplift pattern. Here, the Calatayud and Teruel basins are included. Areas 4 represents the NE sector of the range, where we assumed the maximum uplift rate of the range. The surroundings of the Iberian Chain have been named Area 3 (Central System), Area 5 (Toledo Mountains), and Area 6 (Guadiana Basin). We perform several numerical experiments applying different uplift rates in the numbered regions (fig. 2.5). In these calibration runs, the bedrock erodibility parameter, kc, is set uniform all over the region, and it is varied at each run.

The onset of the regional uplift that affected the Iberian Chain is still highly debated. In order to add time constraints to it we list some considerations (Scotti et al., submitted):

1) The constant low local relief that characterize the entire chain, as well as the river transient state of disequilibrium, speak to a recent unique regional tectonic input.
2) The low relief upland surface is a record of stability of base-level conditions. The deposits relative to its shaping lay down into the mega-lakes that surrounded the Iberian Chain. Considering that these huge lacustrine basins lasted form many millions of years, they should be very close to sea level.
3) The adjacent Central System, that presents much higher values of local relief and rivers close to equilibrium, was affected by a rapid cooling since 5 Myr (De Bruijne & Andriessen, 2002; Ter Voorde et al., 2000).
4) The Paramo Fm. sedimentation, that is the last record of the mega-lakes surrounding the Iberian Chain as well as of the small intermontane basins, ended in Early Pliocene, indicating a strong change in base-level.

5) In the Iberian Chain interior Late Pliocene-Quaternary deposits are lacking except for small internally drained basins, suggesting the dominance of erosion processes.

These general considerations suggest that the onset should range between 2.5 and 4 Myr.

In order to set the best values of the geomorphological and tectonic parameters which produce a realistic topography, we perform a check between the real and simulated topographies at the end of each simulation; in particular, maximum, minimum and mean elevation, within each numbered area (fig. 2.5A), are used as constraint for the final model output. In every area, uplift occurs at a constant rate for all the simulations. The best fitting set of parameters is selected once the values of above-mentioned elevations on the simulated topography fit those extracted from DEM. In table 2.3 are described the ranges of parameters used for 62 simulations performed for model calibration and the values found for the final best fitting topography within each homogeneous area.

Table 2.3. Parameters implemented in the simulations and best fit values obtained.

Parameters	**Min**	**Max**	**Best topography**
K diffusion *(m^2/yr)*	$2x10^{-3}$	$1x10^{-2}$	$5x10^{-3}$
K channeling *(m^{1-2m}/yr)*	$1x10^{-5}$	$3x10^{-4}$	$1.5x10^{-4}$
m/n	0.25	0.4	0.3
Time *(yr)*	2.5 Myr	4 Myr	3.2 Myr
Max river incision rate *(m/yr)*	$1.3x10^{-4}$	$1x10^{-3}$	$2x10_{-4}$

2.5. 3-D modelling of the Iberian Chain topography

2.5.1 Initial model setups

The aim of our modeling is to reproduce how a low-relief landscape located close to sea level could evolve in response to a tectonic disturbance, depending on the scaling laws chosen and the initial topographic conditions. More in detail, to investigate the origin of the present-day topography of the Iberian Chain, we perform three models.. All of them have common features: a) the geomorphology and tectonic structures of the Iberian Chain and its surroundings during the Early Pliocene; b) a low relief surface developed under tectonic quiescence (corresponding to the modern Iberian Chain), surrounded by mountain ranges (the present-day Central System, Maestrazgo Mts.). The initial setting of the three models differs in the following features:

Setting 1: a wide uniform flat surface at around 0 m a.s.l (fig. 2.6A);

Setting 2: two wide endorheic areas (including the present Tajo, Catalayud and Teruel basins) surrounded by low-relief ranges (simulating the Central System, coastal ranges, and the Castilian and Aragonese brenches) (fig. 2.6B);

Setting 3: same as Setting 2, but including a higher relief (around 800 m) corresponding to the modern Maestrazgo Mts., Cameros Mts., and Central System (fig. 2.6C).

2.5.2 Model results

Model 1

In this model (fig. 2.6D-G), after an early stage of disorganised drainage network in the flat surface, a differential uplift (maximum rate of 1mm/yr in the central sector to 0,3 mm/yr along the flanks) occurs inducing head-ward fluvial erosion. Knickpoints rapidly

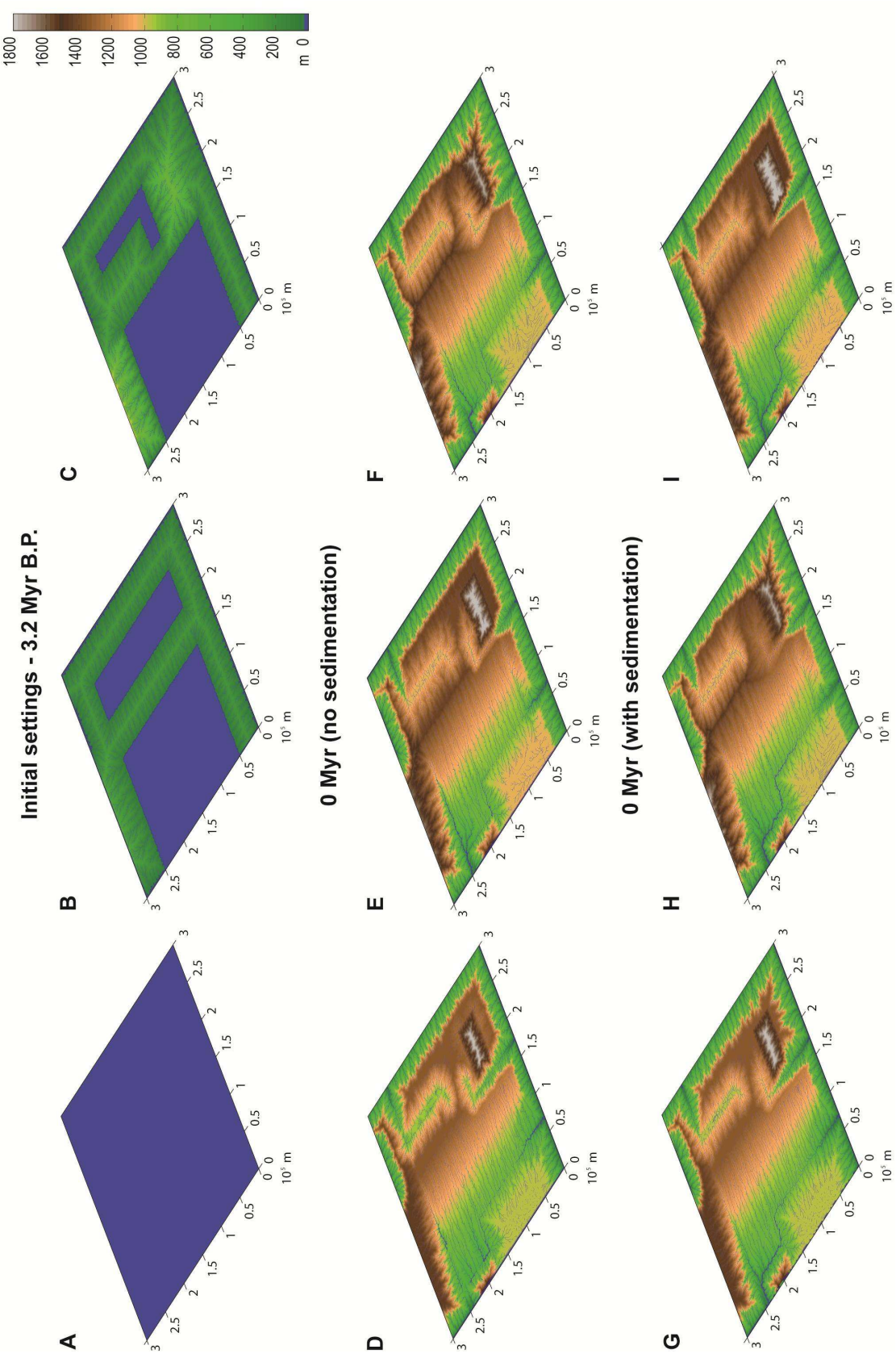

Fig. 2.6. A-C: initial conditions; D-F: topographies shaped by fluvial and hillslope erosion, obtained from setup A-C, under uplifting condition, after running the model for 3.2 Myr; G-I: topographies obtained with the implementation of sedimentation processes.

integrate into the uplifting topography that reaches a maximum elevation of 1300 m after ~3 Myr (table 2.4).

A smoothed low-relief landscape characterizes the interior of synthetic Iberian Chain (fig. 2.6D). It contrasts with deeply incised fluvial valleys cutting into the massif flanks. Since the initial condition is a flat surface, the capture of the internally drained intermontane basins occurs at around 2.5 Myr. Conversely, the simulation of sedimentation in the basins leads to a delay in river piracy (fig.2. 6G).

Models 2 and 3

These two models are very similar (fig. 2.6E-F-H-I), but differences in pre-existing topography strongly influence the head-ward fluvial erosion. The topographic barriers prevent an early capture of the intermontane basins. The delay in river integration into the Iberian Chain induces a pronounced difference between the low-relief surface and the fluvial valley incising the massif flanks. Similarly, the transition from endorheic to esorheic drainage occurs in both models at around 1 Myr (fig. 2.6E-F-H-I). Conversely, the small intermontane basins in the N-NE margin are captured later (around 0.5 Myr) (fig. 2.6E-F-H). In Model 3, the sedimentation in the small intermontane basin corresponding with the present Teruel basin favors its capture by synthetic Turia R. at ~1.2 Myr. In this model, the synthetic landscape reaches elevation similar to the real ones after 3.2 Myr with an uplift rate in the inner sector of 0.45 mm/yr that decreases to 0.25 mm/yr along the flanks, while in the NE sector (Maestrazgo Mts.) is of 0.5 mm/yr (table 2.4). Moreover, the models predict a maximum long-term erosion rates of 0.2 mm/yr (table 2.3). The values of 0.4-0.5 mm/yr are consistent with those calculated from radiometric dating (see § 1.4 and 2.4.1.4).

Table 2.4. Uplift rates implemented in the simulations and best fit values obtained

Uplift rates for each sub-area *(m/yr)*	**Min**	**Max**	**Best topography**
1(gradient)	$1.25x10^{-4}$ - $4x10^{-4}$	$3x10^{-4}$ - $7x10^{-4}$	$2.5x10^{-4}$ – $4.25x10^{-4}$
2	$3x10^{-4}$	$1x10^{-3}$	$4.25x10^{-4}$
3	$4x10^{-4}$	$1x10^{-3}$	$4.5x10^{-4}$
4	$5x10^{-4}$	$1x10^{-3}$	$5x10^{-4}$
5	$5x10^{-4}$	$1x10^{-3}$	$5x10^{-4}$
6	$1.25x10^{-4}$	$5x10^{-4}$	$3x10^{-4}$

2.6. 2-D Modeling of major river profiles

We use simulation of river profiles through time to test which value of erodibility of bedrock *k* fits the real river profile, minimizing the error between simulated and real profiles. The convex-up shape of a river profile is given by the following equation:

$$\frac{dz}{dt} = Ui - ki * Ai^m * Si^n \quad (1)$$

describing the change of elevation for each point *i* of the profile at a given time step *dt*. The first term on the right represents the tectonic uplift rate of the surface on which the river flows, while the second term describes the river incision rate into bedrock, also called the stream power law. Bedrock incision rates are proportional to the parameter *k* or bedrock erodibility. It has been demonstrated that if all governing parameters in eq. (1) are constant through time, at a certain time *t* the uplift rate and incision rate are equal for all points along the profile. In this case we say that the river is in steady state condition. In this study, we model river profiles using data of real rivers, such as

drainage area *A* and channel slope *S* extracted from a 30m DEM of Spain, together with *m*, *n* and *U* parameters in equation (1), obtained by using ad-hoc tools for geomorphlogical analysis of raster data. In particular we use simulations to test the values of *k*, which is unknown and difficult to be straightforward constrained from real profile analysis. Iterative variation of the value of *k*, allows to obtain a final simulated profile similar to the real one. Starting from a guess value of *k*, we use a method to minimize the average error in elevation between the simulated and real profile. The average error between the real and modeled profile can be written as:

$$e_{k_i} = \frac{1}{N}\sum_{i=1}^{N} zi_{sim} - zi_{real} \quad (2)$$

and it is calculated at the end of each simulation for all *n* points along the synthetic profile, and for each new tested value of k_i. Since k_i varies at each simulation, and a change in *k* results in a change in the final simulated profile, then the average error e_{ki} can be defined by the function *f(k)*. *f(k)* describes how well the simulated profile, using the assumed value of k_i, approximates the real profile. The next iteration is performed computing the new value k_{n+1} which must satisfy the condition:

$$f(k_n) \geq f(k_{n+1}) \quad (3).$$

We apply the "gradient descent" method, a first-order optimization algorithm used in numerical analysis to find local minima of a given function, to find the best fitting values of *k* from river profiles. “Gradient descent” is based on the assumption that *f(k)* decreases if steps are taken proportional to the negative of the gradient of the function in the initial point, e.g. k_1.

We can write the gradient of *f(k)* as follows:

$\frac{df}{dk} = -\nabla f(k_1)$ (4),

which provides the direction of the local minimum of this function, starting from the initial guess for minimum k_1.

It follows that if and only if:

$f(k_{2)} = f(k_1) - \gamma\nabla(k_1)$ (5)

(with γ small enough), we obtain $f(k1) \geq f(k2)$.

When this condition is satisfied, the gradient $\nabla f(k)$ is negative for k values increasing or decreasing from k_1 to k_2. The first step in "gradient descent" algorithm consists of picking a guess value k_1 for the local minimum of $f(k)$, considering the sequence of values $k1, k2, k3,..., kn$ such that:

$f(k_{n+1}) = f(k_n) - \gamma\nabla f(k_n),\ n > 0$ (6).

For each value of k, a sequence of $f(k)$ values is then obtained:

$f(k_1) \geq f(k_2) \geq f(k_3) \geq \ ... \geq f(k_n)$ (7).

Such sequence of $f(k)$ values converges toward the desired local minimum. It must be noticed that γ changes at each iteration and represents the amount that must be added to k_1 and to obtain the next value k_2; γ is calculated with the following equation:

$f(k_n) \ - \gamma_n * \nabla f(k_n) = 0$ (8)

where $f(k_n)$ is the average error resulting from a simulation, k_n is the value of bedrock erodibility picked in the previous iteration; $\nabla f(k_n)$ is calculated using $f(k_n)$, $f(k_{n-1})$, k_n and k_{n-1}.

Hence we calculate γ_{n+1}:

$$\gamma_{n+1} = f(k_n)/\nabla f(k_n) \quad (9).$$

The iterative calculation of k stops when a value of $f(k)$ is found such that:

$$f(kn) \leq \varepsilon \quad (10),$$

where ε is an arbitrary value, small enough, and represents the average error tolerance. Calculating the sequence of k_n following the "gradient descent", $f(kn)$ will tend to zero and the corresponding value of k_n can be considered as a good approximation for the local minimum of $f(k)$.

In fig. 2.7 is represented an example of the use of "gradient descent" to minimize the error between a simulated profile and a real one. The profile of the real river is represented by the solid blue curve in the same figure. All variables and parameters in equation (1) are known, except for the value of k to be tested. We make the assumption that at an initial time t_0 the river profile evolves on a flat surface, represented by a straight line at uniform elevation z=0, and that the unknown erodibility parameter k is uniform along the whole river course, as well as the uplift rate U=0.3 mm/y. The first run is performed using a guess value $k1 = 1.5 \times 10^{-4}$. We consider that the final profile (present-day river profile) is achieved at time t=3My (the red dot curve in fig. 2.7), then

the average error between simulated and real profile is calculated. Evaluating the direction to the negative gradient of *f(k)* in *k1*, the increase γ_{n+1} is computed according to equation (10). For the case represented in fig. 2.7, $\nabla f(k)$ is negative for $k > 1.5\times10^{-4}$.

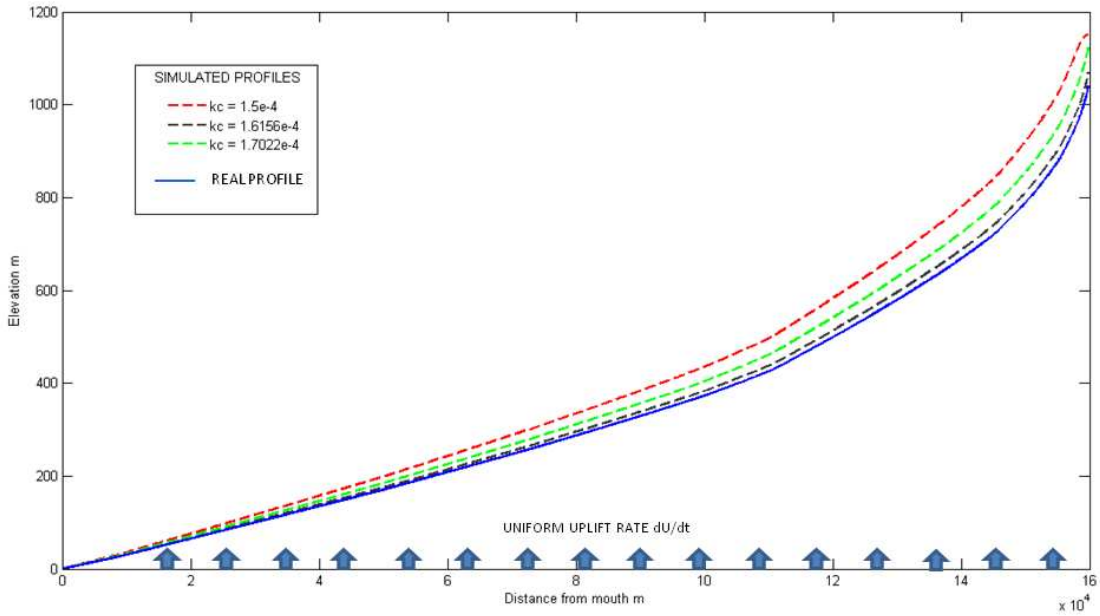

Fig. 2.7. Example of the results for iterative variations of the value of *k* to minimize the error between a simulated stream profiles (dotted lines) and a natural stream profile (solid blue curve) under homogenous uplift conditions.

The computed value of γ_{n+1} is added to k_1, and a new value k_2 is obtained, e.g. $k_2 = 1.6156\times10^{-4}$,as shown in fig. 2.7. Equation (5) predicts that $f(k_2) < f(k_1)$. In fact, computing the sequence of *k* values to the direction of the negative gradient of *f(k)*, following the "gradient descent" algorithm, the simulated profile approaches the real profile and average error e_{ki} is more and more minimized. In fig. 2.8 a plot of *k* and *f(k)* values computed for this example is shown: it can be observed that sequential increases of k_i produce a decrease of e_{ki} values, which gradually tend to zero (condition of local minimum achieved). If $f(k) \leq \varepsilon$, where $\varepsilon = 0.08$ in this case, the best value of *k* is found ($k_3 = 1.7496=10^{-4}$ in figures 2.7-2.8), which sufficiently minimizes the average error e_{ki}.

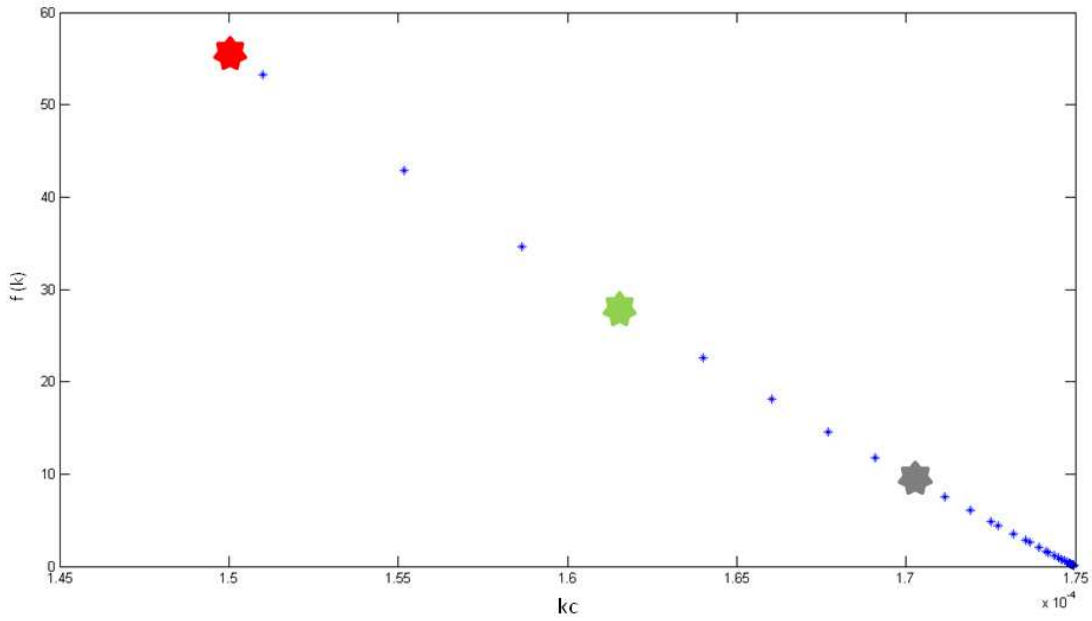

Fig. 2.8. *k* and *f(k)* plot relative to the example of fig. 2.7, showing that the best fit conditions between simulated and natural stream profiles are achieved when *f(k)* decreases to a value $\leq \varepsilon$.

In practice, it is very diffcult to find a river in steady-state conditions, showing a profile as smooth as the example shown in fig. 2.7. In most real cases it is possible indeed to observe sharp slope changes along stream profiles, known with the term "knickpoint". A knickpoint can be created during the natural evolution of a river for different causes: a) changes of bedrock erodibility (lithologic knickpoint), b) base-level changes, c) discharge and sediment load fluctuations, due for example to drainage area piracy among adjacent catchments, or to climate changes at global or regional scale (alternating wet and dry phases).

For the cases shown in this work, we assume that changes in bedrock erodibility *k* along a stream channel exerts a first-order control on all simulated river profiles. Our approach to model river profiles is well illustrated by the example shown in fig. 2.9: a river profile evolves starting from a flat surface uplifted at a constant and uniform uplift rate U = 0.3 mm/y. In this example we have reconstructed a synthetic stratigraphic

model, consisting of a relatively more erodible layer overlapping a relatively less erodible layer: k_1 and k_2 are bedrock erodibility parameters for the upper and lower layer, considering $k_2<k_1$. The lower layer lies initially at a depth of 500 m under the flat surface and both layers have an extent equal to the distance from the source of the river to the mouth. As observed in natural rivers with similar conditions, the river evolves starting from the mouth by upstream erosion. At the end of each time step *dt*, the amount of incision of the river into bedrock dz_{chan}/dt is computed for all points along the profile. If the cumulative amount of incision at a certain time step *t* reaches the depth of the uplifted contact between the two different layers, k_2 replaces k_1 in eq. (1) and a "lithological" knickpoint propagates upstream on the profile. As can be observed in fig. 2.9, the knickpoint coincides with a transition zone between two reaches of the profile with different slopes. In this case the knickpoint propagates upstream following

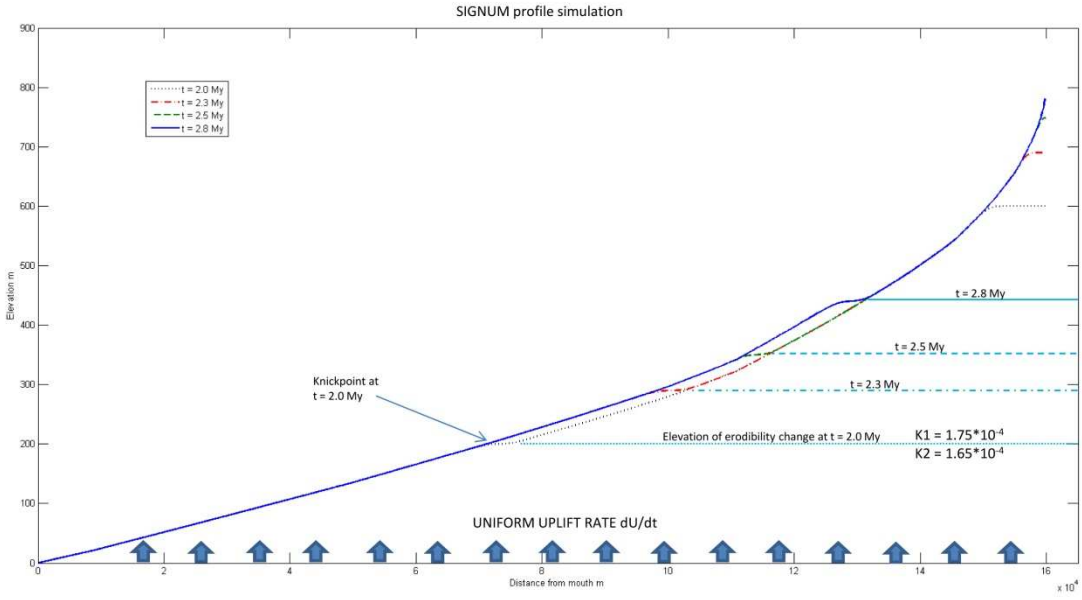

Fig. 2.9. Synthetic stream profile obtained starting from a flat surface under homogeneous uplift conditions (uplift rate U = 0.3 mm/y), implementing a bedrock characterized by two lithologies with different erodibility ($k_2<k_1$). The river evolves starting from the mouth by upstream erosion. When incision reaches the depth of the uplifted contact between the two different layers, a "lithological" knickpoint propagates upstream on the profile.

the model of "slope replacement".

any knickpoints can be found on the same real profile, representing many changes in bedrock erodibility *k*.

Applying the same approach used in the previous modeled examples, we develop a method similar to "gradient descent", adapted to be used in the case of numerous changes in slope that may occur in a river profile.

In fact, "Gradient descent" is an approach similar to Euler's method for solving ordinary differential equations.

The forward explicit Euler's method is a first-order numerical procedure for solving ordinary differential equations (ODEs) with a given initial value. It is the most basic explicit method for numerical integration of ordinary differential equations and is the simplest of Runge–Kutta methods. In numerical analysis the Runge–Kutta methods are an important family of implicit and explicit iterative methods for the approximation of solutions of ordinary differential equations.

Forward Euler's method can be thougth of as the following example: consider the problem of calculating the shape of an unknown curve which starts at a given point x_0 and satisfies a given differential equation. Here, a differential equation can be thought of as a formula by which the slope of the tangent line to the curve can be computed at any point on the curve, once the position of that point has been calculated.

The idea is that while the curve is initially unknown, its starting point, which we denote by x_0 is known. Then, from the differential equation, the slope to the curve at x_0 can be computed, and so, the tangent line. If we take a small step along that tangent line up to a point x_1, along this small step, the slope does not change too much, so x_1 will be close to the curve. If we pretend that x_1 is still on the curve, the same reasoning as for the point

x_0 above can be used. After several steps, a polygonal curve x_0, x_1, x_2, x_3, … x_n is computed. In general, this curve does not diverge too far from the original unknown curve, and the error between the two curves can be made small if the step size is small enough and the interval of computation is finite.

The first step in using the forward explicit Euler method to model river profiles consists of a discretization of our river profile in *n* reaches, as many as the major slope changes found in the real profile, along the X axis, which represents the distance from the mouth. In figures 2.10 are illustrated the fitting runs performed on a real profile (solid blue curve) using the forward Euler method. According to the previous examples, a first simulation is performed on the first upstream reach on the profile, in the total time interval (e.g. t=3 My). We use a first guess value for bedrock erodibility k_1, namely the value we want to test as a minimum for *f(k)*. Hence, we apply the iterative "gradient descent" method to minimize the average error between the first reach of the simulated and the corresponding reach on the real profile. Once the first best fitting value of k_1 is found, the simulation is performed considering the next reach on the profile, and so on for all *n* reaches. In the example shown in figures 2.10, the profile has been discretized into three reaches, assuming that each reach can be modeled with different values of *k*. After *n* iterations on each reach, an average global error e_{kn} is obtained, whose value is less than or equal to the global error tolerance ε. The final result is represented by a synthetic river profile, providing the best approximation for the real irregular curve. As a consequence, the sequence of changes in bedrock erodibility *k* can be reconstructed along the real profile. In fig. 2.10C are shown the best fitting values values for k_1, k_2, k_3 obtained using the forward Euler method.

A

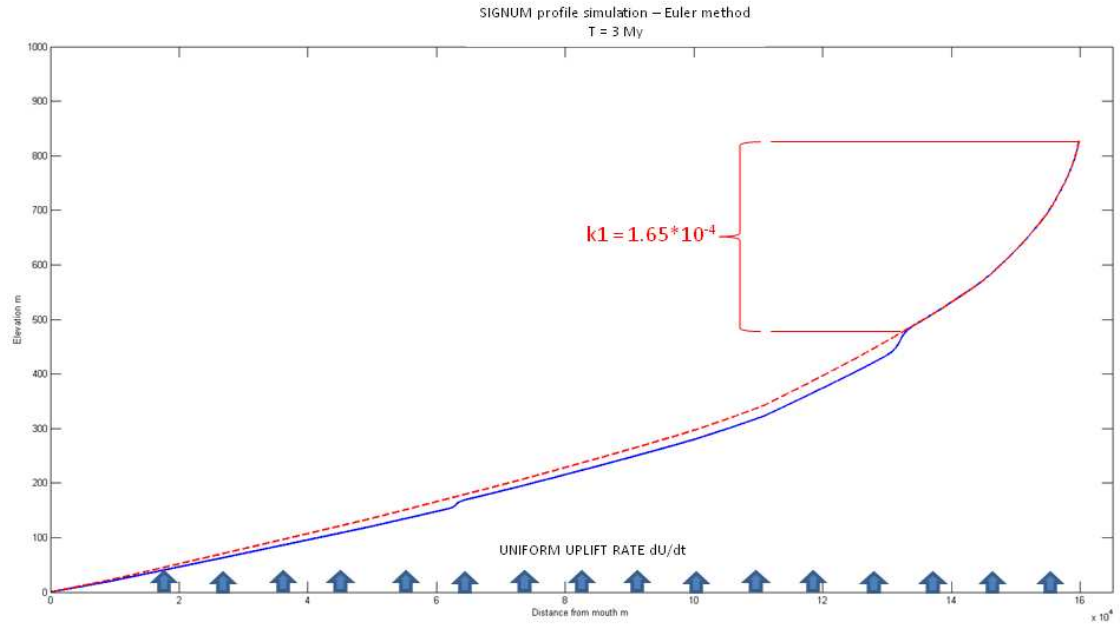
SIGNUM profile simulation – Euler method
T = 3 My
k1 = 1.65*10-4
UNIFORM UPLIFT RATE dU/dt
Elevation m
Distance from mouth m
x 10^4

B

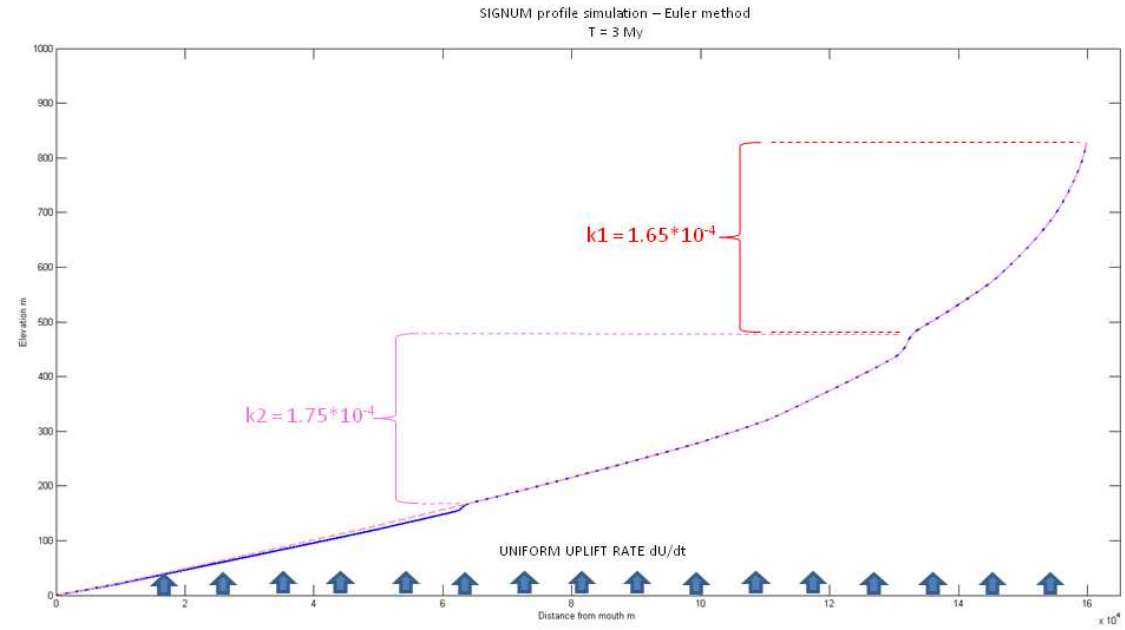
SIGNUM profile simulation – Euler method
T = 3 My
k1 = 1.65*10-4
k2 = 1.75*10-4
UNIFORM UPLIFT RATE dU/dt
Elevation m
Distance from mouth m
x 10^4

C

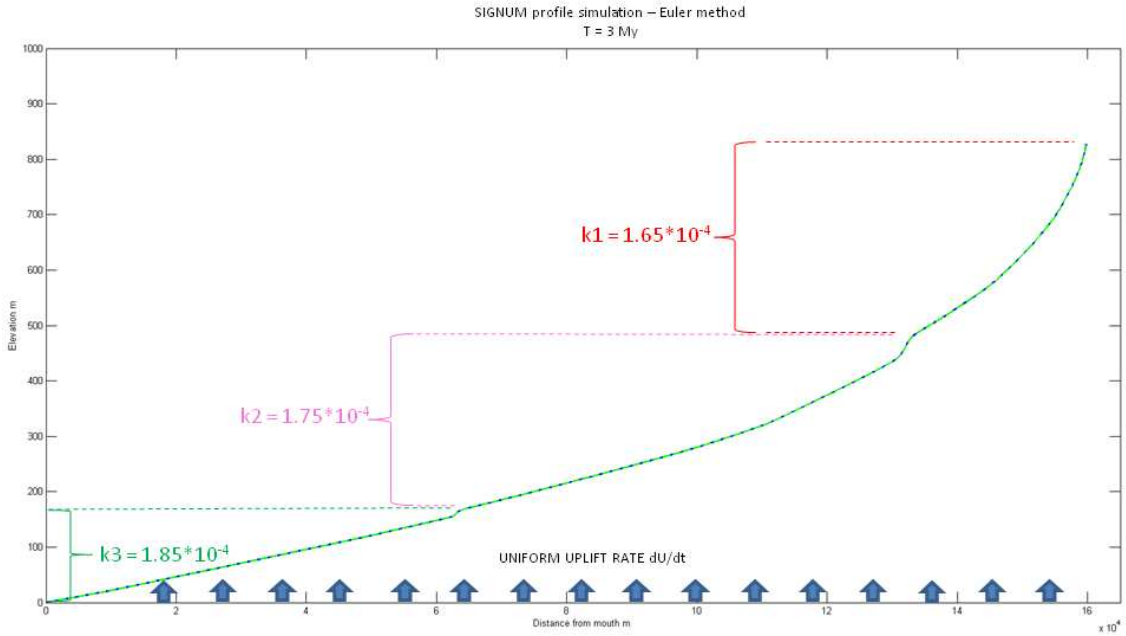

Fig. 2.10. Example of iterations implemented to achieve a synthetic stream profile (dotted lines) that provides the best approximation of a natural irregular curve (solid blue line). The real stream profile is discretizated in 3 reaches. The simulation is performed finding the best fitting value of *k* between natural and synthetic stream profiles firstly for the upstream reach (A), then for the next reach (B) and one-by-one to the mouth of the river (C).

2.6.1. Model results

Table 2.5. Best fit parameters obtained from the 2D inversion of synthetic longitudinal river profiles and the comparison with natural stream profiles.

River	Bedrock erodibility *k* (min-max)	Average error *ε* *(m)*	m, n	Average incision rate *(mm/yr)*
Tajo	1.5-4.8x10^{-4}	0.97 m	0.3, 1	0.52
Tajuña	2.1-4.8x10^{-4}	0.068 m	0.3, 1	0.4156
Mijares	1.05-1.85x10^{-4}	0.94 m	0.3, 1	0.5696

The optimal *k* values (see Table 2.5) obtained from river modeling of the Tajo, Tajuña and Mijares stream profiles correspond to the sedimentary rocks outcropping in the watersheds, as expected from the analysis of the lithologies in the three catchments (see lithology bars in fig. 2.11) and as inferred by previous studies on river modeling (Stock and Montgomery, 1999; Kirby and Whipple, 2001). The good correspondence is also strengthened by the little variation of modeled *k* values in these three rivers using *m*=0.3 and *n*=1. In the higher part of the Tajo River, between 500-400 km of distance from mouth (see Fig. 2.11A), the bedrock is mostly represented by carbonatic rocks, the uplift is almost constant because the river flows perpendicular to the modeled uplift gradient, and *k* assumes values between $1.4x10^{-4}$ $m^{0.4}$ yr^{-1} and $2.5x10^{-4}$ $m^{0.4}$ yr^{-1}: the lower *k* values represent the stronger lithologies of the carbonatic rocks (dolomites and dolomitic limestones), conversely the higher *k* values correspond to the weaker limestones types. In the middle part of the Tajo R. (between 400 – 300 km of d.f.m), the relative higher *k* values obtained ($2.7x10^{-4}$ $m^{0.4}$ yr^{-1} – $3.2x10^{-4}$ $m^{0.4}$ yr^{-1}) can be linked to the more erodible outcropping sedimentary rock types. In this part, the Tajo R. flows out of the highest part of the Iberian Range and then reaches the Madrid Basin, along the direction of the uplift gradient. A regular increase of *k* values is obtained in the lower part of the Tajo R., ranging between $4.8x10^{-4}$ $m^{0.4}$ yr^{-1} for clayey lithologies (between 300 – 200 km d.f.m.) and $4.5x10^{-4}$ $m^{0.4}$ yr^{-1} for the last reach of the profile (200-0 km d.f.m.). In the Tajuña R. we obtain a similar variation of *k* values in the upper part of the profile (400-300 km of d.f.m), with *k* ranging between $2.1x10^{-4}$ $m^{0.4}$ yr^{-1} - $2.5x10^{-4}$ $m^{0.4}$ yr^{-1} for carbonatic rock types and $2.7x10^{-4}$ $m^{0.4}$ yr^{-1} – $2.9x10^{-4}$ $m^{0.4}$ yr^{-1} for the clayey and arenaceous alternations. The Tajuna R. is a tributary of the Tajo R., hence the lower part of the profile (190 - 0 km of d.f.m.) is the same as for the Tajo R. (see Fig. 2.11B). In the Mijares River, where we assume that the uplift is uniform along the profile, the k values vary in a range between 1x10-4 –

A

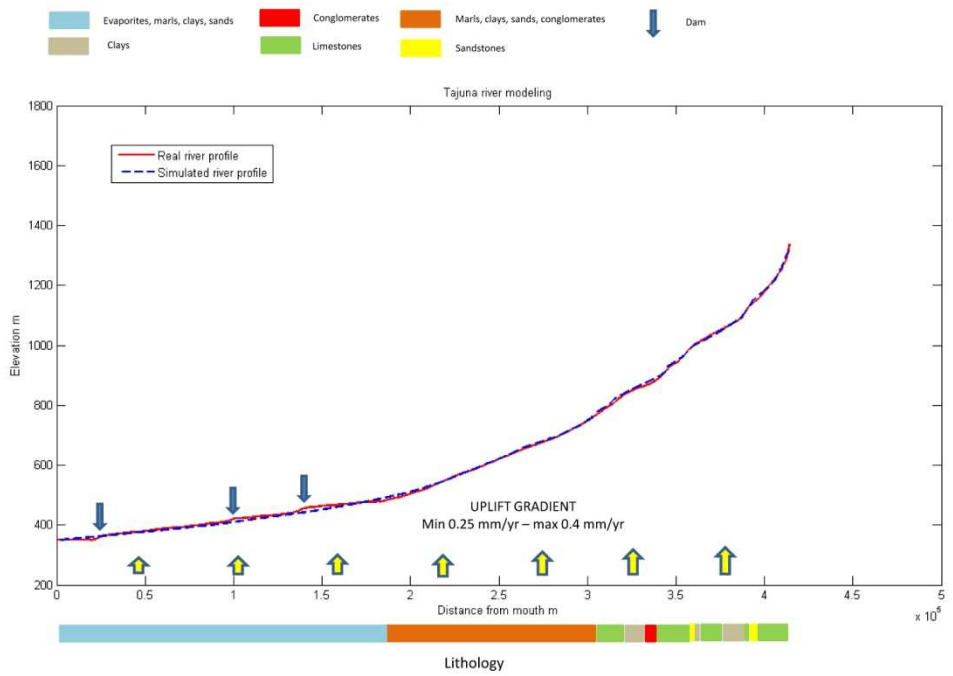
Evaporites, marls, clays, sands
Conglomerates
Marls, clays, sands, conglomerates
Dam
Clays
Limestones
Sandstones
Tajuna river modeling
Real river profile
Simulated river profile
Elevation m
UPLIFT GRADIENT
Min 0.25 mm/yr – max 0.4 mm/yr
Distance from mouth m
x 10^5
Lithology

B

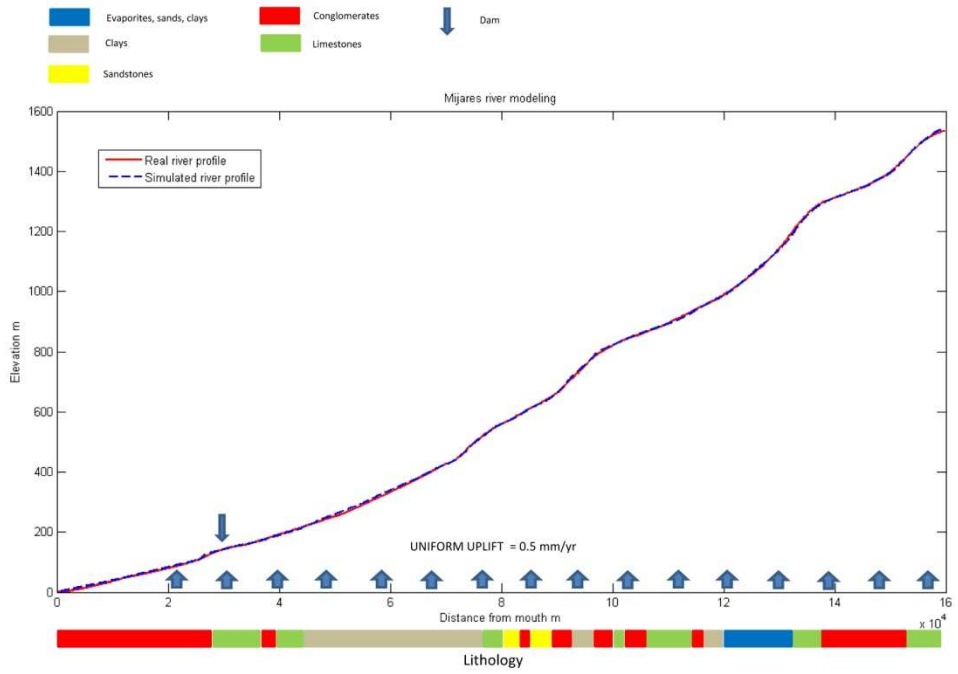
Evaporites, sands, clays
Conglomerates
Dam
Clays
Limestones
Sandstones
Mijares river modeling
Real river profile
Simulated river profile
Elevation m
UNIFORM UPLIFT = 0.5 mm/yr
Distance from mouth m
x 10^4
Lithology

C

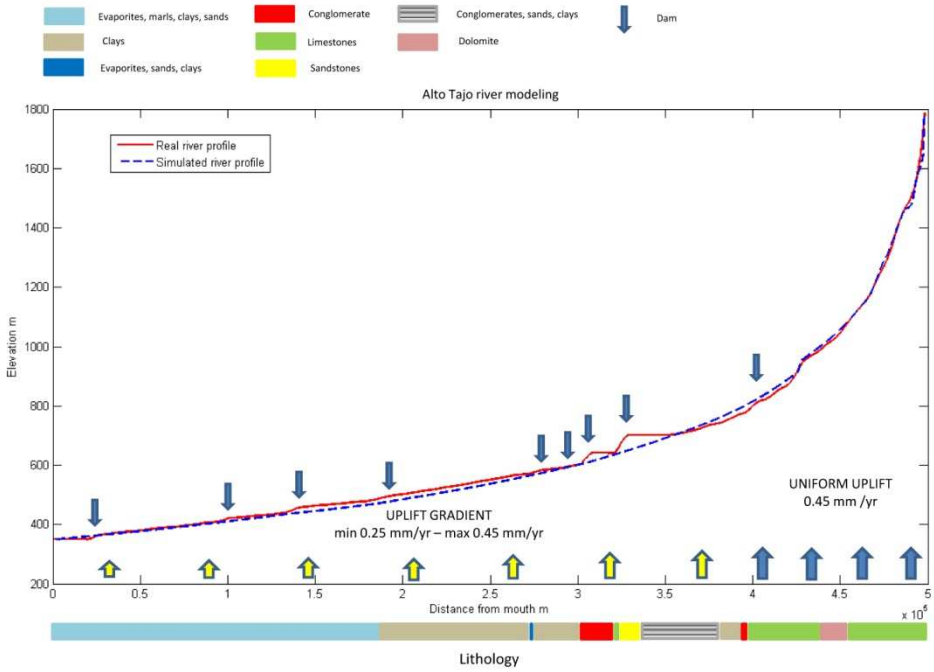

Fig. 2.11. Comparison between the natural stream profiles (solid red lines) of Tajo (A), Tajuña (B) and Mijares (C) R and the synthetic profiles (dotted blue lines) obtained from 2-D inversion and taking into account the erodibility of outcropping litologies.

$1.9x10^{-4}$ $m^{0.4}$ yr^{-1}: the narrower variability of k shows a correspondence with the higher frequency of dolomites, limestones and conglomerates in the Mijares R. catchment compared to the Tajo R. and Tajuna R. Most of the irregularities in the Mijares R. profile can be explained by the higher presence of relatively less erodible rocks (namely limestones, domlomites and conglomerates) alternated to short reaches consisting of weaker bedrock lithologies, (see lithology bar represented below in fig. 2.11C), which allows us to conclude that these knick-zones are mainly lithologically controlled.

The analysis of the concavity of the modeled rivers shows that, even if the intrinsic concavity of the stream power model is m/n = 0.3/1, the modern profile concave shape depends on the orientation of the stream with respect to the rock-uplift gradient existing in the Iberian Chain, and on the lithologic variability along the river course. For

example, the modern Tajo R. shows a higher concavity (0.4) compared to both the Tajuna R. (0.28) and Mijares R. (0.17). The modeling provides a good explanation for this geomorphological feature: most of the higher part of the Tajo river flows through the Iberian Chain, where we assume it has experienced a higher uplift rate compared to the lower part, where the river flows along a decreasing uplift gradient. In addition to the modeled uplift pattern, the bedrock in the upper part of the profile is characterized by more resistant lithologies than in the lower part, as calculated from the profile analyis. Furthermore the irregular concave-up shape of the three river profiles confirms that they are far from steady-state and responding to a recent regional uplift pulse.

The average erosion rates calculated in the last 200 kyr from river profile modeling are also consistent with the erosion rates estimated by U-Th dating of calcareous tufas lying on strath terraces along the courses of Martin, Ruguilla, and Alto Tajo rivers.

2.7. Discussion

The results of the 3D modeling of the Iberian Chain presented in this work show that the hypothesis of a Plio-Quaternary uplift stage of the low-level topography of the Iberian Chain, as interpreted by the previous geomorphological analysis, can explain the observed modern topography and drainage network organization. In particular, the uplift pattern used in the landscape evolution model allows to obtain an optimal topography presenting many features similar to the modern one, such as the uplifting margins of the Iberian Chain, which hampered the erosion of the internally drained basin, the capture of intermontane basins during Late Pleistocene, and the consequent reversal of drainage network in the marginal areas of these basins. The model results suggest that the uplift rates are of the order of 0.25-0.5 mm/yr, which is compatible also with the recent incision rates extracted from strath terraces in the Iberian Chain. Furthermore, the

regional uplift pattern implemented in the model is consistent with the achievement of the actual topography after 3 Myr.

The average erosion rates resulting from the 3-D modeling (0.2 mm/yr) are slightly lower than the incision rates obtained from U/Th dating, suggesting that the optimal value of *k* found for the best fitting topography (*k*=1.5x10-5) cannot be considered as uniform in all the Iberian Chain region during the Plio-Quaternary evolution. A finer reconstruction of the erodibility parameter by 2-D river profile modeling have helped to get values of incision rates similar to those obtained from dating techniques. Furthermore, the erosion coefficient used in the stream power model falls in a range of values ($1x10^{-4}$ – $4.8x10^{-4}$ $m^{0.4}$ yr^{-1}) similar to the estimates of sedimentary rocks published in previous works (Stock and Montgomery, 1999, Kirby and Whipple, 2001).

Our numerical analysis of stream profiles also corroborates the uplift pattern implemented in the 3D model of the Iberian Chain and the strong control that lithology exerts on the channel slope in this area. Furthermore, the results demonstrate the potential of the profile gradient analysis and fitting method presented in this study as a quantitative mean to understand the response of real channels to the spatial variability of bedrock uplift and erodibility.

2.8. Conclusion

We investigated the long-term evolution of an uplifting landscape shaped by fluvial and hillslope erosion. We employed the numerical landscape evolution model SIGNUM, which combines hillslope erosion, fluvial erosion, and is driven by boundary conditions (uplift and relief). The model integrates present-day geomorphological, geomorphic and geological datasets: mean elevation location of thresholds, shape of longitudinal stream

profiles and relative intrinsic concavity and steepness indexes, incision rates, post-depositional deformation, erodibility of the outcropping lithologies.

The model used has been applied to the present-day topography of the Iberian Chain.

We proceeded the following steps:

- reconstruction of three different initial settings;
- model running for 4 Ma for the examined initial conditions ;
- comparison of model predictions with natural topography in a transient stage and after 4 Ma;
- selection of the best initial set up;
- implementation of sedimentation processes;
- validation of the model by the inversion of synthetic longitudinal profiles.

We conclude that:

1) the onset of the tectonic uplift occurs at ~3.2 Myr;

2) the estimate uplift rates are non-uniform and range between 0.5 mm/yr in the interior sector to 0.25 mm/yr;

3) the inversion of the drainage network and the opening of the internally drained basins occurs after the onset of the uplift, and starts at around 2 Ma, confirming what supposed in previous studies on basis of field evidences and geochronological data;

4) coupled regional uplift and topographic barriers preserve the landscape in the inner Iberian Chain at high elevation through time.

References

Alcalá, L., Alonso-Zarza, A. M., Álvarez Sierra, M. A., Azanza, B., Calvo, J. P., Cañaveras, J. C., van Dam, J.A., Garcés, M., Krijgsman, W., van der Meulen, A.J., Morale, J., Peláez-Campomanes, P., Pérez Gonzalez, A., Sánchez Moral, S., Sancho, R., Sanz Rubio, E., 2000. El registro sediment ario y faunístico de las cuencas de Calatayud-Daroca y Teruel. Evolución paleoambiental y pal eoclimática durante el Neógeno. Revista de la Sociedad Geológica de España, 13, 323–343.

Alonso-Zarza, A., 2008. El Neógeno: de las crisis tectónicas a la tranquilidad de los lagos someros. In: Calonge, A., Rodríguez, M.,Segura M. (Eds.), Geología de Guadalajara, Guadalajara (Spain), 151–165.

Alonso-Zarza, A., Calvo, J., 2000. Palustrine sedimentation in an episodically subsiding basin: the Miocene of the northern Teruel Graben (Spain). Palaeogeography, Palaeoclimatology, Palaeoecology, 160, 1–21.

Álvaro, M., Capote, R., Vegas, R., 1979. Un modelo de evolución geotectónica para la Cadena Celtibérica. Acta Geológica Hispanica, 14, 172-177.

Anadón, P., Moissenet, E., 1996. Neogene basins in the Eastern Iberian Range. In: Friend, P., Dabrio C., Tertiary basins of Spain, the stratigraphic record of crustal kinematics. Cambridge University Press, Cambridge (UK),. 68-76.

Anadón, P., Moissenet, P., Simón, J., 1990. The Neogene Grabens of the Eastern Iberian Chain (Eastern Spain). In: Agustí, J., J. Martinell, Iberian Neogene Basins: Field Guideboook.. Paleont. Evol. Especial Publ., 2, 97 – 130.

Armenteros, I., Dabrio, C., Guisado, R., Sanchez de Vega, A., 1989. Megasecuencias sedimentarias del terciario del borde oriental de la Cuenca de Almazan (Soria – Zaragoza). Studia Geologica Salmanticensia, Special Volume 5, 107–127.

Birot, P., 1959. Esquisse morphologique des Monts Celtibériques orientaux. Bull. Comm. Trav. Hist. Sci., Sect. Geogr., 72, 101–130.

Braun, J. and M. Sambridge, 1997. Modelling landscape evolution on geological time scales: a new method based on irregular spatial discretization. Basin Research, 9, 27-52.

Calvo J.P., Daams, R., Morales, J., López-Martínez, N., Agusti, J., Anadon, P., Armenteros, I., Cabrera, L., Civis, J., Corrochano, A., Diaz-Molina, M., Elizaga, E., Hoyos, M., Martin-suarez, E., Martinez, J., Moissenet, E., Muñoz, A., Perez-Garcia, A., Perez-Gonzalez, A., Portero, J.M., Robles, F., Santisteban, C., Torres, T., van der

Muelen, A.J., Vera, J.A., Mein, P., 1993. Up-to-date Spanish continental Neogene synthesis and paleoclimatic interpretation. Revista de la Sociedad Geológica de España, 6, 1–16.

Casas-Sainz, A.M., Faccenna, C., 2001. Tertiary compressional deformation of the Iberian Plate. Terra Nova, 13, 281-288.

Courant, R., Friedrichs, K. & Lewy, H., 1967. On the partial difference equations of mathematical physics. IBM Journal, 215-234.

De Bruijne, C., Andriessen, P., 2002. Far field effects of alpine plate tectonism in the Iberian microplate recorded by fault-related denudation in the Spanish Central System. Tectonophysics, 349, 161–184.

Foufoula-Georgiou, E., Ganti, V. & Dietricht, W.E., 2010. A nonlocal theory of sediment transport on hillslopes. Journal of Geophysical Research, 115, F00A16.

Flint, J. J., 1974. Stream gradient as a function of order, magnitude, and discharge. Water Resources Research, 10, 969–973.

Gasparini, N.M. & Brandon, M.T., 2011. A generalized power law approximation for fluvial incision of bedrock channels. Journal of Geophysical Research, 116, F02020.

Gasparini, N.M., Whipple, K.X. & Bras, R.L., 2007. Predictions of steady state and transient landscape morphology using sediment-flux-dependent river incision models. Journal of Geophysical Research, 112, F03S09.

Gómez, J.J. & Fernández-López, S.R., 2006. The Iberian Middle Jurassic carbonate-platform system: Synthesis of the palaeogeographic elements of its eastern margin (Spain). Palaeogeography, Palaeoclimatology, Palaeoecology, 236 (3–4), 190–205.

Gracia-Prieto, F. J., Gutiérrez-Elorza, M., Leránoz Istúriz, B., 1988. Las superficies de erosión neógenas en el sector central de la Cordillera Ibérica. Revista de la Sociedad Geológica de España, 1 (1-2), 135-142.

Guimerà, J., Más, R., Alonso, A., 2004. Intraplate deformation in the NW Iberian Chain: Mesozoic extension and contractional inversion. Journal of Geological Society of London, 16, 291–303.

Gutiérrez, F., 1996. Gypsum karstification induced subsidence: effects on alluvial systems and derived geohazards (Calatayud Graben, Iberian Range, Spain). Geomorphology, 16, 277–293.

Gutiérrez, F., Gutiérrez, M., Gracia, F. J., Mc Calpin, J. P., Lucha, P., and Guerrero, J., 2008. Plio-Quaternary extensional seismotectonics and drainage network

development in the central sector of the Iberian Chain (NE Spain). Geomorphology, 102, 21–42.

Hack, J. T., 1957. Studies of longitudinal profiles in Virginia and Maryland. U. S. Geological Survey Professional Paper, 294 (B), 45–97.

Howard, A.D., & Kerby, G., 1983. Channel changes in badlands. Geological Society of America Bulletin, 4, 739–752.

Kirby, E. & Whipple, K. X., 2001. Quantifying differential rock-uplift rates via stream profile analysis. Geology, 29, 415–418.

Liesa, C.L. & Simón, J.L. (2009). Evolution of intraplate stress fields under multiple remote compressions: The case of the Iberian Chain (NE Spain). Tectonophysics, 474, 144-159.

López-Martínez, N., Agusti, J., Cabrera, L., Calvo, J., Civis, J., Corrochano, A., Daams, R., Diaz, M., Elizaga, E., Hoyos, M., Martinez, J., Morales, J., Portero, J. M., Robles, F., Santisteban, C., Torres, T., 1987. Approach to the Spanish continental Neogene synthesis and paleoclimatic interpretation. Annales. Instituti Geologici Publici Hungarici, 70, 383 – 391.Ludwig, K. (2003). Using Isoplot/Ex, Version 3. A Geochronological Toolkit for Microsoft Excel. Berkeley Geochronology Center Special Publication, 4.

Pazzaglia, F.J., 2003. Landscape evolution models. Developments in Quasternary Science, 1, 247-273.

Pelletier, J.D., 2008. Quantitative modeling of Earth surface processes. Cambridge: Cambridge University Press.

Peña, J. L., Gutiérrez, M., Ibáñez, M. J., Lozano, M. V., Rodríguez, J., Sánchez, M., Simón, J.L., Soriano, A., Yetano, M. ,1984. Geomorfología de la Provincia de Teruel. Teruel. Instituto de Estudios Turolenses. Excma. Dip. Provincial de Teruel (Spain).

Perea, H., Masana, E., Santanach, P., 2012. An active zone characterized by slow normal faults, the northwestern margin of the València trough (NE Iberia): a review. Journal of Iberian Geology, 38(1), 31-52.

Press, William H.; Teukolsky, Saul A.; Vetterling, William T.; Flannery, Brian P., 1986. "Preface". Numerical Recipes: The Art of Scientific Computing. New York: Cambridge University Press.

Refice A., Giachetta., E. & Capolongo. D., 2012. SIGNUM: A Matlab, TIN-based landscape evolution model. Computers & Geosciences, 45, 293-303.

Roering, J.J., J.W. Kirchner, and W.E. Dietrich, 1999. Evidence for nonlinear, diffusive sediment transport on hillslopes and implications for landscape morphology,Water Resources Research, 35, 853-870.

Scotti, V. N., Molin, P., Faccenna, C., Soligo, M. & Casas-Sainz, A., submitted. The influence of surface and tectonic processes in landscape evolution of the Iberian Chain: quantitative geomorphological analysis and geochronology.

Simón, J. L., 1984. Compresión y distensión alpinas en la Cadena Ibérica oriental. Instituto de Estudios Turolenses, Teruel (Spain).

Simón, J., Arlegui, L., Lafuente, P., Liesa, C., 2012. Active extensional faults in the central-eastern Iberian Chain, Spain. Journal of Iberian Geology, 38(1), 127-144.

Snyder, N., Whipple, K. X., Tucker, G. E., Merritts, D. J., 2000. Landscape response to tectonic forcing: Digital elevation model analysis of stream profiles in the Mendocino triple junction region, northern California. Geological Society of America Bulletin, 112 (8), 1250-1263.

Solé Sabarís, L., 1979. La Meseta. In: Teràn, D., Geográfia de España. Ariel, Madrid (Spain), 42 – 62.

Stock, J.D. & Montgomery, D.R., 1999. Geologic constraints on bedrock river incision using the stream power law. Journal of Geophysical Research, 104, 4983–4993.

Tarantola, A., & Valette B., 1982. Generalized Nonlinear Inverse Problems Solved using the Least Squares Criterion. Reviews of Geophysics and Space Physics, 20(2), 219-232.

Tarboton, D. G., Bras, R. L., Rodriguez-Iturbe, I., 1989. Scaling and elevation in river networks. Water Resources Research, 25, 2037–2051.

Ter Voorde, M., De Bruijne, C., Cloetingh, S., Andriessen, P., 2004. Thermal consequences of thrust faulting: simultaneous versus successive fault activation and exhumation. Earth and Planetary Science Letter, 223, 397-415.

Tucker, G.E. & Bradley, D.N., 2010. Trouble with diffusion: reassessing hillslope erosion laws with a particle-based model. Journal of Geophysical Research, 115, F00A10.

van Dam, J., Sanz Rubio, E., 2003. Late Miocene and Pliocene small mammals from the Calatayud Basin (Central Spain). Coloquios de Paleontología, 1, 115-126.

Villena, J., Pardo, G., Pérez, A., Muñoz-Jiménez, A., González, A.. 1996. Tertiary of the Iberian margin of the Ebro Basin: 1) Stratigraphic synthesis. In: Friend, P.,

Dabrio, C. (eds) Tertiary basins of Spain, Serie World and Regional Geology. Cambridge University Press, 77-82.4

Whipple, K. X., 2004. Bedrock rivers and the geomorphology of active orogens. Annu. Rev. Earth Planetary Sci., 32 , 151-185.

Whipple, K. X. & Tucker, G. E., 1999. Dynamics of the stream-power river incision model: implications for height limits of mountain ranges, landscape response timescales, and research needs. Journal of Geophysical Research, 104, 17,661-17,674.

Whipple, K.X., Wobus, C., Crosby, B., Kirby, E., Sheehan, D., 2007. New Tools for Quantitative Geomorphology: Extraction and Interpretation of Stream Profiles from Digital Topographic Data. Geological Society of America Annual Meeting, Short Course Guide: http://www.geomorphtools.org, Denver.

Willgoose, G., Bras, R.L.& Rodriguez-Iturbe, I., 1991. A physical explanation of an observed link area-slope relationship, Water Resourches Research, 27(7), 1697 – 1702.

Wobus, C., Whipple, K. X., Kirby, E., Snyder, N., Johnson, J., Spyropolou, K., Crosby, B., Sheehan, D., 2006. Tectonics from topography: Procedures, promise, and pitfalls. In: Willett, S., Hovius, N., Brandon, M.T, Fisher, D.M. (Eds), Tectonics, Climate, and Landscape Evolution. Geol. Soc. Am. Spec. Pap., 398, 55 –74.

Chapter 3

SUMMARY AND CONCLUSION

Quantitative geomorphic analyses are useful to investigate the impact of tectonic activity on geomorphic processes and landscape development. The quantitative analyses studied topographic and longitudinal river profiles, drainage networks, spatial distribution of drainage basins and their geometric relationships, having the aim to define controlling factors and reconstruct the evolution of landscape of Iberian Chain. Morphometric analysis have been also coupled with U-Th datings and field investigation of calcareous tufa lying on fluvial strath terraces. Finally, radiometric and morphometric data have been implemented in numerical models as physical parameters and combined by process laws (hillslope diffusion, fluvial incision, sedimentation).

This study demonstrates the importance of the interplay between surface and tectonic processes in shaping long-term landscape evolution, that results firstly sensitive to the initial geometrical configuration and to tectonic uplift rate and pattern.

In detail, results suggest an initial setting characterized by a wide plain surrounded by endorehic areas with a slightly higher relief to the NE sector (fig. 2.6C). The topographic surfaces from which the present-day topography originally evolved influence the outcome of evolution predictions and strongly contrast the adjustment to modern erosional conditions, keeping the landscape in a transient state in which rivers are still adjusting a dominant tectonic input, even though the lack of Late Pliocene-Quaternary deposits, except for small intermontane basins, suggest that erosion is a dominant process. In particular, the initial topographic barriers, together with the uplift pattern, play a fundamental role guiding the orientation of the headward fluvial erosion and preserving an ancient landscape in the interior of the range (fig. 2.6E-F-H-I):

topographic barriers prevent the rapid headward migration of the divides, keeping two distinct landscapes, the relict planation surface and the flank of the range, that therefore share very few topographic similarities: a long-lived, slowly eroding low-relief highland, and younger river valleys characterized by higher slope. Nevertheless, the river incision rate are quite similar throughout the range, recording average values of 0.6 mm/yr.

Since 3.2 Myr, the only remarkable tectonic activity of the area consists of a regional uplift. An uplift pattern of ~0.4 mm/yr is estimated in the inner sector, progressively decreasing toward WSW up to 0.25 mm/yr. A maximum uplift rate of 0.5 mm/yr is also calculated in the north-eastern sector of the Iberian Chain.

The reversal of the drainage network, due to the regressive erosion of the reliefs isolating the lacustrine areas from the Mediterranean Sea and the Atlantic Ocean, could be set after the onset of the uplift. This means that slow uplift rates in a flat region favour the preservation of internally drained basins of the central sector. In detail, similarly to how is proposed in the review of Gutierrez et al. (2008) on the basis of geomorphic and stratigraphic evidences, the Calatayud basin is captured at around 1.5 Myr. The capture and consequently the change to exorheic conditions in the Jucar basins and in the Teruel basin takes place at around 2 Myr.